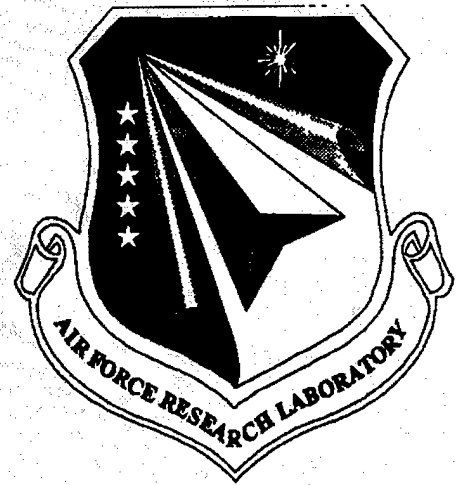


AFRL-ML-WP-TR-1999-4019



TRIBOLOGICAL MODELING

DR. PRADEEP K. GUPTA

**PRADEEP K. GUPTA, INC.
117 SOUTHURY ROAD
CLIFTON PARK, NY 12065-7714**

OCTOBER 1998

FINAL REPORT FOR 09/01/1992 – 10/31/1998

APPROVED FOR PUBLIC RELEASE; DISTRIBUTION UNLIMITED

**MATERIALS AND MANUFACTURING DIRECTORATE
AIR FORCE RESEARCH LABORATORY
AIR FORCE MATERIEL COMMAND
WRIGHT-PATTERSON AIR FORCE BASE OH 45433-7750**

DTIC QUALITY INSPECTED 4

20000107 093

NOTICE

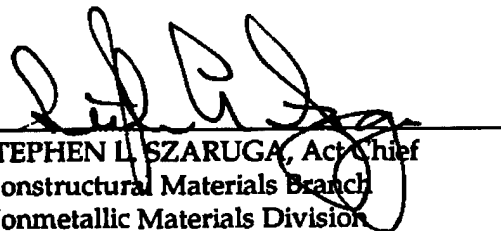
USING GOVERNMENT DRAWINGS, SPECIFICATIONS, OR OTHER DATA INCLUDED IN THIS DOCUMENT FOR ANY PURPOSE OTHER THAN GOVERNMENT PROCUREMENT DOES NOT IN ANY WAY OBLIGATE THE US GOVERNMENT. THE FACT THAT THE GOVERNMENT FORMULATED OR SUPPLIED THE DRAWINGS, SPECIFICATIONS, OR OTHER DATA DOES NOT LICENSE THE HOLDER OR ANY OTHER PERSON OR CORPORATION; OR CONVEY ANY RIGHTS OR PERMISSION TO MANUFACTURE, USE, OR SELL ANY PATENTED INVENTION THAT MAY RELATE TO THEM.

THIS REPORT IS RELEASABLE TO THE NATIONAL TECHNICAL INFORMATION SERVICE (NTIS). AT NTIS, IT WILL BE AVAILABLE TO THE GENERAL PUBLIC, INCLUDING FOREIGN NATIONS.


THIS TECHNICAL REPORT HAS BEEN REVIEWED AND IS APPROVED FOR PUBLICATION.



SHASHI K. SHARMA, Project Engineer
Nonstructural Materials Branch
Nonmetallic Materials Division



STEPHEN L. SZARUGA, Act Chief
Nonstructural Materials Branch
Nonmetallic Materials Division



ROGER D. GRISWOLD, Asst Chief
Nonmetallic Materials Division
Materials & Manufacturing Directorate

Do not return copies of this report unless contractual obligations or notice on a specific document requires its return.

REPORT DOCUMENTATION PAGE			Form Approved OMB No. 0704-0188	
<small>Public reporting burden for this collection of information is estimated to average 1 hour per response, including the time for reviewing instructions, searching existing data sources, gathering and maintaining the data needed, and completing and reviewing the collection of information. Send comments regarding this burden estimate or any other aspect of this collection of information, including suggestions for reducing this burden, to Washington Headquarters Services, Directorate for Information Operations and Reports, 1215 Jefferson Davis Highway, Suite 1204, Arlington, VA 22202-4302, and to the Office of Management and Budget, Paperwork Reduction Project (0704-0188), Washington, DC 20503</small>				
1. AGENCY USE ONLY (Leave blank)		2. REPORT DATE OCTOBER 1998		3. REPORT TYPE AND DATES COVERED FINAL REPORT FOR 09/01/1992 - 10/31/1998
4. TITLE AND SUBTITLE TRIBOLOGICAL MODELING			5. FUNDING NUMBERS C F33615-92-C-5916 PE 62102 PR 2421 TA 01 WU 57	
6. AUTHOR(S) DR. PRADEEP K. GUPTA				
7. PERFORMING ORGANIZATION NAME(S) AND ADDRESS(ES) PRADEEP K. GUPTA, INC. 117 SOUTHBURY ROAD CLIFTON PARK, NY 12065-7714			8. PERFORMING ORGANIZATION REPORT NUMBER	
9. SPONSORING/MONITORING AGENCY NAME(S) AND ADDRESS(ES) MATERIALS AND MANUFACTURING DIRECTORATE AIR FORCE RESEARCH LABORATORY AIR FORCE MATERIEL COMMAND WRIGHT-PATTERSON AFB, OH 45433-7750 POC: SHASHI K. SHARMA, AFRL/MLBT, 937-255-9029			10. SPONSORING/MONITORING AGENCY REPORT NUMBER AFRL-ML-WP-TR-1999-4019	
11. SUPPLEMENTARY NOTES				
12a. DISTRIBUTION AVAILABILITY STATEMENT APPROVED FOR PUBLIC RELEASE, DISTRIBUTION UNLIMITED			12b. DISTRIBUTION CODE	
13. ABSTRACT (Maximum 200 words) Analytical modeling of tribological behavior of interacting bodies is undertaken in three parts: modeling stresses at the surface and in the coatings of a coated solid, friction or traction at the interface between two contacting solids, and modeling of wear under given conditions of operation. Stress modeling of coated solids is accomplished by plane strain numerical solutions for line contact problems and finite element solutions of the more complex elliptical contacts. Both mechanical and thermal stresses in the solid are modeled. Semi-empirical relations are derived by regression analysis of experimental traction-slip data for several solid lubricants. The traction equations are readily applicable for the design and performance simulation of mechanical components. Wear is modeled as a multi-process phenomena. A generalized wear equation is developed such that one of the terms consists of Archard-type sliding wear while others represent thermally activated phenomena with varying activation energies. The model thus provides wear prediction as a function of load, speed and temperature. Similar to the traction model, coefficients of the wear equations are derived by fitting the model to experimental data. Good correlations of the model are demonstrated with two sets of experimental wear data.				
14. SUBJECT TERMS Modeling, tribology, stress, coated solids, friction, traction, wear, solid lubricants			15. NUMBER OF PAGES 132	
			16. PRICE CODE	
17. SECURITY CLASSIFICATION OF REPORT UNCLASSIFIED	18. SECURITY CLASSIFICATION OF THIS PAGE UNCLASSIFIED	19. SECURITY CLASSIFICATION OF ABSTRACT UNCLASSIFIED	20. LIMITATION OF ABSTRACT SAR	

Table of Contents

Report Documentation Page	i
Table of Contents	iii
List of Figures	v
List of Tables	vii
Foreword	viii
 1. EXECUTIVE SUMMARY	 1-1
 2. INTRODUCTION	 2-1
 3. STRESS MODELING IN PLANE-STRAIN	 3-1
3.1 The Plane-Strain Model	3-1
3.2 Computer Code LAYER	3-7
3.3 Typical Results	3-9
 4. FINITE ELEMENT MODELING	 4-1
4.1 Two-Dimensional Plane-Strain Problem	4-1
4.2 Generalized Three-Dimensional Problem	4-12
4.3 Thermal Modeling	4-30
 5. MODELING OF FRICTIONAL BEHAVIOR	 5-1
5.1 Friction or Traction Models	5-2
5.2 Regression Analysis for Model Coefficients	5-5
5.3 Contact Temperatures	5-6
5.4 Model Correlations	5-9
5.5 Nominal Friction Values for Some Materials	5-24
5.6 Other Models for Frictional Interactions	5-26
 6. WEAR MODELING	 6-1
6.1 Proposed Wear Model	6-2
6.2 Model Correlations	6-5
 7. MODEL INTEGRATION	 7-1
7.1 Operating Environment	7-1
7.2 Component Analysis	7-1
7.3 Potential Materials	7-1
7.4 Stress Analysis of Coatings	7-2
7.5 Surface Friction and Thermal Dissipations	7-2
7.6 Combined Mechanical and Thermal Stress Analysis	7-2
7.7 Analysis of Wear and Component Life	7-2
 8. RECOMMENDATIONS FOR FUTURE DEVELOPMENT	 8-1

9.	REFERENCES	9-1
	APPENDIX A	
	Macros of Building the Coated Solid	A-1
	APPENDIX B	
	Manual Analysis Procedure	B-1

List of Figures

3-1	Basic coordinate frame for a coated solid	3-2
3-2	Schematic layout of coated stress modeling computer code, LAYER	3-8
3-3	Typical normal stress solutions for a coated solid	3-10
3-4	Typical shear stress solutions resulting from normal surface loading	3-11
4-1	Typical regioned solid for the two-dimensional plane-strain problem with two coatings	4-2
4-2	Start of the mapped meshing procedure for the two-dimensional plane-strain problem	4-3
4-3	Meshing a region adjacent to an already meshed region	4-5
4-4	Fully meshed solid for modeling the two-dimensional plane-strain problem	4-6
4-5	Applied elliptical pressure and translational restraints for the plane-strain problem	4-8
4-6	von-Mises stress distribution for the plane-strain problem	4-9
4-7	Orthogonal shear stress distribution for the plane-strain problem	4-10
4-8	Distribution of maximum shear stress for the plane-strain problem	4-11
4-9	Regioned solid for modeling the three-dimensional stress problem	4-12
4-10	An enlarged view of the three-dimensional solid	4-13
4-11	Regioning details of the elliptical contact area	4-14
4-12	Start of the mesh process for the three-dimensional solid	4-16
4-13	Meshed outer annulus of the top coating	4-17
4-14	Meshed first region of the inner annulus around the contact	4-18
4-15	Meshed first region of the elliptical contact	4-19
4-16	Fully meshed solid for the three-dimensional problem	4-20
4-17	Enlarged view of finite element mesh in the elliptical contact region	4-21
4-18	Normalized grid pattern in the elliptical contact zone	4-22
4-19a	Applied ellipsoidal load and fixed base restraints for the three-dimensional problem	4-23
4-19b	Section of the three-dimensional solid along minor axis of the contact ellipse	4-24
4-20a	von-Mises stress distribution in the three-dimensional solid, along the minor axis of contact ellipse	4-25
4-20b	von-Mises stress distribution along major axis of the contact ellipse	4-26
4-21	Global shear stress variation along minor axis of the contact ellipse	4-27
4-22a	Variation of maximum shear along minor axis of the contact ellipse	4-28
4-22b	Variation in maximum shear stress along major axis of the contact ellipse	4-29
4-23	Surface grid pattern for defining the heat flux	4-30
4-24a	Temperature distribution on a sectional plane along major axis of the contact ellipse resulting from an ellipsoidal heat flux on the surface	4-33
4-24b	Temperature distribution on a sectional plane along minor axis of contact ellipse resulting from an ellipsoidal heat flux on the surface	4-34
4-25a	von-Mises stresses on a sectional plane along major axis of contact ellipse resulting from an ellipsoidal heat flux on the surface	4-35

4-25b	von-Mises stresses on a sectional plane along minor axis of contact ellipse resulting from an ellipsoidal heat flux on the surface	4-36
4-25c	Orthonal sher stress resulting from an ellipsoidal heat flux on the surface	4-37
4-26a	von-Mises stresses on a sectional plane along major axis of contact ellipse resulting from a uniform cooling of the solid from 500 to 20°C	4-38
4-26b	von-Mises stresses on a sectional plane along minor axis of contact ellipse resulting from a uniform cooling of the solid from 500 to 20oC	4-39
5-1	Commonly observed traction slip behavior	5-2
5-2	Contact zone schematic	5-7
5-3	Basic coordinates in the contact zone	5-8
5-4	Traction behavior of 0.40 μm coating of Ga-In-W-Se2 52100 steel specimens	5-9
5-5	Model correlation with experimental traction data obtained with Ga-In-W-Se2	5-10
5-6	Model correlation with experimental traction data obtained with ceramic disk specimens with no lubricant at room temperature	5-11
5-7	Model correlation with experimental traction data obtained with ceramic disk specimens with no lubricant at 649oC	5-12
5-8	Model correlation with experimental traction data obtained with ceramic disk specimens with TiO2 powder lubricant at room temperature	5-13
5-9	Model correlation with experimental traction data obtained with ceramic disk specimens with TiO2 powder lubricant at 649oC	5-14
5-10	Model correlation with experimental traction data obtained with ceramic dis specimens, contaminated with Inconel 718, with TiO2 powder lubricant at 649oC	5-15
5-11	Model correlation with experimental traction data obtained with ceramic disk specimens with boron nitride powder lubricant at 30oC	5-16
5-12	Model correlation with experimental traction data obtained with ceramic disk specimens with boron nitride powder lubricant at 649oC	5-17
5-13	Model correlation with experimental traction data obtained with ceramic disk specimens with MoS2 powder lubricant at 30oC	5-18
5-14	Model correlation with experimental traction data obtained with ceramic disk specimens with MoS2 powder lubricant at 427oC	5-19
5-15	Model correlation with experimental traction data obtained with ceramic disk specimens with MoS2 powder lubricant at 649oC	5-20
5-16	Model correlation with experimental traction data obtained with ceramic disk specimens with ZnMoO2S2 powder lubricant at 30 and 585oC	5-21
5-17	Model correlation with experimental traction data obtained with POM disk specimens	5-22
5-18	Model correlation with experimental traction data obtained with K162B (TiC) ball and silicon carbide disk specimens at high operating temperature	5-23
6-1	Model correlation to experimental wear data obtained with titanium alloys	6-6
6-2	Model correlations to experimental wear data obtained with a pin of composite material against an M50 steel disk	6-7
7-1	Model application for practical design	7-4

List of Tables

5-1 Nominal Friction Values for Some Materials

5-24

FOREWORD

The objectives of this program is to develop analytical models for understanding stresses, friction and wear as applicable to coated solids with solid lubricant films. Specific development of models for stress distribution, friction and wear respectively constitute the three phases of this program. Technical effort on the project was started on September 15, 1992. The Air Force project engineer was K. R. Mecklenburg from September 1992 to January 1998. In January 1998, Mr. Mecklenburg retired from the Air Force and Dr. Shashi Sharma assumed the project management responsibilities until end of the performance period till October 1998.

1. EXECUTIVE SUMMARY

The primary objective of this program is to develop procedures to model stresses, surface friction or traction and wear resulting from sliding and thermal interaction between coated solids. The emphasis is on development of model equations, numerical procedures and computer codes, which may be used for practical design. The overall project was divided into three phases:

Phase I:	Stress modeling
Phase II:	Friction modeling
Phase III:	Wear modeling

An existing plane-strain contact formulation for one coating on an elastic substrate was the starting point for modeling of stresses in coated solids. The formulation was based on Fourier transform of Airy stress function. The analysis was generalized to permit modeling of an arbitrary number of coatings. The formulation was implemented in the form of a computer code, LAYER, written in FORTRAN-90. The code serves as an efficient design tool. In addition to coated solids, the model may be used for solids with varying elastic properties as a function of depth by simply dividing the solid in discrete layers with different properties. While the computer code LAYER provides quick solutions to 2-D problems, finite element effort was undertaken to develop solutions for the more generalized 3-D problems associated with elliptical contacts. The widely used MSC/NASTRAN with the ARIES pre- and post-processors was used. Fairly unique grid patterns were generated to model the steep pressure gradients at the edge of contact. All mesh generation procedures were automated by writing appropriate macros for the ARIES pre-processor. Thus recreation of the solid and related mesh is straightforward and therefore, the macros have significant design potential. Aside from modeling of mechanical stresses, finite element procedures were also used to solve the thermal problem where the temperature distribution in the solid is computed for a prescribed surface heat flux. The computed temperature distribution is then input to the static module of MSC/NASTRAN to compute the various stresses in the solid. The procedures were also used to compute residual stresses in the solid resulting from coating deposition at high temperatures.

Procedures for modeling friction or traction are more empirical in nature. Based on past work on lubricant traction modeling, a traction-slip relation with three empirical constants is postulated. The model is then fitted to experimental traction data and the model coefficients are derived by nonlinear regression. The entire procedure is implemented in another computer code, SLTRAC, which may be used to development coefficients for future materials. The model is very well correlated with the experimental data obtained with several solid lubricants. The coefficients derived may be immediately used for the design and performance simulation of mechanical components, such as, rolling bearings and gears. In addition to regression analysis of experimental data, the computer code SLTRAC also computes contact temperature using flash temperature-type theories. The graphic output from the code consists of both traction and average contact temperature as a function of slide-to-roll ratio with prescribed contact load, rolling velocity and inlet temperature.

Modeling of wear has been a relatively more complex task. Traditionally wear has been related to contact loads and sliding speeds, with very little emphasis on effects of temperature, which is an important parameter for most solid lubricant materials. In order to model the effect of

thermal environment, overall wear of interacting solids is partitioned into several processes. One of the processes consist of traditional Archard-type wear resulting from sliding. The other processes are based on thermal activation with varying activation energies, and they, therefore, constitute different temperature dependent phenomena. The generalized equation consists of an arbitrary number of processes. Appropriate coefficients of the models may be derived by fitting the model to actual experimental data. Good correlation of the model is shown for two sets of available experimental data. As more experimental data with newly developed solid lubricating materials become available, the model may be used to develop a data base of coefficients which may be readily used for wear prediction in solid lubricated applications.

As a final part of this investigation, procedures for implementing the models developed above to practical applications are schematically outlined. The procedures basically integrate the above three models to provide practical guidance for design and also materials development for future applications.

2. INTRODUCTION

The tribological behavior of the materials present at the interface between machine elements subjected to sliding interaction very often dominate the overall behavior and life of the entire mechanical system. Friction and wear of bearings, gears, cams and similar components, are significant problems in a wide range of both DOD and commercial applications. Some examples include, rolling bearings used in turbine engines, gyroscopes, precision gimbals, cryogenic turbopumps and cryo-coolers. Similarly, wear of piston rings, cylinder liners, gears, cams and cam followers in automotive applications is an important problem, particularly in adiabatic diesel engines, where operating temperatures are quite high. The use of lubricating oils and greases is well known for reduction of friction and wear and as a result, an improvement in life of the overall mechanical system. However, these conventional lubricants can only perform satisfactorily in a limited range of operating temperatures. In the very high temperature environment of modern gas turbine applications, solid lubricants offer, perhaps, the only means of lubricating the interacting mechanical elements. Similarly, for space applications in the cryogenic temperature range, solid lubrication offers the only potential for reducing friction and wear between mating surfaces.

Very often tribological enhancement of interacting surfaces and solid lubrication is accomplished by applying one or more coatings of certain materials, which offer favorable tribological characteristics. In gyro bearings, hard coats of Tungsten Carbide or Titanium Carbide over the 440C stainless steel balls have shown to result in higher preload capability, higher life and improved torque stability. Similarly, in oscillatory bearings for precision gimbals, multiple coatings of vastly different materials have shown significant reduction in friction and wear. In fact, surface treatments which result in reduction in friction and wear have a rather universal significance. However, when thin coats or films of different materials are applied, adherence between the coatings as a function of both the applied operating conditions, such as loads, surface friction and temperatures, and the residual stresses, resulting from the coating process itself, are critical problems. The residual stress problem has been particularly significant with very hard materials, such as diamond. In addition to the stresses resulting from the applied conditions, the thermomechanical behavior of the coatings may vary from fully isotropic to highly anisotropic. This adds further complications to the mechanical behavior of coatings in a given operating environment. Aside from the above tribological applications, surface coatings play an important role in infrared (IR) devices used for guidance and tracking. Here, the functionality of the device imposes an additional requirement that the coating material be IR transparent. For example, survival of the coatings on the IR dome in the "Maverick Missile" against erosion due to rain drops at very high speeds and other similar environmental conditions is a critical problem. The relative low life against erosion of the present Zinc Sulfide and Zinc Silicide coatings is a critical problem. A very thin coat of a hard material, such as diamond, has been proposed as a solution. However, the high temperature requirement for application of diamond films creates a significant problem. In fact, deposition of diamond may require an intermediate coat of another more compatible material such as Germanium Carbide, which, however, is not completely IR transparent. Similar coupling between material behavior and operating requirements is also important in electronic packaging, circuit boards, thermal management in space power systems and a variety of other applications. In the above wide application spectrum, the fundamental mechanics leading to the distribution of stresses and deformations in the coated solids is, indeed, a common subject. In fact, due to the greatly different constitutive behavior of the coatings in comparison to that of the substrate, an

acceptable design of a coating-substrate system is dependent on realistic modeling of the stresses in the coatings in a prescribed operating environment. The stress distribution in the coating determines its mechanical survival; the tensile stresses in the coating are often responsible for fracture initiation while both the shear and tension at the coating/substrate interface affect adhesion, or mechanical bond, of the coating to the substrate. A rigorous analytical modeling of these stresses is, therefore, essential.

In addition to the applied loads on the coating surface, the friction forces lead to surface shear stresses in the contact, which alter the stress distribution in the coating and the coating/substrate interface. In fact, the surface shear loading results in tension at the coating/substrate interface, and therefore, the survival of the coating is affected. Along with the mechanical problem, the surface shear or friction results in heat which is conducted through the coated solid. The resulting temperature distribution produces thermal stresses, which are superposed on the mechanical stress fields. Since, the material properties are very often dependent on temperature, the frictional effects become intricately coupled with the mechanical problem. This requires a simultaneous modeling of stress and friction problems. As the coating surface is subjected to sliding interaction, a wear process sets in to define the operating life of the coating in a given environment. However, as the coating thickness changes due to wear, the overall stress distribution and the thermal interactions are affected. In fact, the wear process itself may be a thermally activated phenomena, and since the material properties, such as hardness, often depend on temperature, the wear process also becomes coupled with the stress and friction problems, discussed above. For the development of practical design tools for such coupled interactions, it is necessary to first develop and validate models for each of the three basic processes, e.g., stress distributions, frictional interactions, and the wear process. Thus, the primary objective of the present investigation is to develop models for each of these three basic processes.

Practical significance of the analytical model extends far beyond the prediction of design variables, such as optimum coating thickness, for given applications. Once the models have been validated for their predictive strengths, they may be effectively used to parametrically evaluate critical parameters, such as, shear and tensile stresses at the coating to substrate interface, thermal stresses induced by the difference in thermal coefficient of expansion between the coatings and substrate and realistic endurance limits when the coated elements are subjected to cyclic loading, to arrive at significant recommendations for the required materials for more advanced applications. Thus, the analytical models may indeed serve as viable tools for materials selection and development.

Modeling of stresses in coated solids is divided in two parts. First, plane-strain techniques are used to develop numerical procedures and computer codes for the somewhat simplified two-dimensional problems. Since plain-strain approximation may be fairly valid for a broad range of practical application, such analytical tools and computer codes will have a significant practical potential. For more complex problems with three-dimensional elliptical contacts, the well established finite element procedures are used to model the stress problems. The widely used MSC/NASTRAN package is used to accomplish this task. In addition to the mechanical stress problem, finite element techniques are also used to solve the thermal problem where the interacting solid may be subject to a surface heat flux. These solutions provide a temperature distribution in the solid which may be input to the stress modules to compute thermal stresses. Similarly, residual

stresses arising from deposition of coating material at high temperature, and subsequent cooling of the coated solid to room temperature, may also be modeled easily with the finite element procedures. Plane strain analysis and finite element modeling, respectively, constitute chapters 3 and 4 of this report.

Modeling of surface friction is more empirical in nature. The approach consists of postulating a traction-slip equation with appropriate coefficients, which may be computed by regression analysis of experimental data. The approach has been effectively used in the past for a large number of liquid lubricants, where the model coefficients represent physical properties such as viscosity, shear modulus and critical shear stress. Very often traction predictions strictly based on the fundamental properties of the lubricant, liquid or solid, do not quite agree with experimental measurements. The modeling approach, therefore, has been to fit the model to actual experimental data and derive the "effective" value of the constitutive constants. Although such an approach lacks adequate physical interpretation of the model, it provides validated models with good predictive strengths for design purposes. Friction modeling is the subject of chapter 5 of this report.

Wear modeling is even more empirical than the approach to friction or traction relations. Traditionally, wear rate is considered to be proportional to load and sliding velocity with no effect of temperature. For modern materials, solid lubrication and high-temperature operating environments, temperature is an important variable. In fact, temperature is the most fundamental variable which provides coupling between the basic processes discussed above, e.g., stresses, friction and wear. The technical approach in the present investigation, therefore consists of dividing overall wear into multiple processes, one of which could be the classical sliding wear, while the other processes are thermally activated with varying activation energy. Although the various coefficients in the generalized wear equation are simply derived by curve fitting the model to experimental data, the thermally activated processes may represent chemical reactions such as oxidation. Thus, the wear model developed herein may correspond to actual physical and chemical processes. Chapter 6 presents the wear model.

Although the models for each process, e.g., stresses, friction and wear, are developed independently, there is a significant interaction between the processes when the models are applied to practical problems. For example, the heat generated in the contact due to frictional effects results in a temperature distribution, which in turn produces thermal stresses. Also, when the material properties are dependent on temperature, both stress distributions and wear rates may be affected by the thermal dissipations resulting from the frictional effects. Similarly, since the stress distributions are dependent on coating thickness, the wear process, where the coating thickness continues to decrease, affects stress distributions. Such variables, therefore, provide the coupling between the three independent models while modeling the overall performance and operating life of a mechanical component. To address such interactions, an integrated approach to apply the models for practical design is outlined in a schematic manner. Such design guidance is the subject of chapter 7 of this report, which is followed by some recommendations for future development.

3. STRESS MODELING IN PLANE-STRAIN

Due to a rather wide application potential, the analytical modeling of the contact mechanics and interfacial interactions in coated solids have been of significant interest in the recent years. In the past, both, solution to the contact problem and stress distribution in the coating as a function of the prescribed boundary loading have been attempted. The solution to the contact pressure profile in the case of cylindrical contact between coated elastic solids has been obtained to varying degrees of sophistication by a number of investigators [1-6]. Most of the early work [1-5] considered an asymptotic problem of a very thin or thick coating. Meijers [3], while considering an elastic layer over a rigid substrate demonstrated that the solutions for a thin and thick layer overlap so well that these solutions may apply to arbitrary layer thicknesses with excellent approximation. Wu, Chiu and Pao [4,5] considered the classical stress function approach to the contact problem of coated solids and they clearly demonstrated the mathematical complexity of the problem, particularly the numerical convergence problem as the material of the coating tends to become incompressible. Gupta and Walowit [6] resolved this problem by considering a Fourier transform of the Airy stress function and they obtained solutions where both the coating thickness and the coating to substrate modulus ratios may assume arbitrary values; in addition, they demonstrated that the Poisson's ratio may also be arbitrary and therefore, the incompressible materials may be properly modeled. In the area of stress distribution in the coating, most investigators considered either a uniform or an elliptical boundary loading. Lemcoe [7] considered a uniform pressure over the contact zone on a hard coating resting over a relatively soft substrate. Results for the stress distribution in the coating and substrate were presented for the cases when the coating is either in frictionless contact or bonded to the substrate. Barovich, et al. [8], used an elliptical pressure profile and obtained stress distribution when the ratio of modulus of elasticity of the coating to that of the substrate varied in the range of 0.25 to 4. Later Ku, et al. [9], considered surface shear and presented similar results for both elliptical and uniform shear prescribed at the coating surface. Based on the general solution to the contact problem [6], Gupta, Walowit and Finkin [10] considered an arbitrary pressure and shear loading on the coating surface and they presented results for stress distribution in the coating, substrate and at the coating/substrate interface for a wide range of material properties. For practical designs, the Fourier transform approach of Gupta and Walowit [6,10] was implemented in a FORTRAN computer code, LAYER [11].

In terms of practical applications, the plane-strain models are applicable to a wide range of application. In roller bearings, the line contact between roller and race is certainly a plane-strain problem. In most ball bearings, although the contact is elliptical, the ratio of major to minor axis of the contact ellipse is often greater than 5; thus, a line contact approximation may be quite reasonable. Similarly, contact problems in gears, cams and cam followers may be modeled reasonably well with plane strain approximation. Contact between the piston rings and liners in another application where the plane strain approximation is valid.

3.1 The Plane-Strain Model

In the present investigation, the plane-strain models developed by Gupta and Walowit [6] and Gupta, et al. [10], form the base line. The analytical formulation is based on a formulation derived from Fourier transform of the classical Airy stress function. With reference to the coordi-

nates shown below in figure 3-1, the stresses, σ_x , σ_y and τ_{xy} are respectively given by the rela-

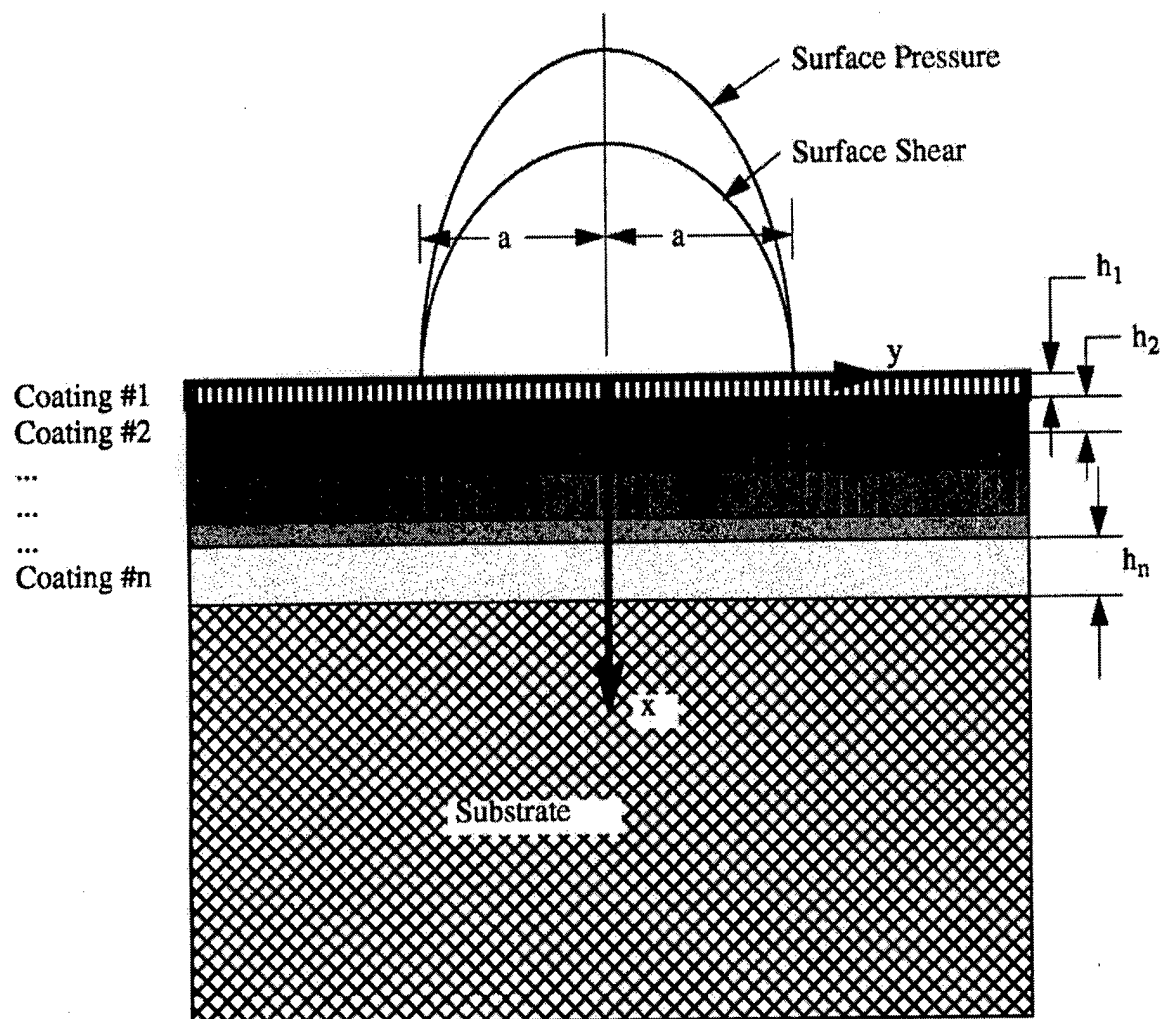


Figure 3-1. Basic coordinate frame for a coated solid.

tions:

$$\sigma_x = \frac{\partial^2 \psi}{\partial y^2} = -\frac{1}{2\pi} \int_{-\infty}^{\infty} \omega^2 G e^{-i\omega y} d\omega \quad \text{Eqn (3-1)}$$

$$\sigma_y = \frac{\partial^2 \psi}{\partial x^2} = \frac{1}{2\pi} \int_{-\infty}^{\infty} \frac{d^2 G}{dx^2} e^{-i\omega y} d\omega \quad \text{Eqn (3-2)}$$

$$\tau_{xy} = -\frac{\partial^2 G}{\partial x \partial y} = \frac{1}{2\pi} \int_{-\infty}^{\infty} i\omega \frac{dG}{dx} e^{-i\omega y} d\omega \quad \text{Eqn (3-3)}$$

and the displacements:

$$u = \frac{1-\nu^2}{2\pi E} \int_{-\infty}^{\infty} \left[\frac{d^3 G}{dx^3} - \frac{(2-\nu)}{1-\nu} \omega^2 \frac{dG}{dx} \right] e^{-i\omega y} \frac{d\omega}{\omega^2} \quad \text{Eqn (3-4)}$$

$$v = \frac{1-\nu^2}{2\pi E} \int_{-\infty}^{\infty} \left[\frac{d^2 G}{dx^2} + \frac{\nu}{1-\nu} \omega^2 G \right] i e^{-i\omega y} \frac{d\omega}{\omega} \quad \text{Eqn (3-5)}$$

where ψ is the Airy stress function which satisfies the biharmonic equation and G is the Fourier transform of ψ , symbolically

$$\nabla^4 \psi = 0 \quad \text{Eqn (3-6)}$$

and

$$G = \frac{1}{2\pi} \int_{-\infty}^{\infty} \psi e^{-i\omega y} dy \quad \text{Eqn (3-7)}$$

By eliminating ψ in equations (6) and (7) and by solving the resulting differential equation in G , a solution of the following form is obtained

$$G = (A + Bx)e^{-|\omega|x} + (C + Dx)e^{+|\omega|x} \quad \text{Eqn (3-8)}$$

where A, B, C and D are constants to be determined from the boundary conditions. These constants are, in general, functions of ω and the coating material. Thus for each coating, labeled as 1 to n , in figure 3-1, there will be four stress function constants. The boundary conditions for the computation of these constants consist of

1. Prescribed normal and shear stress at the surface of the top coating.
2. The normal and shear stress at each interface in the two materials are equal.
3. The displacement in the two materials are also equal at the interface.
4. For elastic substrate the normal and shear stress should vanish at infinite depth.
5. For rigid substrate the displacements vanish at the substrate surface.

If the coatings in figure 3-1 are labeled as ($i = 1, n$) then the $4n$ algebraic equations, corresponding to the four stress function coefficients for each coating, have to be formulated in terms of the above boundary conditions.

For the development of these equations it will be convenient to define the following dimensionless variables:

$$\eta = (y/a), \xi = (x_i/a), s = \omega a, d_i = (h_i/a), \text{ and } z = |s| \quad \text{Eqn (3-9)}$$

Now by substituting the surface boundary conditions $\sigma_{x_1}|_{x_1=0} = p$, and $\tau_{x_1 y}|_{x_1=0} = q$, in equations (3-1) and (3-3) and by taking an inverse Fourier transform of the resulting equations, the following two equations may be derived:

$$s^2 A_1 + s^2 C_1 = P = \int_{-\infty}^{\infty} p(\eta) e^{is\eta} d\eta \quad \text{Eqn (3-10)}$$

and

$$-zsA_1 + sB_1 + zsC_1 + sD_1 = Q = \int_{-\infty}^{\infty} q(\eta) e^{is\eta} d\eta \quad \text{Eqn (3-11)}$$

For developing the equations corresponding to the boundary conditions at the interface between two coatings, it will be convenient to define the following additions functions:

$$\phi_i = \frac{2 - \nu_i}{1 - \nu_i} \quad \text{Eqn (3-12)}$$

$$\phi'_i = \frac{\nu_i}{1 - \nu_i} \quad \text{Eqn (3-13)}$$

$$\gamma_i = \frac{(1 - \nu_i^2)E_{i-1}}{(1 - \nu_{i-1})E_i} \quad \text{Eqn (3-14)}$$

If n is the number of coatings, then for equations 12 and 13, $1 \leq i \leq n$ for rigid substrate, and $1 \leq i \leq (n+1)$ for elastic substrate, where the subscript $(n+1)$ corresponds to the elastic substrate. In equation (14) the subscript, i , will vary from 2 to n for rigid substrate, while it varies from 2, $(n+1)$, for the elastic substrate.

In addition, at any value of ξ coordinate, and the integrating variable ω , a matrix Z is defined to contain the coefficients of the stress function and its derivatives, as follows:

$$Z \begin{bmatrix} A \\ B \\ C \\ D \end{bmatrix} = \begin{bmatrix} G \\ \frac{dG}{dx} \\ \frac{d^2 G}{dx^2} \\ \frac{d^3 G}{dx^3} \end{bmatrix} \quad \text{Eqn (3-15)}$$

Here Z is a (4x4) matrix of the coefficients which are derived from the stress function equation. The coefficients are functions of the coordinate ξ and the integrating variable ω .

The boundary conditions of equal normal and shear stresses, and the two displacements, at the interface between coating i and $i+1$, where i varies from 1 to $n-1$, are written as

$$\sigma_{x_i}|_{\xi_i = d_i} = \sigma_{x_{i+1}}|_{\xi_{i+1}} = 0 \quad \text{Eqn (3-16)}$$

$$\tau_{xy_i}|_{\xi_i = d_i} = \tau_{xy_{i+1}}|_{\xi_{i+1}} = 0 \quad \text{Eqn (3-17)}$$

$$u_i|_{\xi_i = d_i} = u_{i+1}|_{\xi_{i+1}} = 0 \quad \text{Eqn (3-18)}$$

$$v_i|_{\xi_i = d_i} = v_{i+1}|_{\xi_{i+1}} = 0 \quad \text{Eqn (3-19)}$$

Now by using equations (1), (3), (4), and (5), and by using the notations introduced in equations (12-15), the above four equations may be written in terms of the stress function coefficients

$$\begin{bmatrix} Z_{11}|_{d_i} & Z_{12}|_{d_i} & Z_{13}|_{d_i} & Z_{14}|_{d_i} & -Z_{11}|_0 & -Z_{12}|_0 & -Z_{13}|_0 & -Z_{14}|_0 \\ Z_{21}|_{d_i} & Z_{22}|_{d_i} & Z_{23}|_{d_i} & Z_{24}|_{d_i} & -Z_{21}|_0 & -Z_{22}|_0 & -Z_{23}|_0 & -Z_{24}|_0 \\ U_1|_{d_i} & U_2|_{d_i} & U_3|_{d_i} & U_4|_{d_i} & -\gamma_{i+1}U_1|_0 & -\gamma_{i+1}U_2|_0 & -\gamma_{i+1}U_3|_0 & -\gamma_{i+1}U_4|_0 \\ V_1|_{d_i} & V_2|_{d_i} & V_3|_{d_i} & V_4|_{d_i} & -\gamma_{i+1}V_1|_0 & -\gamma_{i+1}V_2|_0 & -\gamma_{i+1}V_3|_0 & -\gamma_{i+1}V_4|_0 \end{bmatrix} \begin{bmatrix} A_i \\ B_i \\ C_i \\ D_i \\ A_{i+1} \\ B_{i+1} \\ C_{i+1} \\ D_{i+1} \end{bmatrix} = 0$$

$$\text{Eqn (3-20)}$$

where

$$U_j|_{d_i} = Z_{4j}|_{d_i} - \delta_i s^2 Z_{2j}|_{d_i})_{j=1,4} \quad \text{and} \quad U_j|_0 = Z_{4j}|_0 + \delta_{i+1} s^2 Z_{2j}|_0)_{j=1,4} \quad \text{Eqn (3-21)}$$

$$V_j|_{d_i} = Z_{3j}|_{d_i} + \delta_i s^2 Z_{1j}|_{d_i})_{j=1,4} \quad \text{and} \quad V_j|_0 = Z_{3j}|_0 + \delta_{i+1} s^2 Z_{1j}|_0)_{j=1,4} \quad \text{Eqn (3-22)}$$

The boundary conditions at the interface between the last coating (coating # n) and the substrate will depend on the type of substrate. For elastic substrate, the normal and shear stress, and the displacements in the coating will match those in the substrate, while both displacements will vanish at the interface for a rigid substrate. Thus the equations for elastic substrate are

$$\begin{bmatrix} Z_{11}|_{d_n} & Z_{12}|_{d_n} & Z_{13}|_{d_n} & Z_{14}|_{d_n} & -Z_{11}|_0 & -Z_{12}|_0 \\ Z_{21}|_{d_n} & Z_{22}|_{d_n} & Z_{23}|_{d_n} & Z_{24}|_{d_n} & -Z_{21}|_0 & -Z_{22}|_0 \\ U_1|_{d_n} & U_2|_{d_n} & U_3|_{d_n} & U_4|_{d_n} & -\gamma_{n+1} U_1|_0 & -\gamma_{n+1} U_2|_0 \\ V_1|_{d_n} & V_2|_{d_n} & V_3|_{d_n} & V_4|_{d_n} & -\gamma_{n+1} V_1|_0 & -\gamma_{n+1} V_2|_0 \end{bmatrix} \begin{bmatrix} A_n \\ B_n \\ C_n \\ D_n \\ A_{n+1} \\ B_{n+1} \end{bmatrix} = 0 \quad \text{Eqn (3-23)}$$

Here the subscript $(n+1)$ is used for the substrate. Also, the requirement that the stresses must vanish at infinite depth in the semi-infinite elastic substrate, which results in the condition $C_{n+1} = D_{n+1} = 0$, has been used in the above equation (23).

For the rigid substrate the two displacement in the last coating at the coating/substrate interface must vanish. These displacement equations may be written as

$$\begin{bmatrix} U_1|_{d_n} & U_2|_{d_n} & U_3|_{d_n} & U_4|_{d_n} \\ V_1|_{d_n} & V_2|_{d_n} & V_3|_{d_n} & V_4|_{d_n} \end{bmatrix} \begin{bmatrix} A_n \\ B_n \\ C_n \\ D_n \end{bmatrix} = 0 \quad \text{Eqn (3-24)}$$

Here the definition of the functions U and V is identical to that defined in equations (3-21 and 3-22) with the coating index i set to n for the last coating.

In summary, for semi-infinite elastic substrate and n coatings, there are $(4n+2)$ unknowns, $A_i, B_i, C_i, D_i|_{i=1,n}, A_{n+1}$ and B_{n+1} . The corresponding equations available to compute these unknown coefficients consist of equations (3-10) and (3-11), $(4n-4)$ equations from equation (3-20) with $(i = 1, n-1)$, and four equations for equation (3-23).

For the rigid substrate with n coatings, there are $4n$ unknowns, $A_i, B_i, C_i, D_i|_{i=1,n}$. The required number of equations consist of equations (3-10) and (3-11), $(4n-4)$ equations from equation (3-20) with $(i = 1, n-1)$, and two equations for equation (3-24).

Once the stress function coefficients are computed, based on the above equations, they may be substituted in equations (3-1 to 3-5) and the resulting integrals may be evaluated numerically to compute the various stress and displacement fields in the coated solid. A ten-point Gaussian quadrature algorithm was found to be adequate for these computations. This completes the analytical formulation for computation of subsurface stresses in the coatings for a prescribed surface loading.

For solution to the contact problem, where parabolic displacements are prescribed on the surface of the top coating, the Green's function type approach used by Gupta and Walowit [1] for a single coating bonded to a semi-infinite elastic substrate is directly applicable. For computation of Green's functions the surface pressure $p(\eta)$, in equation (10), is replaced by a unit line load, the surface shear stress is set to zero, and then the normal surface displacement equations in terms of surface pressure are equated to the prescribed parabolic displacement to compute the surface pressure distribution. Except for the stress function coefficients, which are derived from the above generalized formulation, the analytical procedure for the solution to the contact problem is identical to that already published by Gupta and Walowit[1]. This formulation is, therefore, omitted here.

3.2 Computer Code LAYER

The above numerical procedure for modeling stresses in a coated solid is implemented in the earlier computer code, LAYER, developed by Gupta [11]. There are three parts to this updated code: input module, the main compute module, and the graphics module. The input module is based on the X-Windows and Motif libraries, available as a part of the most Unix operating system, and it is written in the standard ANSI C language. The main compute module is written in standard FORTRAN-90 language. Also, the graphics module conforms to the FORTRAN-90 standard and it employs the ISO-PHIGS graphics library. The interconnection between the three modules is shown schematically in figure 3-2. The input module, based on the user input supplied via interactive screens, prepares an input data file. This file is input to the compute module, which basically has two parts: the solution to the contact problem, and subsurface stresses in the coated solid. For solving the contact problem, first the stress function coefficients are computed for a line load condition, these coefficients are input to the computation of Green's function and formulation of the surface pressure and displacement equations, and finally the pressure-displacement equations are inverted to obtain solution to the contact problem. For computation of stresses, the stress function coefficients are computed for the prescribed surface loading and these are input directly to the Fourier integrals defining the various stress components.

The main compute module, as shown schematically in figure 3-2, has three modes of operation, which are selected by value of the input variable MODE. Under MODE=0, only the contact problem is solved. With MODE=1, the surface pressures, as obtained from the contact problem solution, are input to subsurface stress computing procedures and the final output consists of both the surface pressures and the subsurface stress distributions in the coatings. When the subsurface

stress distributions are required for any prescribed surface loading, MODE=3 may be used. Surface pressure loading is prescribed in the input data in this case.

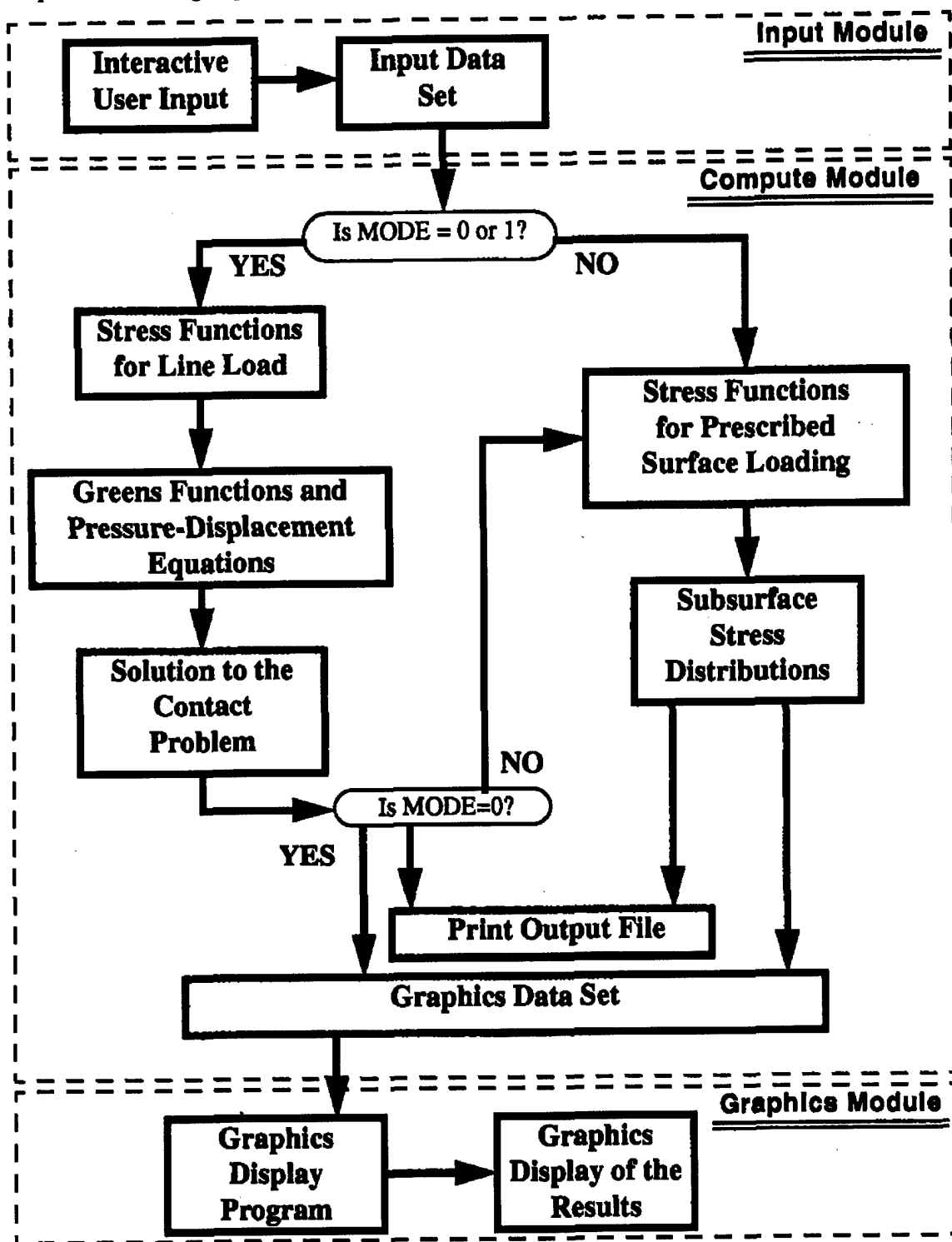


Figure 3-2. Schematic layout of coated stress modelling computer code, LAYER.

Output from the compute module consists of two files: a print file and a graphics file. The print file simply contains the formatted print output and it may be printed on any printer, while the graphics file is an ASCII data file which may be input to the graphics module to obtain a visual presentation of the results.

3.3 Typical Results

Consider a coated solid with three coatings and an elastic substrate. Let the top coat be of a ceramic material with one micron thickness. The material of the central and lower coatings is arbitrarily selected to have an elastic modulus of, respectively, 0.75 and 0.70 times that of the top coats, while the thickness of these coatings is set to 2 and 3 micron. Typical normal stress solutions for this solid with a contact half width of 10 microns are shown in figure 3-3. The solid graphs represent the normal stress σ_x at the various depth coordinate. The normal loading on the surface is obtained by solving the contact problem. Note that the normal stress is highest on the surface, and it gradually reduces as a function of the depth coordinate as expected.

The subsurface shear stress for the above example is shown in figure 3-4. Note the increasing shear stress as a function of the depth coordinate. This behavior is similar to the classical Hertzian contact where the subsurface shear first increases as a function of depth and then gradually vanishes with increasing depth. The critical parameters here will be the shear stress at the interface which may lead to coating fracture.

The graphics facility which produces the typical results shown in figures 3-3 and 3-4, offers interactive menu buttons on top of the screen. Thus, all stress components may be immediately examined as a function of certain input parameters which are available under the "parametric" menu button. This greatly facilitates the design optimization process.

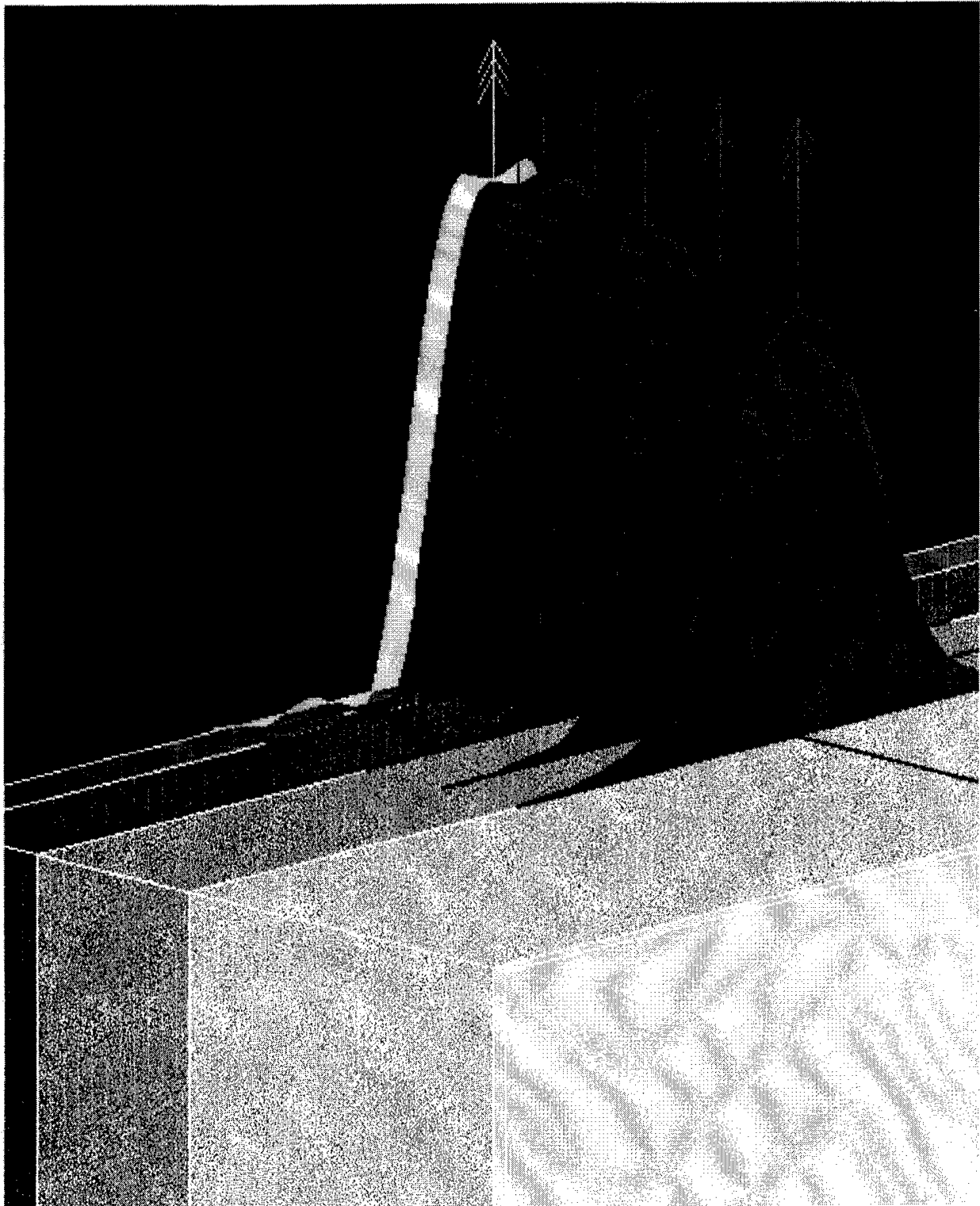


Figure 3-3. Typical normal stress solutions for a coated solid.

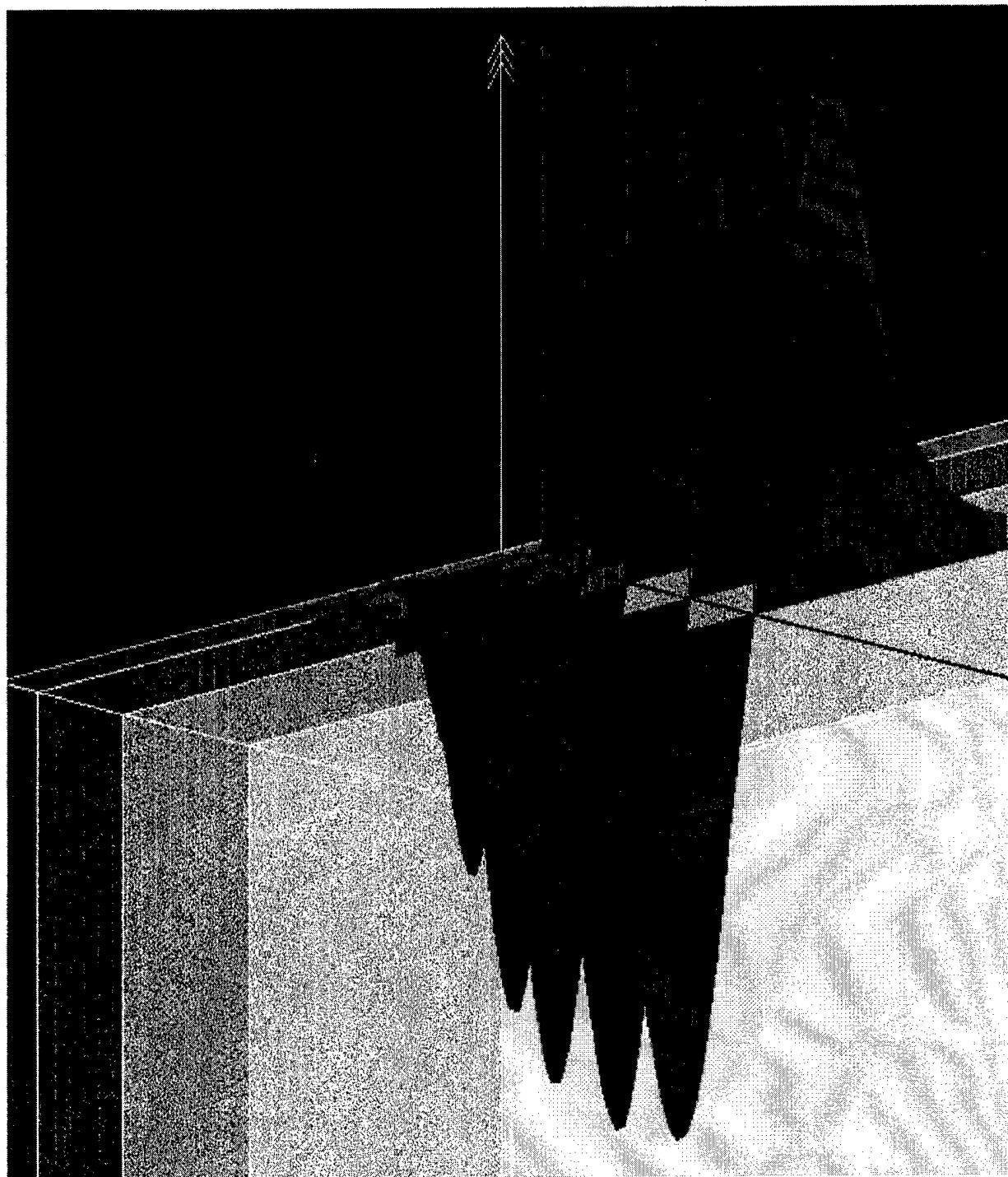


Figure 3-4. Typical shear stress solutions resulting from normal surface loading.

4. FINITE ELEMENT MODELING

Finite element methods have been very widely used to model stresses and thermal problems in a wide range of application. Very recently have also been applied to modeling friction problem in coated solids [12,13]. A number of finite element packages are commercially available and they are readily usable for practical problems. In the present investigation the widely used MSC/NASTRAN package [14] was used to carry out finite element modeling of coated solids. First, a plane-strain problem was modeled in two dimensions and then the more complex three-dimensional problem with elliptical contact was considered. It is well known that preparation of the mesh is generally the most time consuming task in any finite element work. Perhaps, processing of the results is the second laborious task. In other words, data pre- and post-processing effort is significant in any finite element modeling work. In an overall sense, the basic steps involved in the finite element modeling task are:

1. Generation of the solid
2. Meshing of the various regions of the solid
3. Application of applied loads and restraints
4. Finite element analysis
5. Processing of the results

Steps 1 to 3 constitute data pre-processing, step 4 is actual analysis and step 5 represents data post-processing to present the results in different engineering formats. The MSC/NASTRAN package includes the ARIES pre- and post-processors, which provide an interactive geometrical modeler which greatly helps in modeling the geometry and generating the mesh pattern for NAS-TRAN analysis. Similarly, the ARIES post-processor provides engineering displays of all the results. This interface was used in the current effort. The overall modeling effort for both the two- and three-dimensional problems is discussed below.

4.1 Two-Dimensional Plane-Strain Problem

The first step in the modeling effort is to create a simple rectangular solid, which is then "regioned" into different areas to represent the coatings and applied load zone. Regioning is an operation in the modeling step where an area or volume is defined by intersection of two solids or surfaces. Although the region, so defined, is still a part of the original solid, but its material and properties may be different from that of the base solid. Thus, a coating rigidly bonded to a solid can be defined by the regioning operation. Similarly, it is convenient to define an area over which the load is applied by another regioning operation. The "Geometry" application available in the ARIES interface can be used interactively to perform all these geometrical modeling steps. Before using this application, however, certain start-up steps may be necessary, such as setting the coordinate frame, units of measurement, etc. These steps are contained in the Macro: startup, listed in Appendix A. Thus the setup is simply accomplished by simple execution of the macro, by typing *startup* at the command line. The "Geometry" application may now be used to create the solid. After the modeling steps have been successfully performed, the associated "journal file" may be used to create another macro, listed as Macro: solid2d, in Appendix A. The modeling process may now be automated by simply executing this macro by typing a command *solid2d* on the command line. The various inputs, such as coating thickness and size of contact zone are requested by

appropriate interactive prompts. For an example with two coatings on the surface, the solid as created by executing the macro is shown below in figure 4-1.

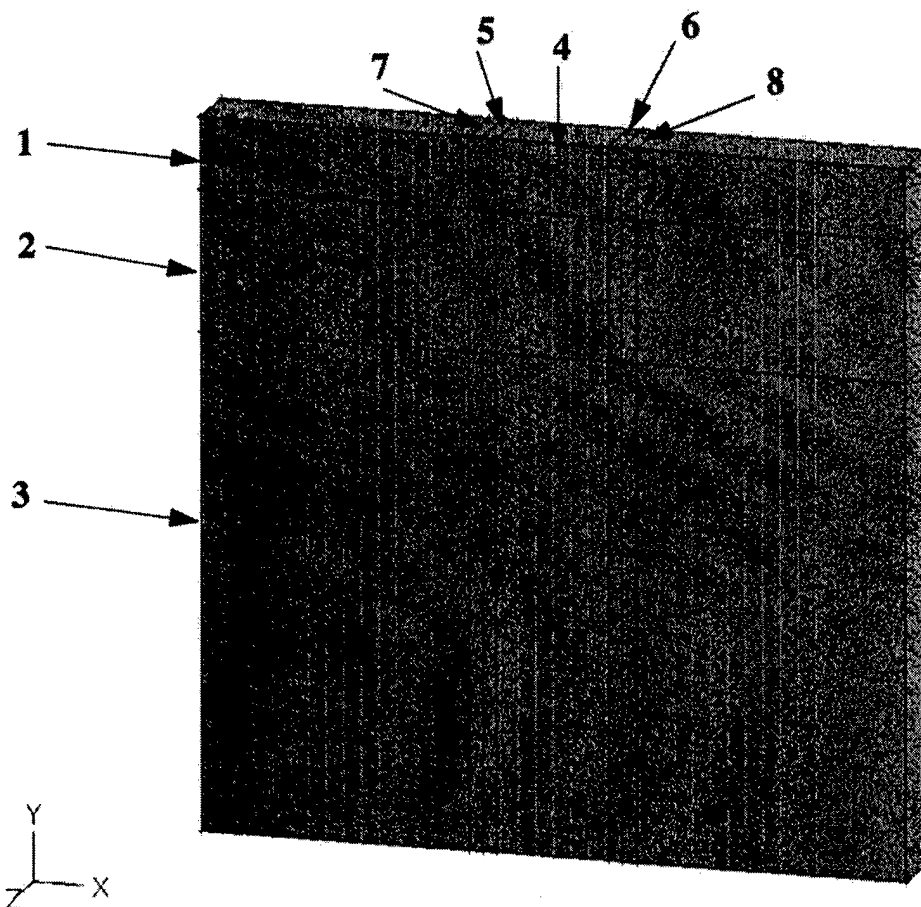


Figure 4-1

Typical regioned solid for the two-dimensional plane-strain problem with two coatings.

First, a base rectangular solid is created, and then it is regioned into three parts, corresponding to the top coating (region #1), the second coating (region #2) and the substrate (region #3). This regioned solid is then further regioned to define the central part of the load zone (region #4), the areas near the edges of and within the load zone (regions #5 and #6), and the two areas near the edges of and external to the load zone (regions #7 and #8). With the solid defined in this manner, the material properties in regions 1, 2 and 3 may be defined independently to create a base solid with two coatings having different material properties. The finite element mesh sizes in the central region (#4) may be different from those in the edge regions (#5, #6, #7 and #8) for improved computational accuracy near the edge of contact zone where the pressure gradients are generally high. The relative size of region near the edges, shown in figure 4-1, was determined by substantial trial and error with steep pressure gradients representative on elliptical surface loading, as found in common contact problems.

The next step in the modeling process is to create a mesh. Before starting this process, however, it may be necessary to edit the materials in the ARIES database, to make sure that the

desired materials are available. For the present example three materials are added to the database, e.g., "SoftCoat," "HardCoat" and "Substrate," which respectively correspond to a soft solid lubricant coating over a ceramic coating, which is bonded over a steel substrate.

For the two-dimensional plane strain problem it is only necessary to mesh the end face of the solid. Due to the simple rectangular areas in the solid face, shown in figure 4-1, each rectangular area can be interactively meshed by using a rectangular element and by prescribing the number of nodes on a given edge. This is done by using the "mapped mesh" technique in the "FEM" application in the ARIES interface. The process may be started by meshing the region A, in the top coatings, as shown below in figure 4-2, where the solid is displayed at an enlarged scale for

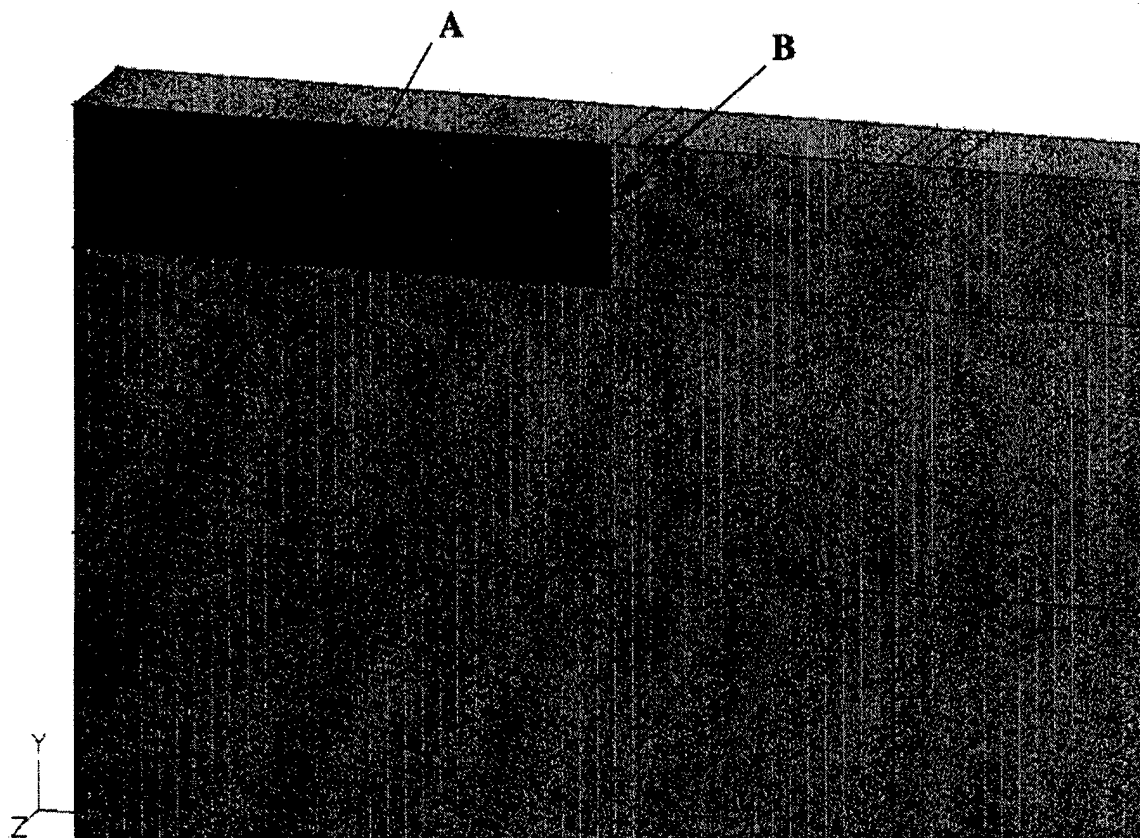


Figure 4-2
Start of the mapped meshing procedure for the two-dimensional plane-strain problem.

clarity. The interactive commands in the "Finite Element" application which produce the mesh shown in figure 4-2 consists of the following:

Aries
FEM
edit
femodel

model1

*** click Aries button for main menu
*** select FEM application
*** click edit button
*** specify name as "model1" next to femodel button

at_axis		*** click at_axis as model reference coordinate system
analysis_code	msc_nastran	*** select msc_nastran as the analysis code
analysis_type	linear_static	*** analysis type is linear static
plane_strain		*** select the plane strain type
element_set	set1	*** name element set as "set1"
quadrilateral		*** specify a quadrilateral element type
;;;		*** keep clicking the right mouse to remove menus
generate		*** click mesh generation menu button
mapped_mesh		*** select mapped mesh
override	yes	*** set material override to yes
material	SoftCoat	*** select material "SoftCoat" from data base
pick	face	*** click pick, then face button
		*** then click on the region to be meshed
;		*** done or right mouse to accept highlighted region
edge_nodes		*** click edge nodes button to specify edge nodes
num_elem	4	*** specify number of elements as 4
pick	edge	*** click pick, then edge button
		*** then click on an edge along depth of region
;		*** right mouse to accept and generate nodes
num_elem	10	*** number of elements along the surface
pick	edge	*** click pick, then edge button
		*** then click an edge along the surface
;		*** right mouse to accept
;		*** right mouse again to get out of the menu
mesh		*** click mesh to generate mesh
;;;		*** right mouse clicks to accept and out of the menu

The process can now be repeated to mesh the remaining areas, one at a time. Note that for subsequent regions in the top coating, it is only necessary to prescribe nodes on the top edges, also the initial steps to specify analysis type and model name, may not be necessary in meshing the remaining area in the top coating. For example, after completing mesh A, the mesh in the adjacent region B, is created by the following commands:

generate		*** click mesh generation menu button
mapped_mesh		*** select mapped mesh
override	yes	*** set material override to yes
material	SoftCoat	*** select material "SoftCoat" from data base
pick	face	*** click pick, then face button
		*** then click on the region to be meshed
;		*** done or right mouse to accept highlighted region
edge_nodes		*** click edge nodes button to specify edge nodes
num_elem	4	*** number of elements along the surface
pick	edge	*** click pick, then edge button
		*** then click an edge along the surface
;		*** right mouse to accept
;		*** right mouse again to get out of the menu

mesh
;;;

*** click mesh to generate mesh
*** right mouse clicks to accept and out of the menu

This will mesh the region B as shown in figure 4-3 below. The process is repeated to mesh the remaining regions in the top coating.

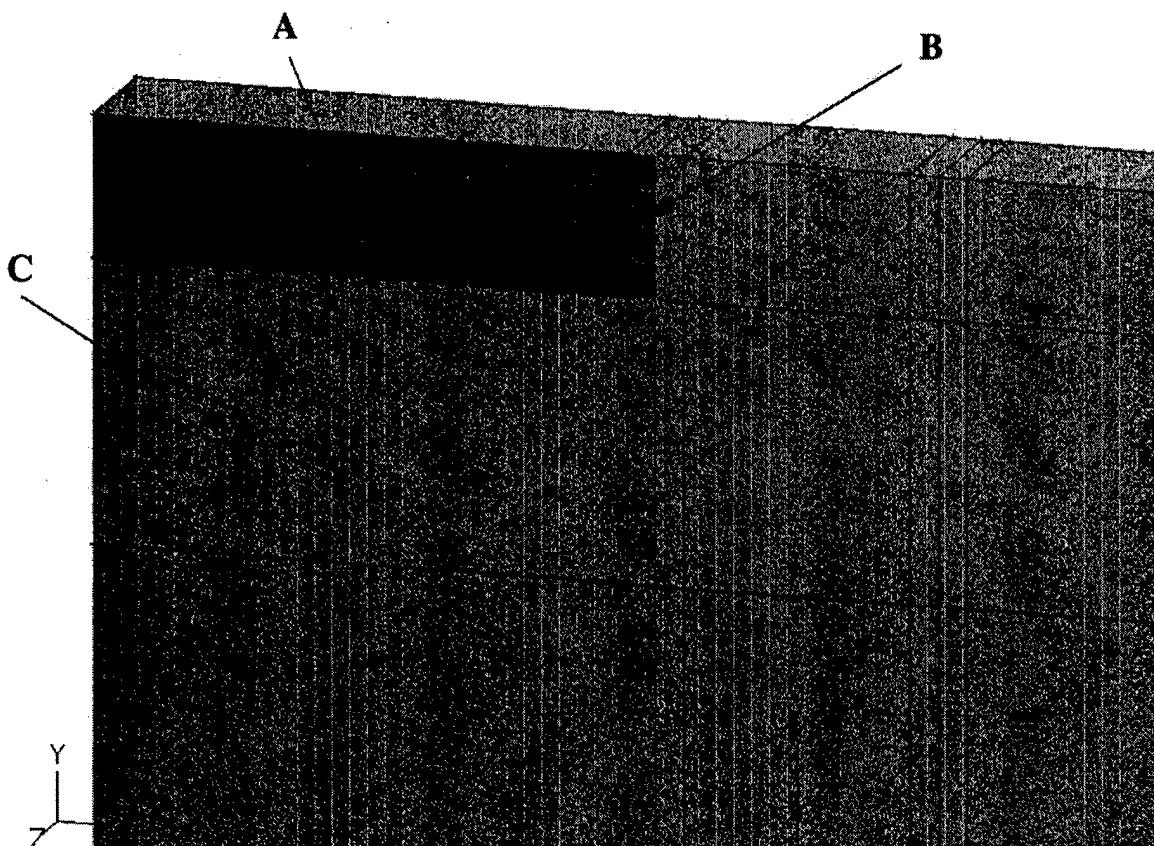


Figure 4-3
Meshing a region adjacent to an already meshed region.

Once the top coating is meshed, meshing the remaining area becomes even simpler. For example, meshing the edge region C (see figure 4-3) in the second coating simply requires specification of element set name, the material of coating, and nodes on the edge along depth of the coating. Once this region is meshed, the remaining areas in the second coat require no specification of nodes, because all nodes are defined by adjacent elements. After completing the mesh in the second coating, this procedure is also used to mesh the substrate. The completely meshed solid is shown in figure 4-4.

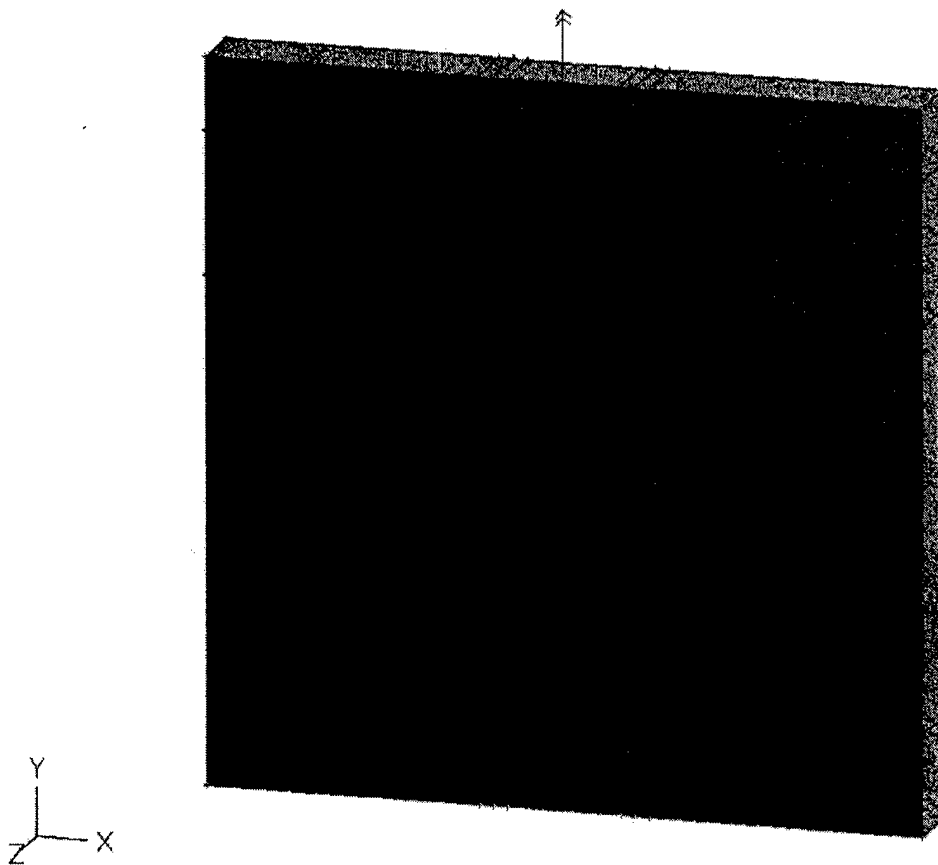


Figure 4-4

Fully meshed solid for modeling the two-dimensional plane-strain problem.

The next step in the finite element modeling process is to prescribe the applied loads and restraints. The ARIES "Environment" application is used to prescribe both, the restraints and the applied loads. For the two-dimensional plane-strain problem, the applicable restraints simply consist of imposing translational restraints on the base, or the bottom edge of the solid. With ARIES running and the solid already displayed in the main window, this can be easily accomplished by the following commands:

```
Aries
Environment
edit
restraint_case
fixed_base
;;;
add
translational_restraint
```

```
click this button to get the main menu
select the "Environment" application
click the edit button
click restraint_case button to specify name
name the restraint case as "fixed_base"
several clicks on right mouse button to close all menus
select add button to add restraints
select translational restraint option
```

pick	edge	turn on pick edge option and select all button edges of the solid
;		right mouse to accept
components_1	z	turn off z-component
;		accept zero value for components x and y
:::		accept and close all menus by clicking right button

After closing all menus, the restraint symbols will appear on the button edge, confirming that the prescribed restraints have been applied.

An elliptical pressure distribution on the top surface is considered as the applied loading. This requires the use of ARIES point processor, to apply the elliptical distribution of pressure in a piece-wise linear fashion. A macro "ell_pres" (see Appendix A) is written to prescribe the pressure points for a given contact half width and maximum pressure. With the ARIES "Environment" application still running, the following commands are used to prescribe the surface loading:

edit		click edit button
load_case		select load case option
normal		name the load case as "normal"
pick	edge	pick the edges corresponding to central and the two edge zones within the contact (top edges of zone 4,5 & 6 shown in figure 4-1)
;		right mouse to accept the selected edges
component_1	x	turn off x component
component_1	z	turn off z component
;		
VALUE		option for defining pressure values along the y axis
input_variable		independent input variable is the x coordinate value
x		
;		accept above options
interpolation		turn on interpolation option
piecewise_linear		select the piecewise linear option
ell_pres		execute the macro ell_pres macro to enter all values of pressure and the position along the x axis.
:::		a few clicks on the right mouse to accept and close menus

The macro will interactively request the contact half width and the value of maximum pressure at the center of contact. The value of half width is 0.001 m (this is set in the macro solid2d) and the central pressure is set to 1.0 GPa in the present example. Since all the stress solutions are scaled relative to the central pressure, the solutions may be appropriately scaled for any other value of central pressure.

The applied pressure and restraints as applied by the above procedure are shown in figure 4-5 below.

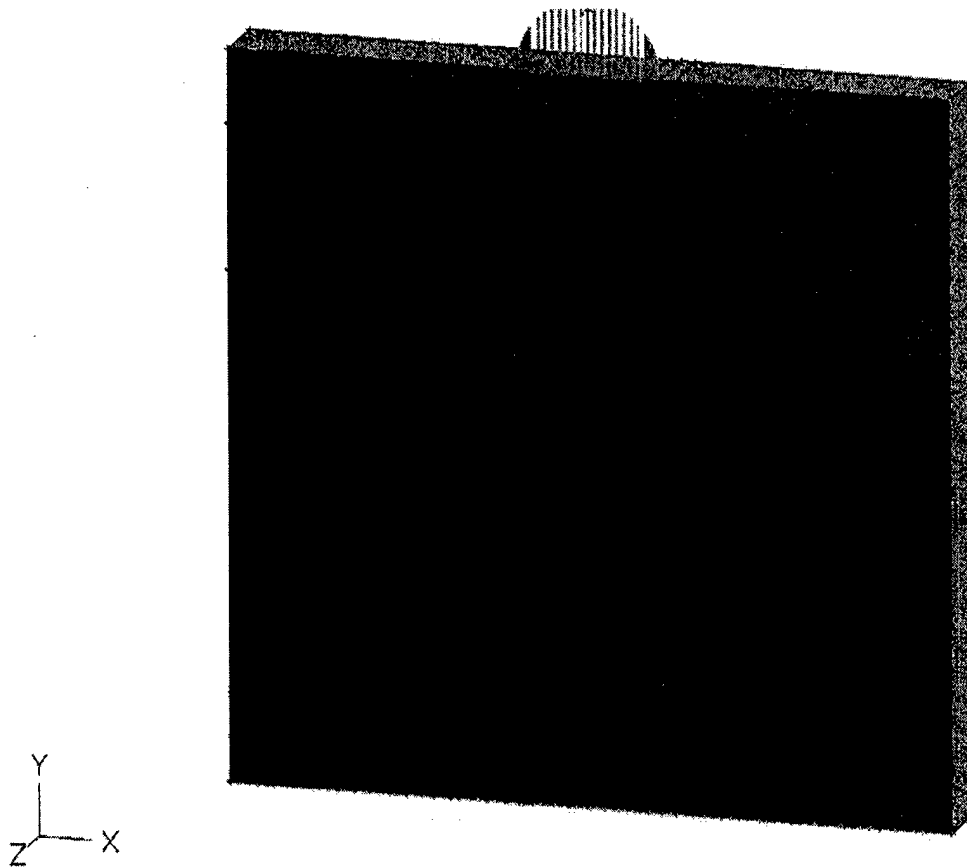


Figure 4-5
Applied elliptical pressure and translational restraints for the plane-strain problem.

The model is now ready for finite element analysis, which can be started by clicking the "Analyze" button under the "FEM" application in the ARIES interface. Since the loads and restraints are prescribed on the edges, the automatic nodal loads and restraints option must be turned on in the analyze menu; this will permit computation of the nodal loads and restraints before starting the analysis.

Once the analysis is complete, the "Results" application in the ARIES system is used to view the results. Virtually all stress, strain and displacement components can be displayed by the "Results" application. Figures 4-7, 4-8 and 4-9 respectively, show the von-Mises stress, the global shear stress, and the maximum shear stress distribution in the solid. These are the most common components which are used to assess failure in the coatings as a function of applied loads. Note that all solutions are for a 1.0 GPA maximum stress at the surface. For other stress values, these solutions may be appropriately scaled.

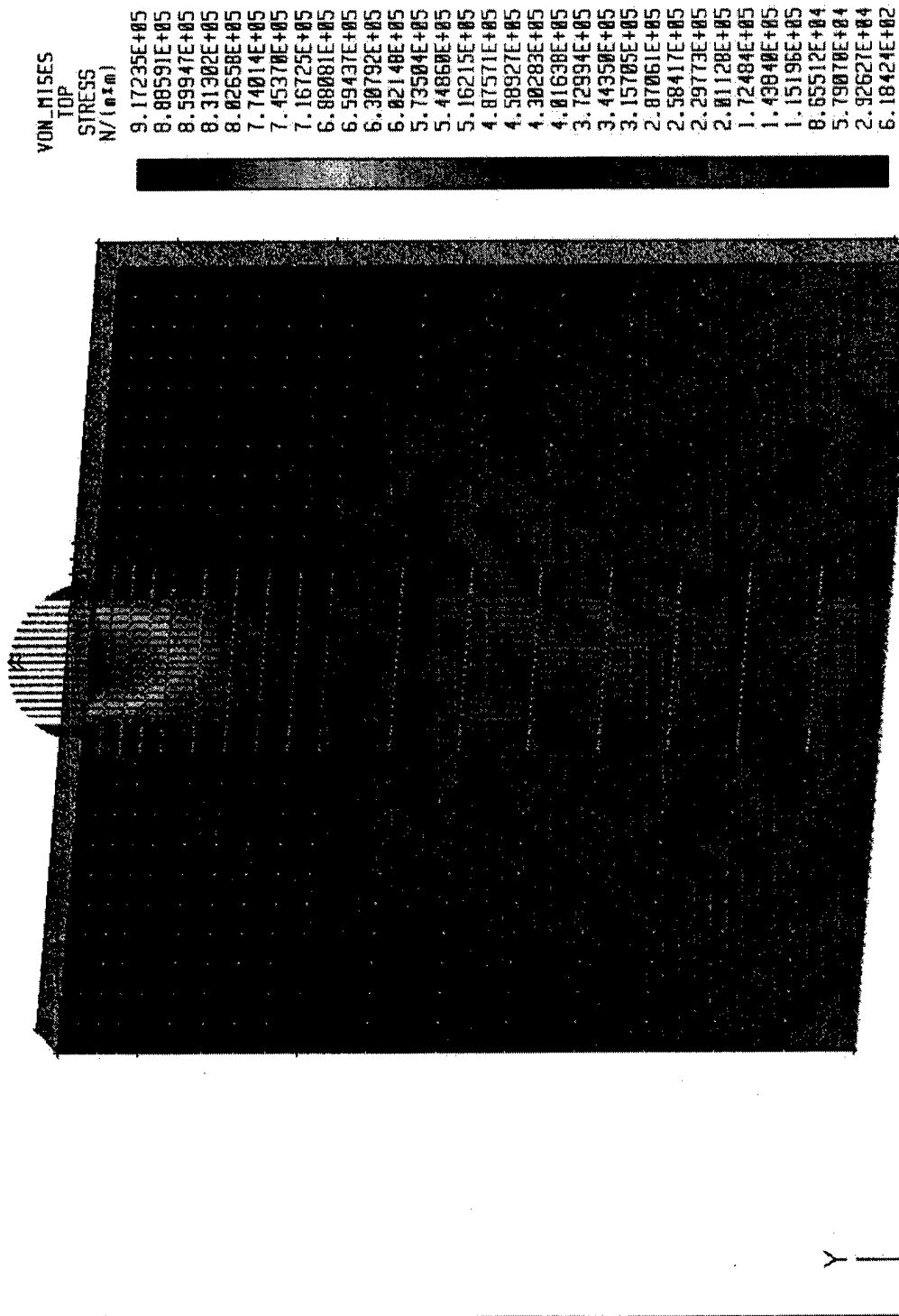


Figure 4-6
von-Mises stress distribution for the plane-strain problem.

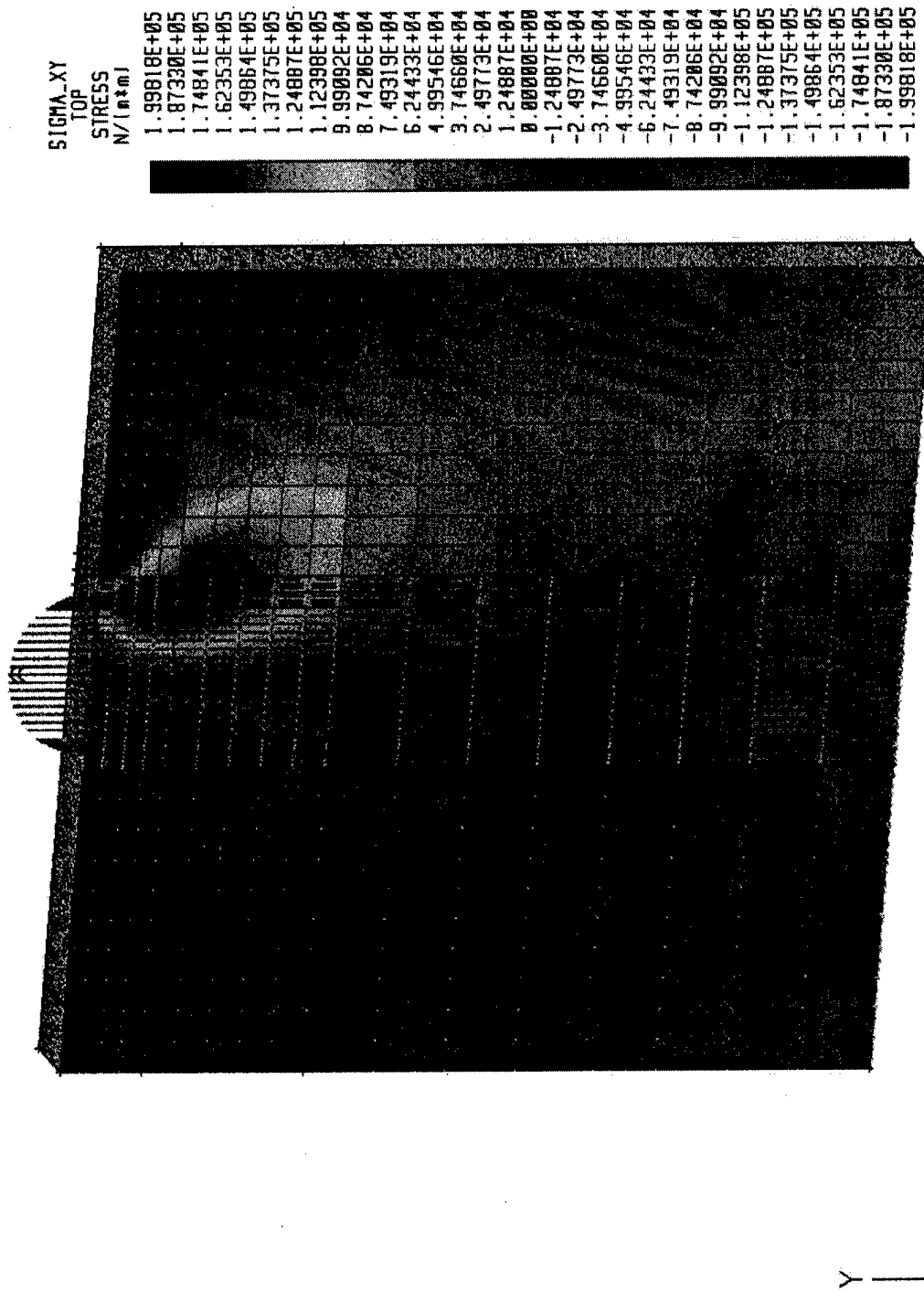


Figure 4-7
Orthogonal shear stress distribution for the plane-strain problem.

SIGMA_XY
TOP
STRESS
N/(mm²)

1.99818E+05
1.87330E+05
1.74841E+05
1.62353E+05
1.49864E+05
1.37375E+05
1.24887E+05
1.12398E+05
9.99092E+04
8.74206E+04
7.49319E+04
6.24433E+04
4.99546E+04
3.74660E+04
2.49773E+04
1.24887E+04
0.00000E+00
-1.24887E+04
-2.49773E+04
-3.74660E+04
-4.99546E+04
-6.24433E+04
-7.49319E+04
-8.74206E+04
-9.99092E+04
-1.12398E+05
-1.24887E+05
-1.37375E+05
-1.49864E+05
-1.62353E+05
-1.74841E+05
-1.87330E+05
-1.99818E+05

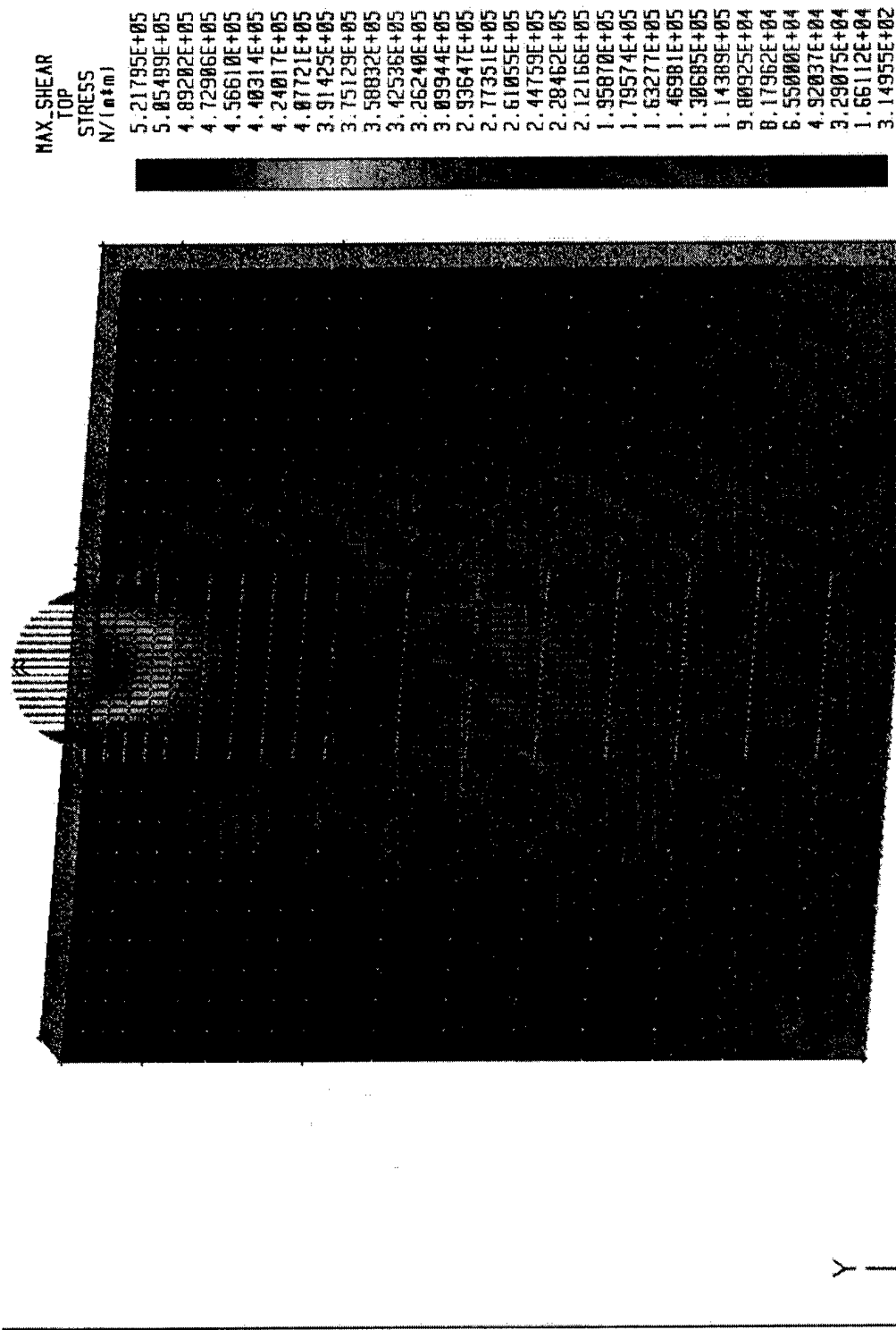


Figure 4-8

Distribution of maximum shear stress for the plane-strain problem.

4.2 Generalized Three-Dimensional Problem

The common three-dimensional contact problem consists of a solid with surface loading over an elliptical area. Although the modeling approach for such a problem is quite similar to that discussed above for the simplified two-dimensional plan-strain problem, all the steps are substantially more complex. In particular, meshing of the elliptical contact area, determining the mesh size near, and along, the contact edge for modeling of high pressure gradient with acceptable accuracy, and applying the surface loading in a piecewise linear fashion. After a number trial runs, and significant experimentation with different mesh configuration, it was found that it is perhaps, best to divide the elliptical contact zone into several concentric elliptical regions, and prescribe a constant pressure, of varying magnitude, over each of these regions, to simulate an ellipsoidal pressure distribution. With such established guideline a macro, solid3d, as listed in Appendix A, was written to generate the regioned three-dimensional solid shown below in figure 4-9.

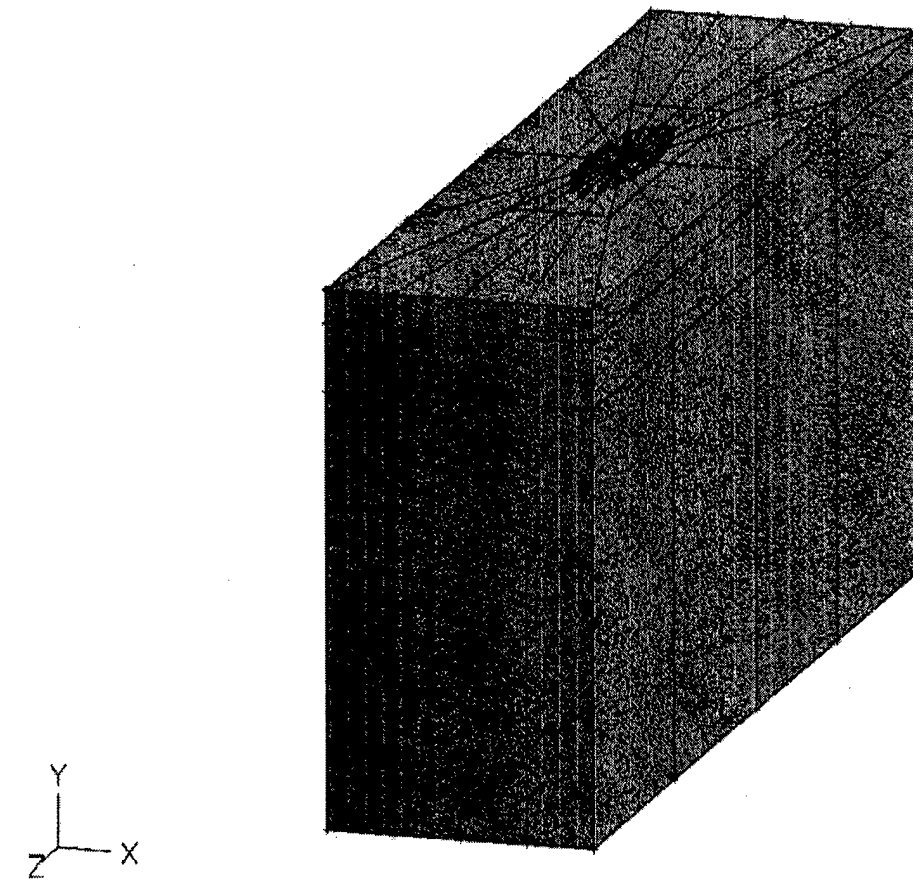


Figure 4-9
Regioned solid for modeling the three-dimensional stress problem.

Each of the regions in the solid may be meshed individually with brick elements for acceptable accuracy in the finite element analysis. A somewhat enlarged view of the solid is

shown in figure 4-10, where the regions in the outer annulus around the contact are numbered from 1 to 16. A meshing sequence for these regions will be discussed later.

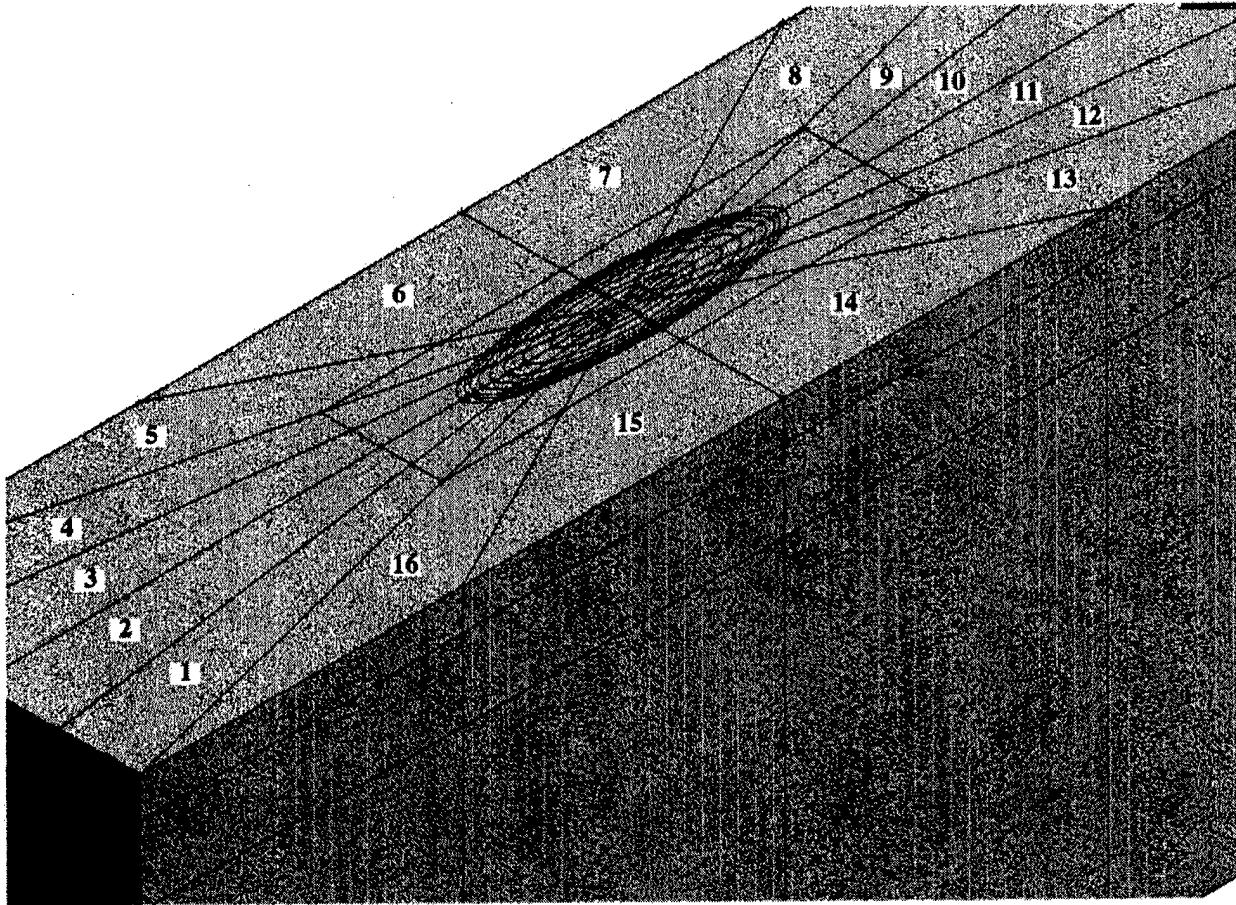


Figure 4-10
An enlarged view of the three-dimensional solid.

Similar to this outer annulus, there is an inner annulus bounded by the a rectangle and the outer elliptical edge of the contact region. There are also sixteen regions in this area. The zone formed by the concentric ellipses will also have the sixteen regions, until we reach the center of contact, which is defined by a rectangular region. The greatly enlarged view of contact shown in figure 4-11 shows these regions more clearly. The labels 1 to 16 in this inner region will be referred to later when discussing the meshing procedure. In general, each one of the regions seen in figures 4-10 and 4-11 may be independently meshed to create virtually any mesh size variation over the solid. However, the regions in the contact area, as seen in figure 4-11, are such that only one element per region is adequate to model the contact stress problem. Thus, in most cases, no more than one mesh point will be necessary in these regions.

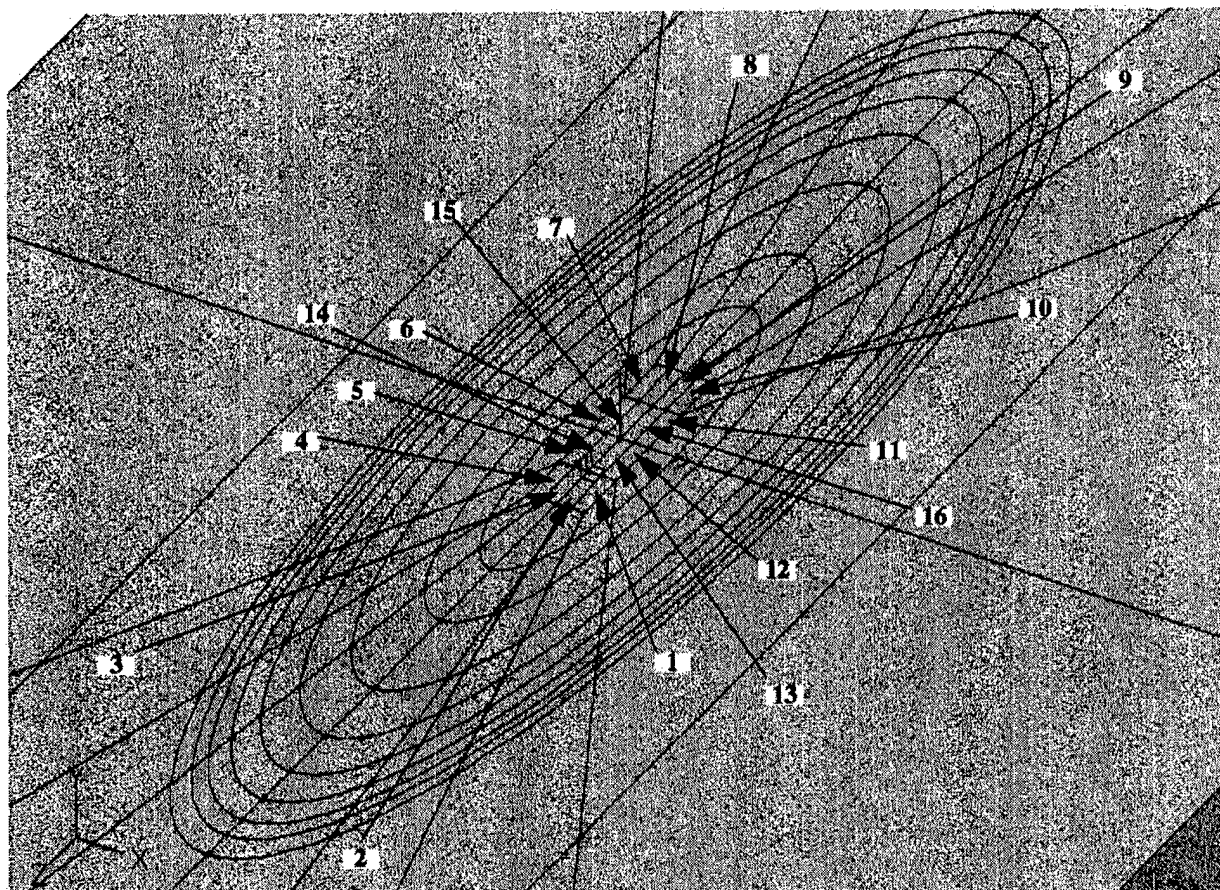


Figure 4-11
Regioning details of the elliptical contact area.

Since there are a large number of regions in the three-dimensional solid, a number of macros have been developed to mesh the solid. The process is started by first manually meshing region 1 of figure 4-10. This is done by following a procedure similar to that listed earlier for the two dimensional solid. However, since the geometry is substantially more complex, it is essential to display the solid at an enlarged scale so that each region is visible, and pickable by the pick processor without any ambiguity. The pick processor normally works with screen coordinates and size of the trap box. The viewport-zoom options are used to magnify the image. Also, a diametric or an isometric view is often more friendly to the pick processor. Now, assuming that the image is on the screen with appropriate magnification, the following steps will mesh the desired region 1 of figure 4-10:

Aries		get to the main ARIES menu
FEM		select FEM application
edit		go to edit menu
femodel	fem3d	name the femodel as "fem3d"
element_set	elset1	name the element set as "elset1"
brick		select brick element type
type	HEXA	with six degrees of freedom
;;;;		accept and remove all menus
generate		get the mesh generation menu
mapped_mesh		select the mapped mesh option
override	yes	click the material override button
material	SoftCoat	select "SoftCoat" as material of top coating
pick	region	get to pick processor to select a region
;		click on region 1 (as seen in fig 10) then right mouse to accept
edge_nodes		click the edge_nodes option
numb_elem	4	set number of edge nodes to 4
pick	edge	turn of pick processor for edges
;		click on the edge along depth of top coating and then right mouse to accept
num_elem	5	set the number of edge nodes to t
pick	edge	turn on the pick-edge processor
;		click on the edge along the radial direction (towards center of contact) and then right mouse to accept
numb_elem	1	set number of edge nodes to 1
pick	edge	turn on the pick-edge processor again
;		now pick the edge along the circumferential direction, i.e. the third orthogonal direction, and then right mouse to accept
;		right mouse to accept all nodes
mesh		click mesh to mesh the region
;		accept the mesh when completed.

The resulting mesh is shown in figure 4-12. Meshing this first region sets the number of elements along depth of the top coating and along the radial direction. This prescribes certain constraints on meshing of the other regions in the top coat. In other words, the number of nodes may only vary along the circumferential direction in the remaining regions of the top coating. The number of edge nodes along the circumferential direction is set to 1 in the present example, and this is done for all regions in the top coating.

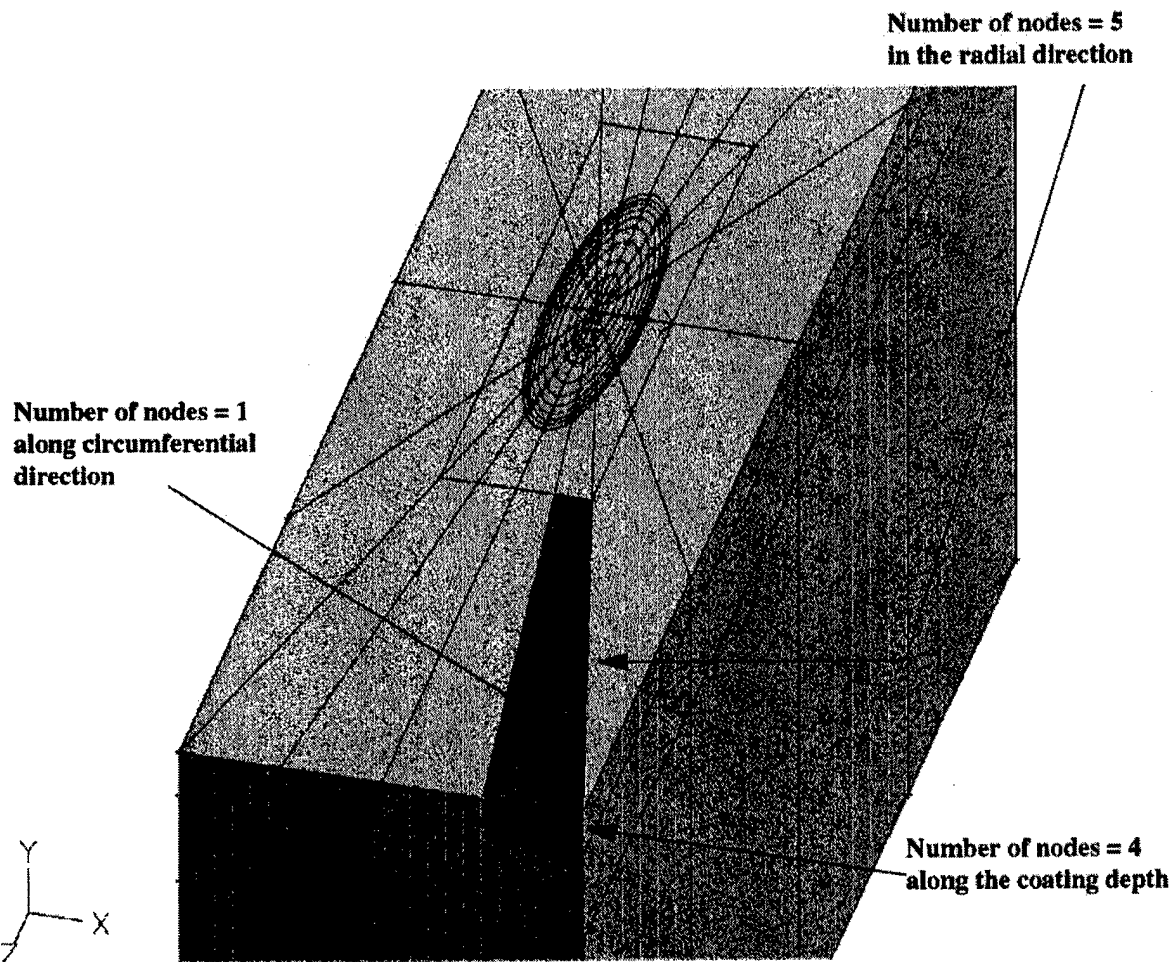


Figure 4-12
Start of the mesh process for the three-dimensional solid.

Once the first region is meshed and the number of nodes along the two orthogonal directions are established, the macro "mesh1" (as listed in Appendix A) may be executed to mesh the remainder of the outer annulus of the top coat. Several inputs, with regard to geometry of the solid and the number of nodes desired in the circumferential direction, are requested by the macro. The resulting mesh is shown in figure 4-13.

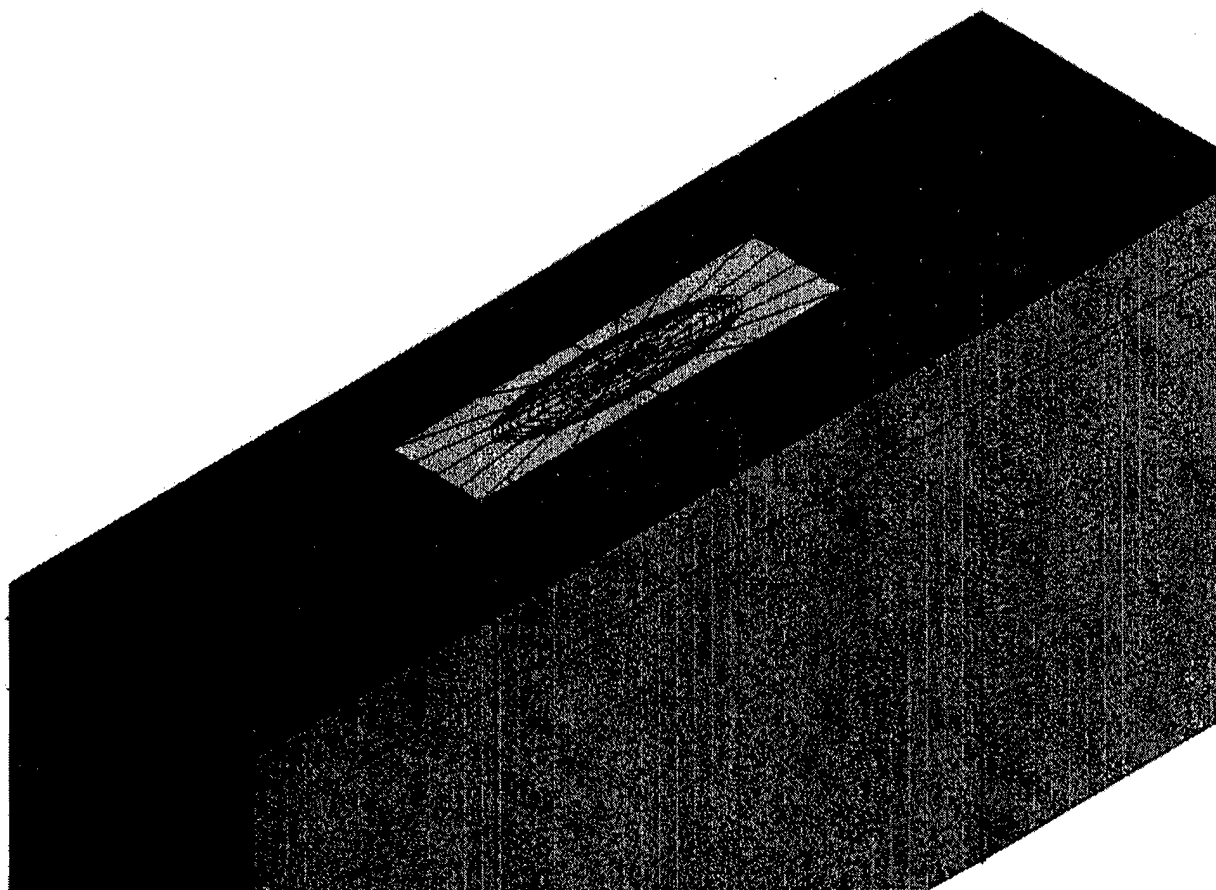


Figure 4-13
Meshed outer annulus of the top coating.

After completing the above mesh, the MODIFY-VISIBILITY-MESH option may be used to blank out the meshed regions, this will give better access to the unmeshed regions. Now the VIEWPORT-ZOOM option may be used to further increase magnification of the image. Meshing of the first region in the second annulus around the elliptical contact is also performed manually to specify the number of nodes along the radial direction. The procedure is identical to that listed above for the first region of the outer annulus. A view of the meshed first region in the second annulus around the contact is shown in figure 4-14. Note that the meshed regions of figure 4-13 are removed in figure 4-14.

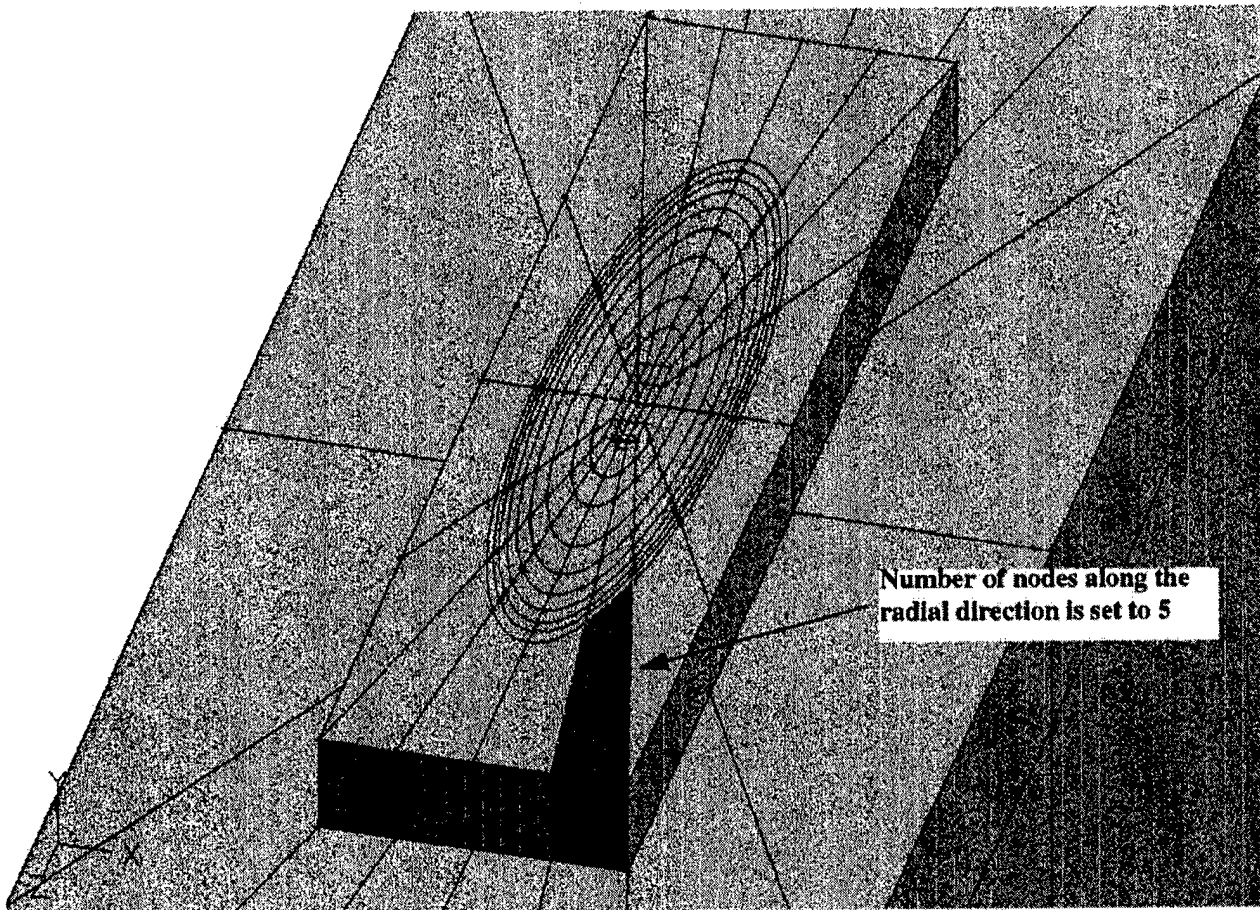


Figure 4-14
Meshed first region of the inner annulus around the contact.

Now, to mesh the remaining regions in this second annulus, no specification of nodes is required, since the number of nodes is already defined by the meshed generated thus far. The mesh is generated by executing macro "mesh2". Note, however, that the image must be displayed on the screen with an enlarged scale for the pick operation to work properly. In the event the pick operation fails, all the regions will not be meshed and a number of error messages may be generated. If this happens, the generated meshes may be deleted, the VIEWPORT-ZOOM option may be used to further increase the magnification to facilitate the pick operation, and then the macro may be executed again to perform the meshing operation.

After the annulus is meshed successfully the "MODIFY-VISIBILITY-MESH" option is used to remove the meshed region from the display and then the unmeshed region is further magnified. Now the first annulus in the elliptical contact region must be clearly visible. The first region in this annulus is again meshed manually so that the number of nodes along the radial direction may be prescribed. As discussed earlier, the concentric elliptical regions are generated such that only one node may be necessary in the present example. However, the option of increasing the number of nodes is always available. The meshed first element of the contact zone is shown in figure 4-15.

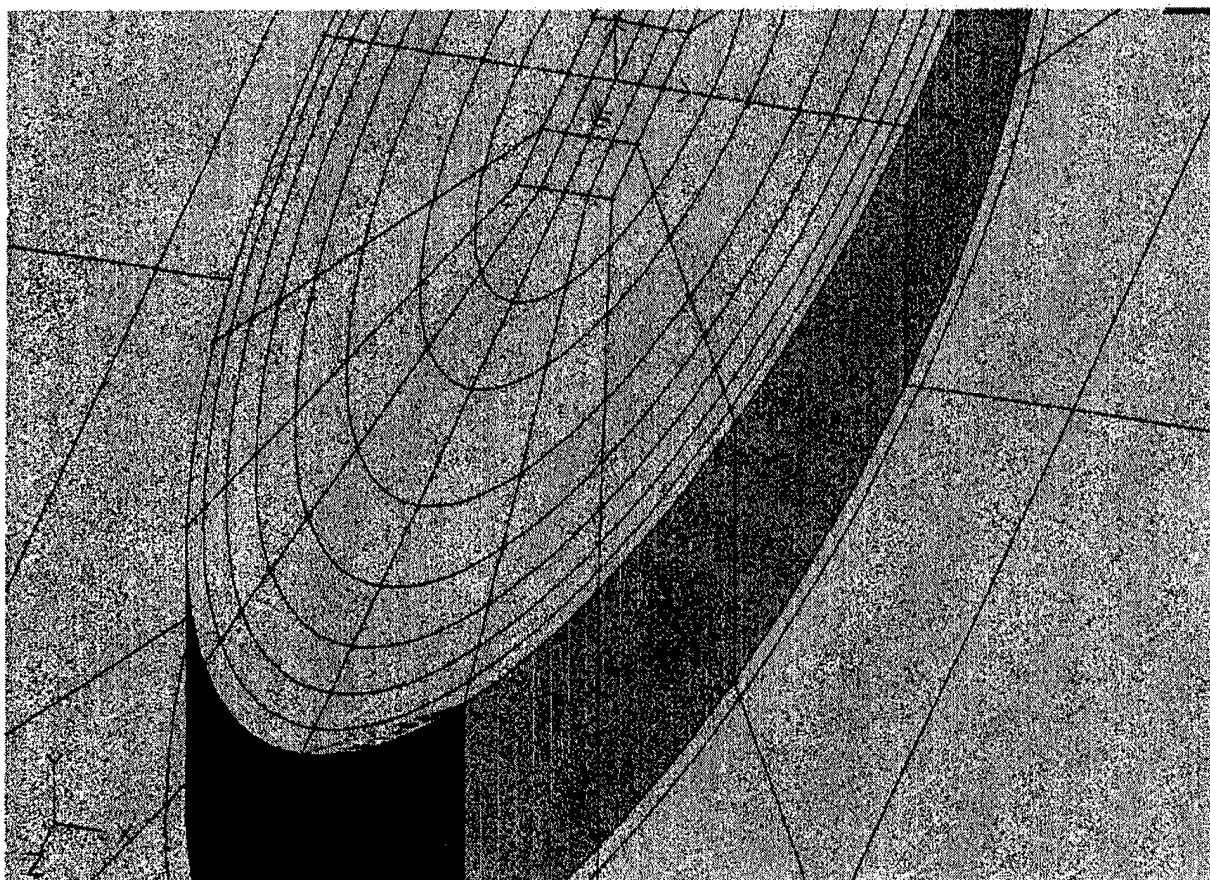


Figure 4-15
Meshed first region of the elliptical contact.

Now the macro "mesh2" may once again be used to mesh the remaining regions of the first elliptical annulus. The process is then repeated to mesh all the other concentric regions in the contact; one annulus at a time. The first region is meshed manually and then macro "mesh2" is used to mesh regions 2 to 16. Continued removal of the meshed regions and increase of magnification of the displayed image may be necessary for the macro to work properly.

The rectangular area in the center of contact will require no specification of number of nodes along any edge, since all definitions are complete by the meshes already generated. The procedure for meshing these regions is, therefore, more simplified. The regions 1 to 12 (see figure 4-11) are meshed by executing macro "mesh3" and the last four regions (13 to 16 in figure 4-11) are meshed by macro "mesh4". This completes meshing of the top coating.

All meshes in the top coat are removed from the screen, using the MODIFY-VISIBILITY-MESH option and the meshing process for the second coat is similarly carried out. The material for the second coat is set to "HardCoat" and the number of nodes along the depth of the coating is set to 4. No other specification is necessary. The macro "mesh2" is used to mesh all the regions, except the central rectangular regions, where macros "mesh3" and "mesh4" are used. The process is then repeated for the substrate. The completed mesh is shown in figure 4-16 and an enlarged view is shown in figure 4-17.

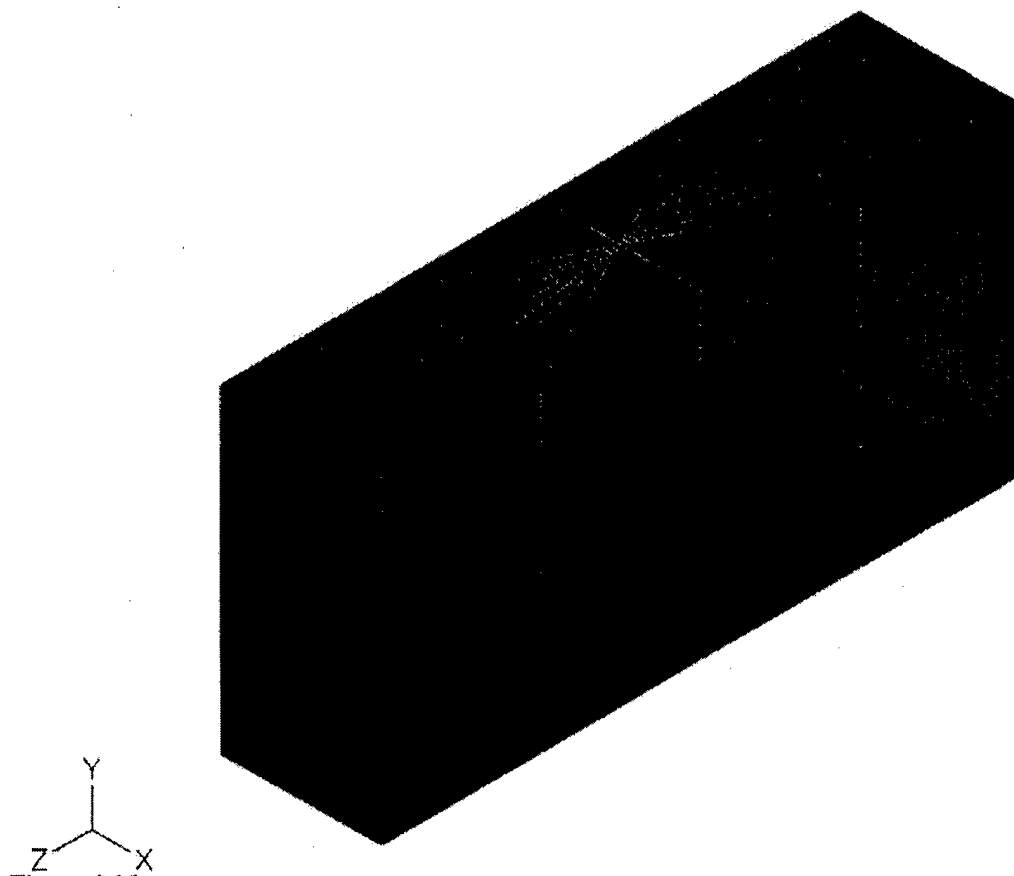


Figure 4-16
Fully meshed solid for the three-dimensional problem.

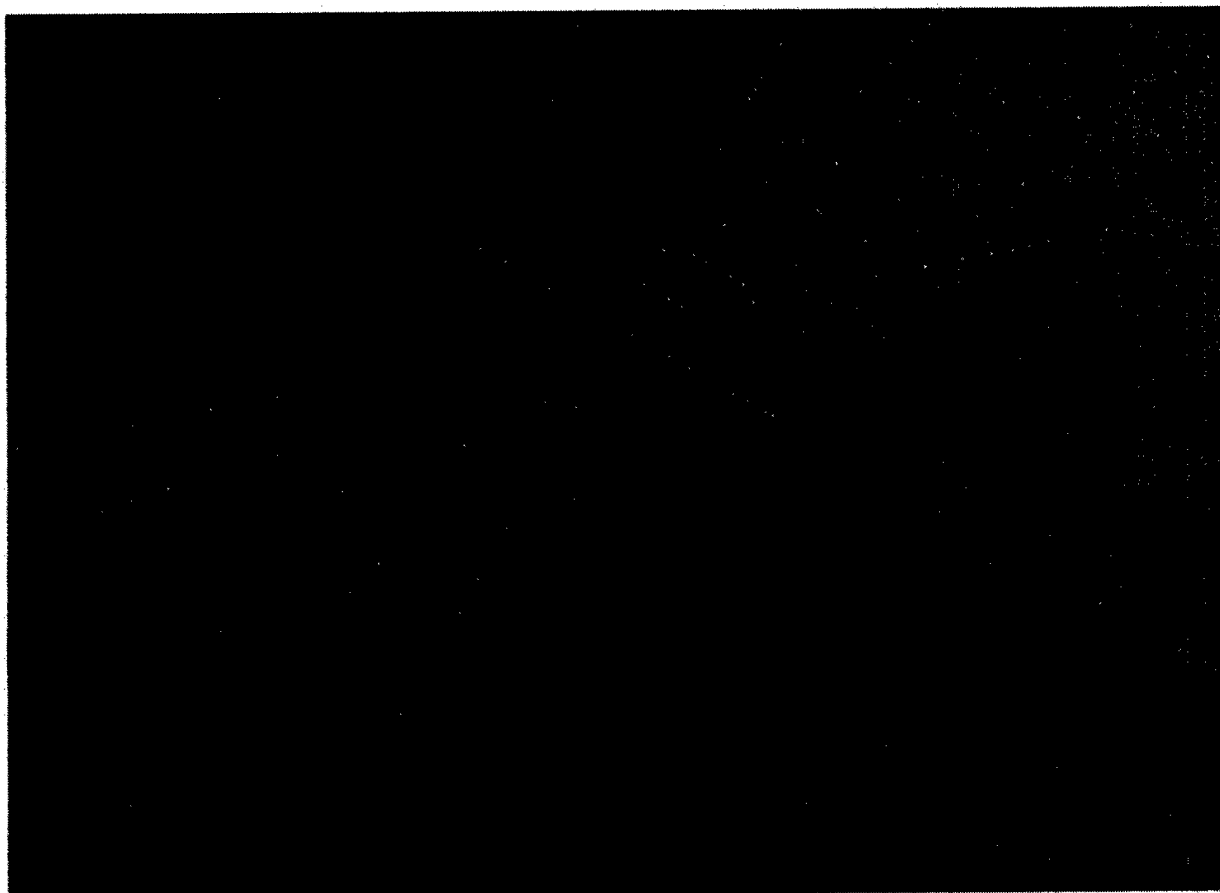


Figure 4-17
Enlarged view of finite element mesh in the elliptical contact region.

The next step in the modeling process is to prescribe the restraints and applied load. Similar to the two-dimensional problem, the restraints consist of a fixed base. In the three-dimensional problem, these are simply applied as translational and rotational restraints on the bottom surface of the solid. Thus, if the bottom view is displayed, then the face of each region selected, via the pick processor, and the constraints can be imposed using the "Environment" application in the ARIES interface. This procedure is identical to that discussed above for the two-dimensional problem.

Specification of surface loading for the three-dimensional problem is significantly more

complex. Since, ARIES does not offer a piecewise linear processor in two dimensions, it becomes essential to compute pressures on the face of every region. Such a requirement is the primary reason for partitioning the contact zone into concentric elliptical regions. For an ellipsoidal pressure profile, as defined by the equation,

$$p = \sqrt{1 - \left(\frac{x}{a}\right)^2 - \left(\frac{z}{b}\right)^2} \quad \text{Eqn (4-1)}$$

the pressure will be constant along these ellipses. In fact the normalized half widths of the concentric ellipses are selected for a certain value of normalized pressure. These values, along with the value of normalized pressure in the region are shown schematically in figure 4-18.

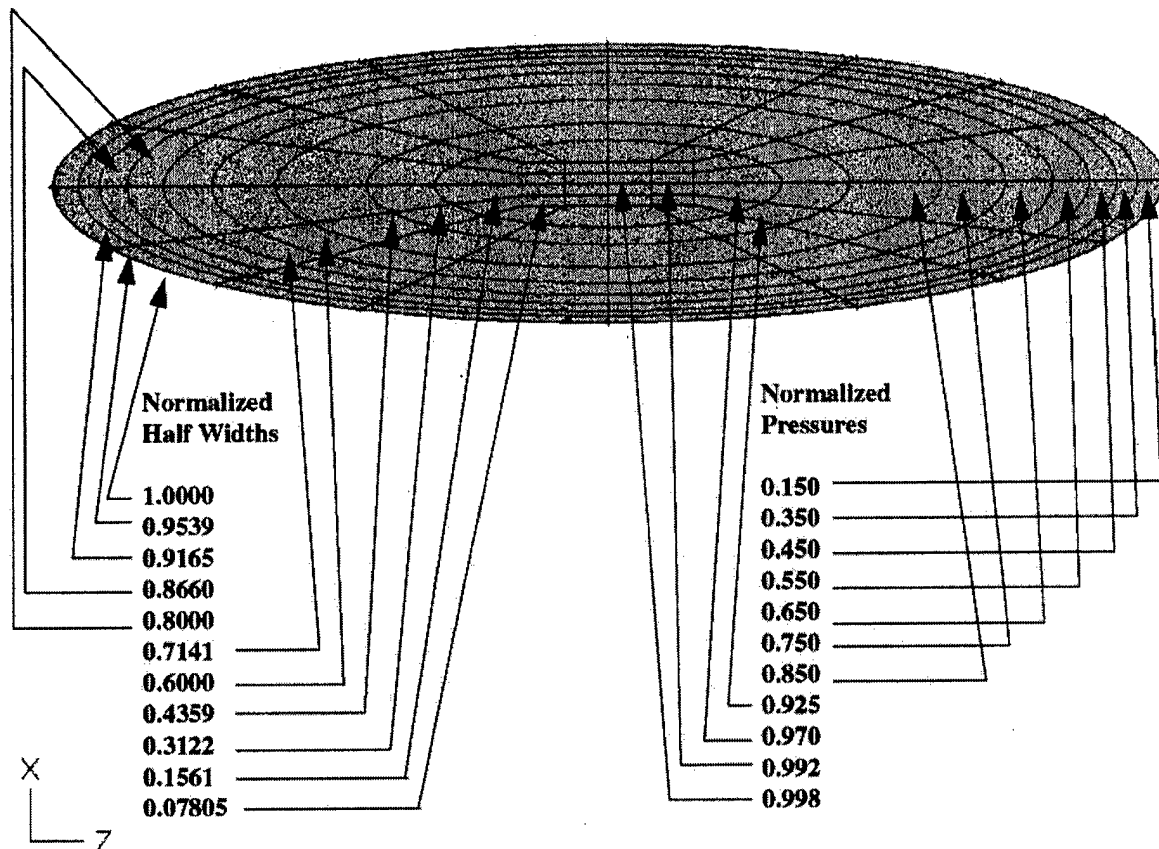


Figure 4-18
Normalized grid pattern in the elliptical contact zone.

With the regions defined with the above coordinates, specification of pressure in the contact zone is straightforward. With the ARIES "Environment" application running, the viewport commands may be used to display the top view of the solid at a reasonable magnification so that all elliptical profiles are clearly visible, as seen in figure 4-18. Then using the procedures similar to that discussed for the two-dimensional problem, a load set may be created to prescribe the var-

ious face pressures. The faces of region may be selected using the pick processor and the magnitude of pressure may be prescribed as listed in figure 4-18. Note that the values listed in the figure are average values using a piecewise linear variation of pressure. This will create a step-type pressure variation which will be close to the true ellipsoidal distribution. Such an applied load is shown below in figure 4-19a.

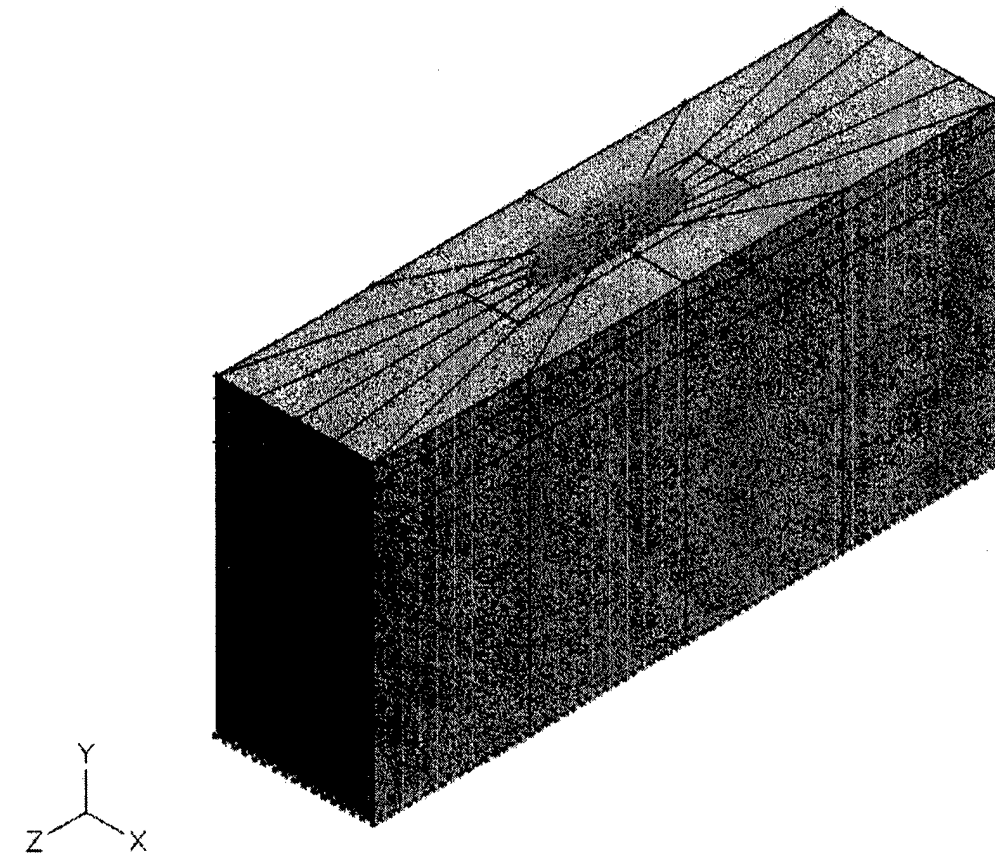


Figure 4-19a

Applied ellipsoidal load and fixed base restraints for the three-dimensional problem.

A section of the solid in the X-Y plane, along the minor axis of contact ellipse, is shown in figure 4-19b. The elliptical variation of the contact load is more clearly seen here; magnitude of the central pressure is 1.0 GPa.

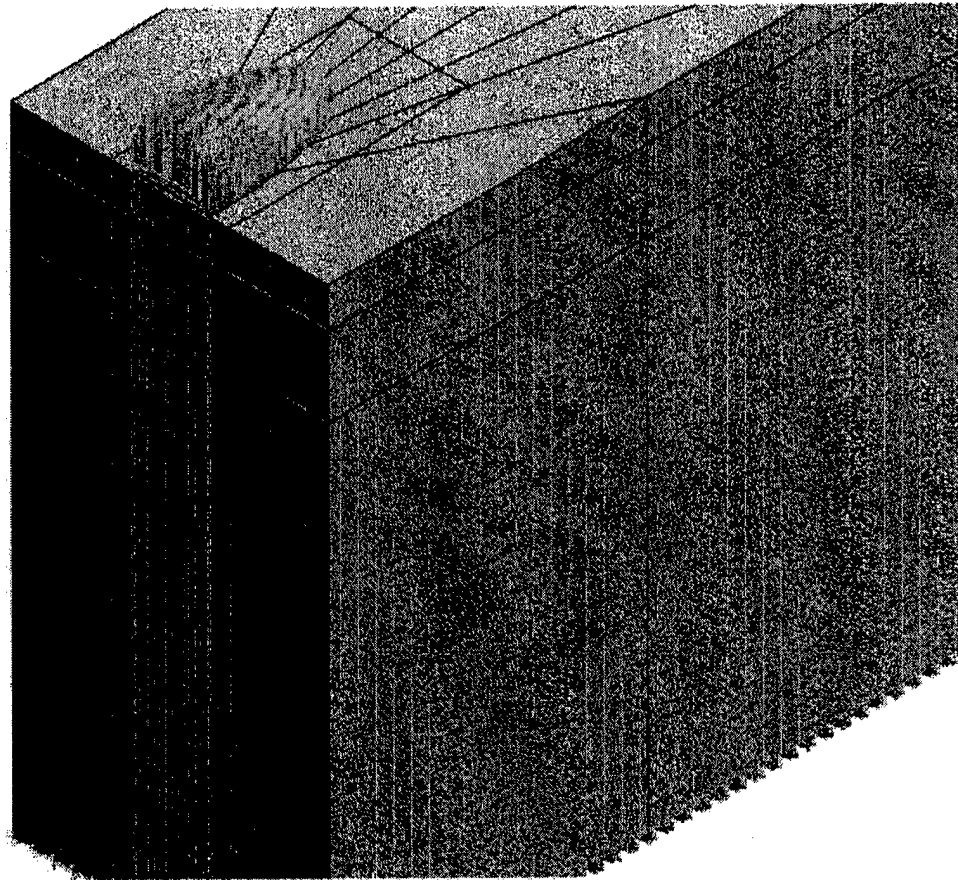
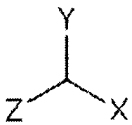


Figure 4-19b
Section of the three-dimensional solid along minor axis of the contact ellipse.

With the applied loads and restraints prescribed and the solid fully meshed, formulation of the problem is fully complete. Generation of loads and restraints at the nodal points is an automatic step in the analysis process. The analysis is again started by clicking the "Analyze" button under the "FEM" application in the ARIES interface. Once the analysis is complete, the results may be examined by running the "Results" application. Again, a number of displays and plots are available to examine the results to any desirable depth. The von-Mises stress distribution in the

solid along the minor and major axis on the contact ellipse is shown in the sectional view shown, respectively, in figures 4-20a and 4-20b along the X-Y and Y-Z planes.

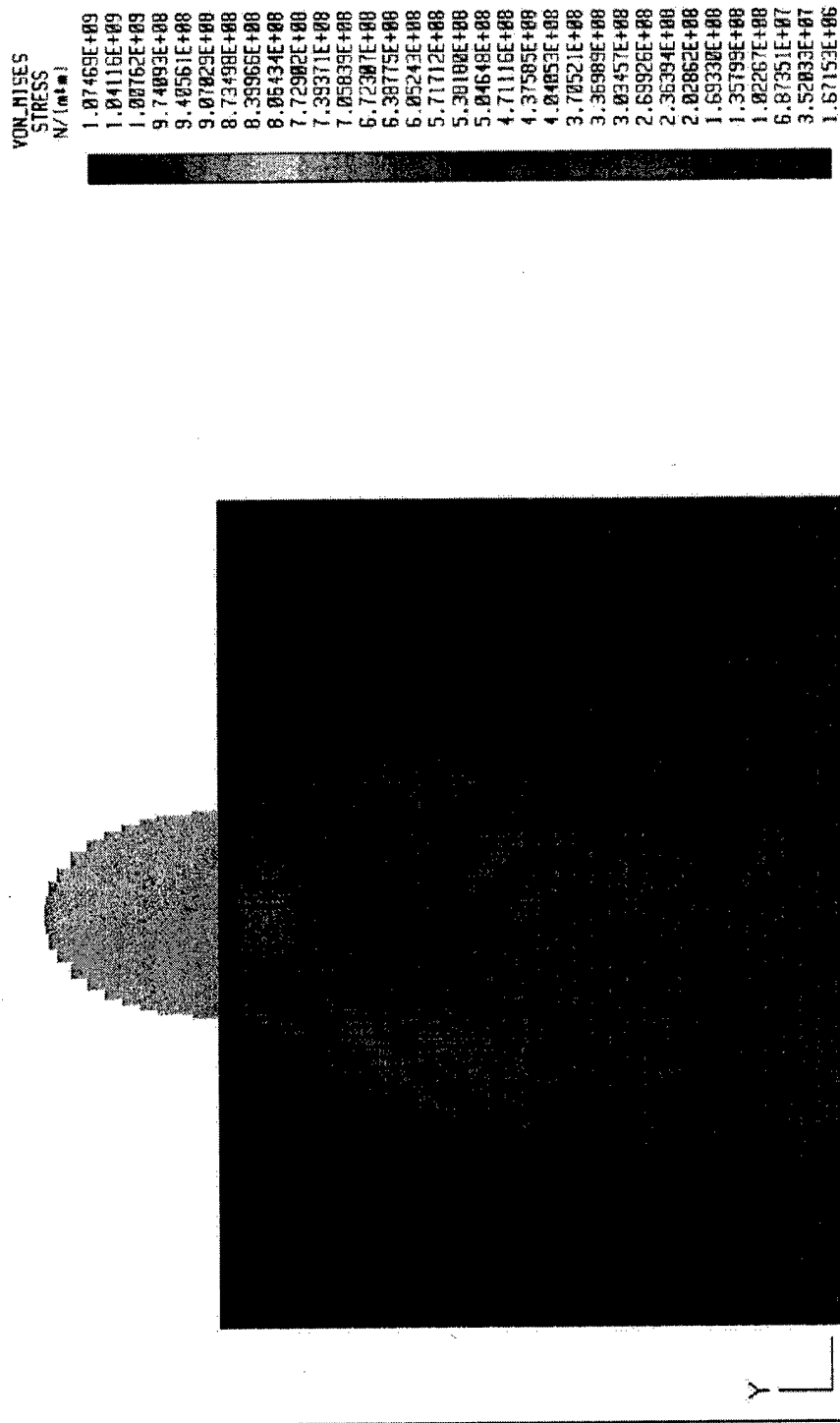


Figure 4-20a
von-Mises stress distribution in the three-dimensional solid, along the minor axis of contact ellipse.

VON_MISES
STRESS
N/(mm²)

1.07459E+09
1.04116E+09
1.00762E+09
9.74033E+08
9.40561E+08
9.07029E+08
8.73498E+08
8.39966E+08
8.06434E+08
7.72902E+08
7.39371E+08
7.05839E+08
6.72307E+08
6.38775E+08
6.05243E+08
5.71712E+08
5.38180E+08
5.04648E+08
4.71116E+08
4.37585E+08
4.04053E+08
3.70521E+08
3.36989E+08
3.03457E+08
2.69926E+08
2.36394E+08
2.02862E+08
1.69330E+08
1.35799E+08
1.02267E+08
6.87351E+07
3.52033E+07
1.67153E+06



Figure 4-20b
von-Mises stress distribution along major axis of the contact ellipse.

The global shear stress, τ_{xy} , along minor axis of the contact ellipse is shown in the sectional view in figure 4-21. The shear stress along the major axis is of course zero. Variation of the

maximum shear stress, as shown in figures 4-22a and 4-22b, is essentially identical to the von-Mises stress.

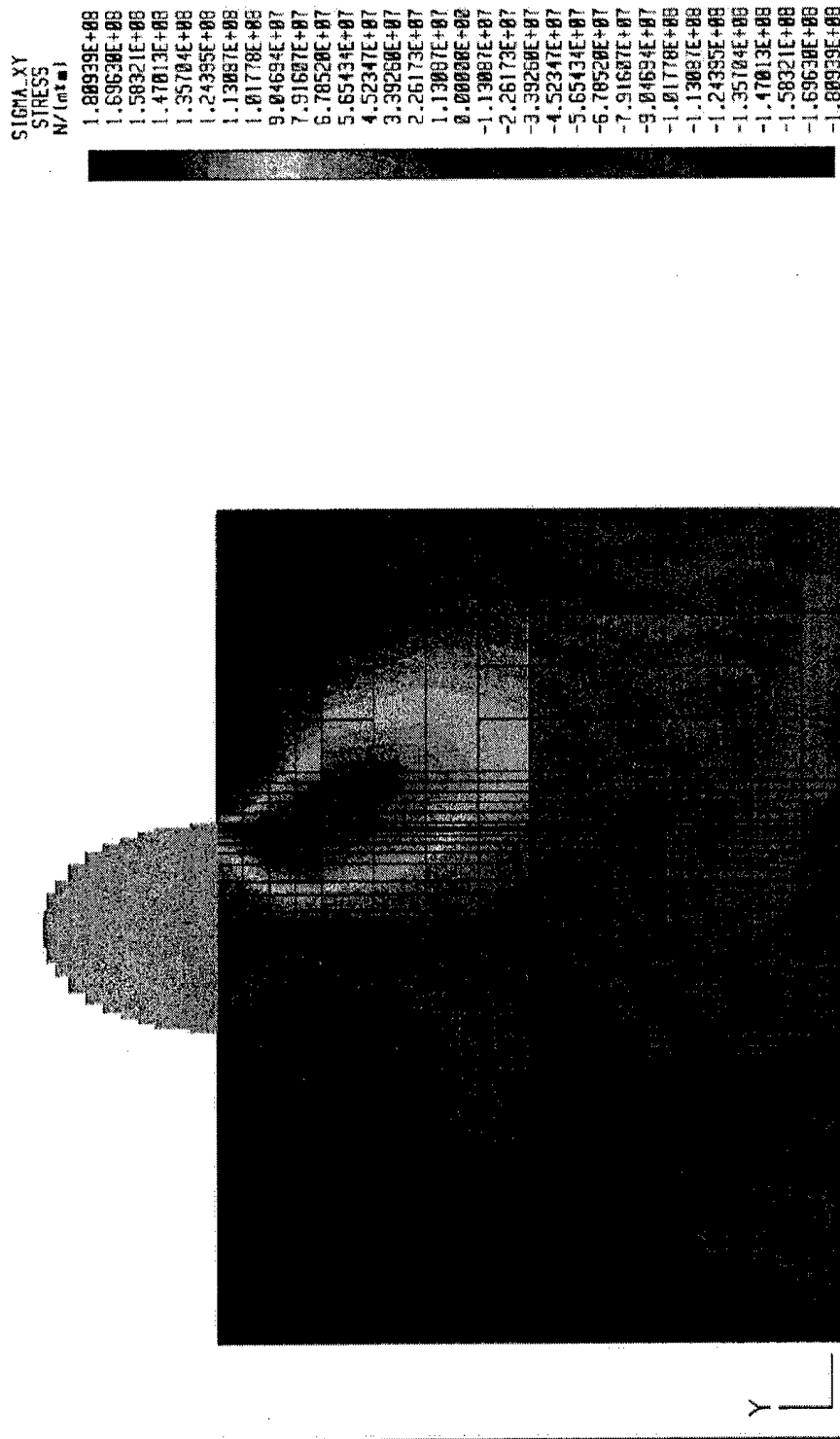


Figure 4-21
Global shear stress variation along minor axis of the contact ellipse.

MAX SHEAR
STRESS
N/(mm²)

6.14977E+08
5.95788E+08
5.76599E+08
5.57410E+08
5.38221E+08
5.19032E+08
4.99843E+08
4.80654E+08
4.61465E+08
4.42276E+08
4.23087E+08
4.03898E+08
3.84709E+08
3.65520E+08
3.46331E+08
3.27142E+08
3.07953E+08
2.88764E+08
2.69575E+08
2.50386E+08
2.31197E+08
2.12008E+08
1.92819E+08
1.73630E+08
1.54441E+08
1.35252E+08
1.16063E+08
9.68751E+07
7.6861E+07
5.68472E+07
3.68282E+07
1.68119E+07
9.30314E+05

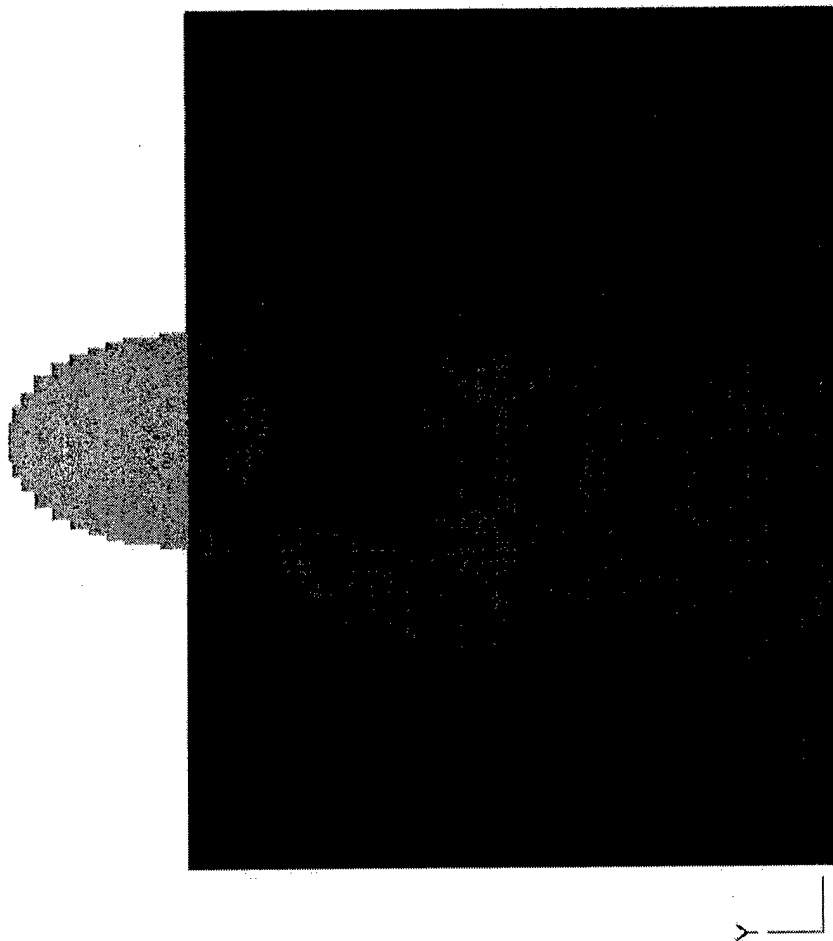


Figure 4-22a
Variation of maximum shear along minor axis of the contact ellipse.

MAX_SHEAR
STRESS
N/(m²·m)

6.14977E+08
5.95788E+08
5.76599E+08
5.57410E+08
5.38221E+08
5.19032E+08
4.99843E+08
4.80654E+08
4.61465E+08
4.42276E+08
4.23087E+08
4.03898E+08
3.84709E+08
3.65520E+08
3.46331E+08
3.27142E+08
3.07954E+08
2.88765E+08
2.69576E+08
2.50387E+08
2.31198E+08
2.12009E+08
1.92820E+08
1.73631E+08
1.54442E+08
1.35253E+08
1.16064E+08
9.68751E+07
7.6861E+07
5.68497E+07
3.68382E+07
2.01193E+07
9.30314E+05

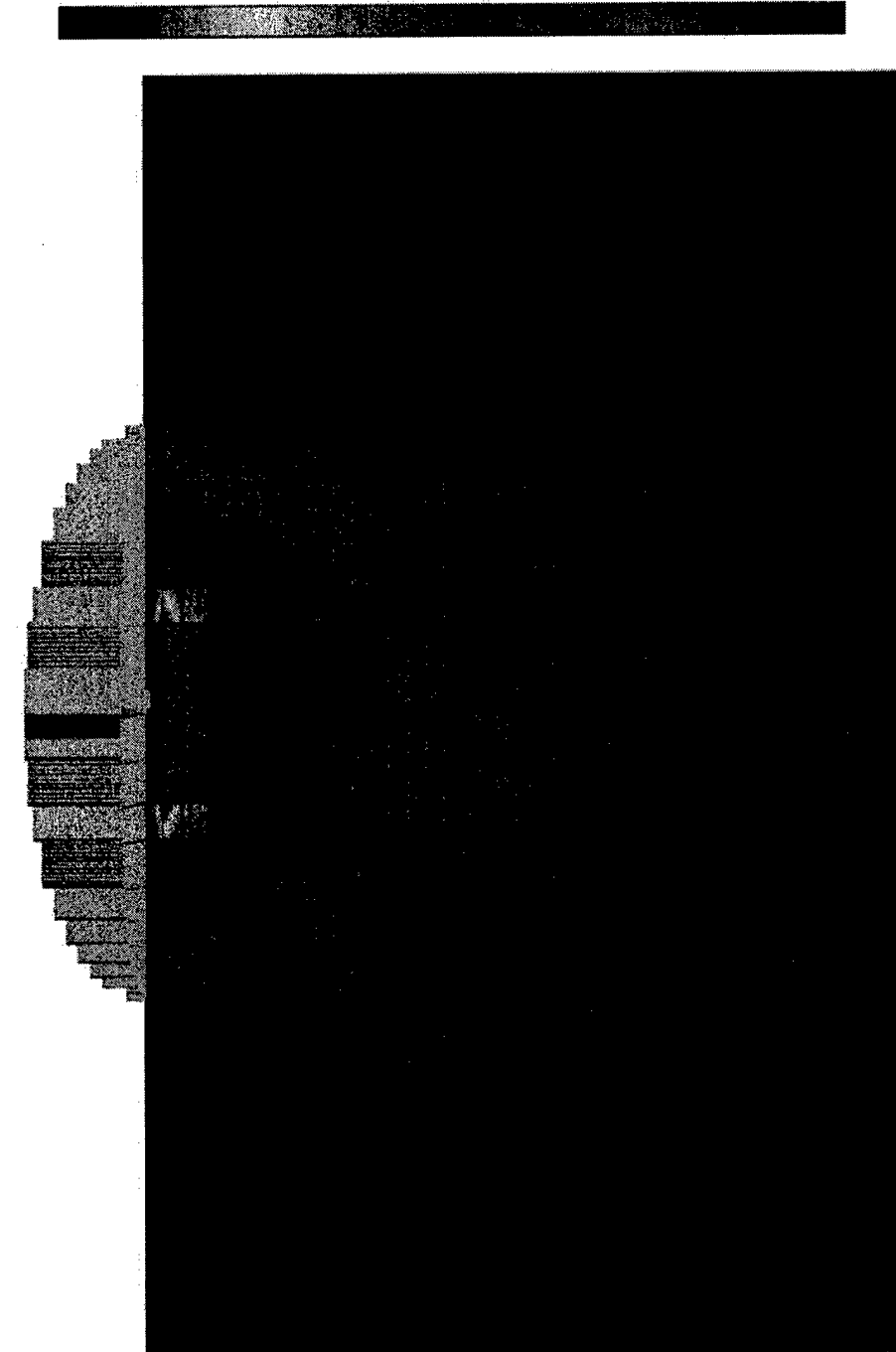


Figure 4-22b
Variation in maximum shear stress along major axis of the contact ellipse.

4.3 Thermal Modeling

When the concentrated contact is subjected to a sliding interaction, in addition to the shear stress, substantial heat may be generated in the contact. At any point in the contact if the sliding velocity is u and the friction or traction coefficient is κ , then the heat generated per unit area, q , may be written as

$$q = \kappa p u \quad \text{Eqn (4-2)}$$

where p is the contact pressure at the point in the contact region.

Thus, knowing the pressure and slip distributions in the contact, the heat flux over the contact can be readily computed. For simplicity, consider the three-dimensional contact problem modeled earlier and let the slip and traction coefficient over the contact be constant. Thus, the heat flux over an elliptical incremental area, as shown in figure 4-23, will be given by equation (4-2) where the pressure is computed by equation (4-1) described earlier.

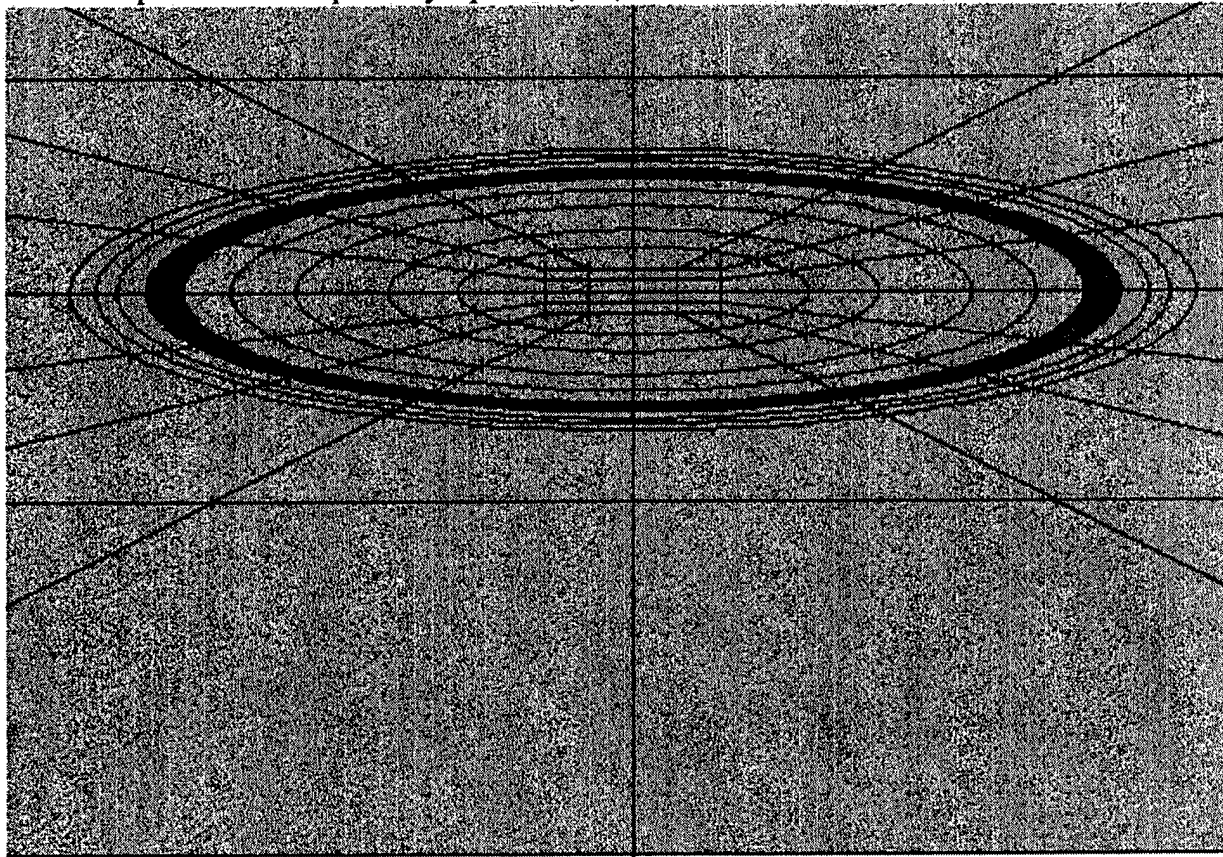


Figure 4-23. Surface grid pattern for defining the heat flux.

Now assuming the central contact pressure is 1.0 GPa, a traction coefficient of 0.001 and a constant slip velocity over the contact of 1 m/s, the heat flux in the center of contact will be $1.0 \times 10^6 \text{ W/m}^2$. The distribution will of course be ellipsoidal and the normalized values given in figure

4-18 can be readily used to compute the distribution.

The finite element modeling for the thermal problem is now straightforward. First, the three-dimensional solid geometry is selected as the edit target in the Aries preprocessor and then the finite element model created earlier is selected to specify the thermal loads and boundary conditions. The thermal loads consist of surface heat flux. This is prescribed by picking an elliptical ring in the contact, and then specifying the flux value as the normalized value given in figure 4-18, multiplied by the flux in center of contact of 10^6 W/m^2 . Figure 4-23 shows the incremental area at a normalized coordinate of 0.80 with a flux value of $0.650 \times 10^6 \text{ W/m}^2$. Appropriate zooming and magnifying functions may be used while interactively picking the various areas. Specification of thermal loading will be complete when the flux is prescribed on the entire elliptical contact zone. Temperature boundary condition is assumed such that the temperature on bottom and side surfaces of the solid is 20°C , i.e., room temperature. This is done by adding "nodal enforced temperatures" on an area. The entire area on sides and bottom of the solid may be picked to specify the value of temperature at all nodes in the selected area.

Once the thermal loads and boundary conditions are prescribed, the finite element analysis can be carried out to compute the temperature distribution in the solid, and then the mechanical stresses generated from the thermal expansions corresponding to the temperature field. With the Aries pre-processor to MSC NASTRAN, this is best accomplished by carrying out the analysis manually. This permits the output to be written to a file which could be read later to compute the resulting stress distribution. Thus, in the preprocessor, an option for manual analysis is selected and a name for the input data file is prescribed. The analysis is now carried out manually in accordance to the steps listed in Appendix B. After the analysis is complete, the results could be fed back to the Aries database for post-processing; this procedure is also listed in Appendix B. The resulting temperature distributions along the major and minor axis of contact are shown in figures 4-24a and 4-24b, respectively.

To compute the thermal expansion and corresponding stresses, the linear static analysis is once again carried out. This time the restraints consists of fixed based, as done earlier, while the loads consists of the nodal temperatures computed above. This is simply done by prescribing a reference room temperature, 20°C , and nodal temperatures available in the results file "NAS-TRAN.ANF" generated during the manual analysis procedure, as listed in Appendix B. Analysis of stresses is then carried out under the expansion loads. The resulting von-Mises stresses on the sectional planes along the major and minor axes of the contact ellipse are shown, respectively, in figures 4-25a and 4-25b. The orthogonal shear stress along the minor axis is shown in figure 4-25c.

In actual system design, the above stresses may be superposed on the stresses computed earlier due to mechanical loading, both normal and shear, on the surface to compute the overall stresses in the coatings resulting from both the mechanical and thermal interactions. Thus potential failures resulting from combined mechanical and thermal effects can be readily identified.

Residual stresses generated in a solid as a result of thermal cycling during fabrication of the solid is another thermal problem of practical interest. Generally, most of the manufacturing processes used to deposit coatings on the surfaces of various components employ a rather high

temperature environment. The mechanical part is basically heated to a high temperature and then the coating is deposited. After the deposition process, the solid is of course cooled to room temperature. When the thermal coefficient of expansion of the coating and substrate materials are greatly different, such a thermal cycle could produce significant residual stresses in the solid, which may affect the overall failure stresses and mechanisms when the solid is subjected to external mechanical and thermal loads.

Modeling of this residual stress problem using the finite element procedures is indeed quite straightforward. The three-dimensional solid and the finite element model as developed above are selected in the Aries preprocessor and a restraint case of fixed base is prescribed. Reference temperature is now set equal to the manufacturing process temperature, say 500°C, and then the default temperature for all the nodes is set to room temperature, say 20°C. A linear static analysis is then carried out to compute stresses resulting from the thermal expansions. The von-Mises stresses in the sectional planes along the major and minor axes are shown respectively in figures 4-26a and 4-26b.

Since all the finite element modeling steps presented above are linear, the solutions can be readily superposed to evaluate the combined effect. In summary, following are four parts to the overall modeling problem:

1. Stresses due to normal contact pressure as the surface
2. Stresses due to surface shear stress due to a traction coefficient
3. Thermal stresses resulting from the frictional heat generated in the contact
4. Residual stresses resulting from thermal cycling in the manufacturing process

Modeling of each of the above problems has been discussed above. Although a very simple three-dimensional contact is considered in the present investigation, the modeling steps could be followed for mechanical components with complex geometries, such as rolling bearings, gears and cam followers. Stress corresponding to each effect could be first computed and then superposed to determine the overall effect.



Figure 4-24a. Temperature distribution on a sectional plane along major axis of the contact ellipse resulting from an ellipsoidal heat flux on the surface.

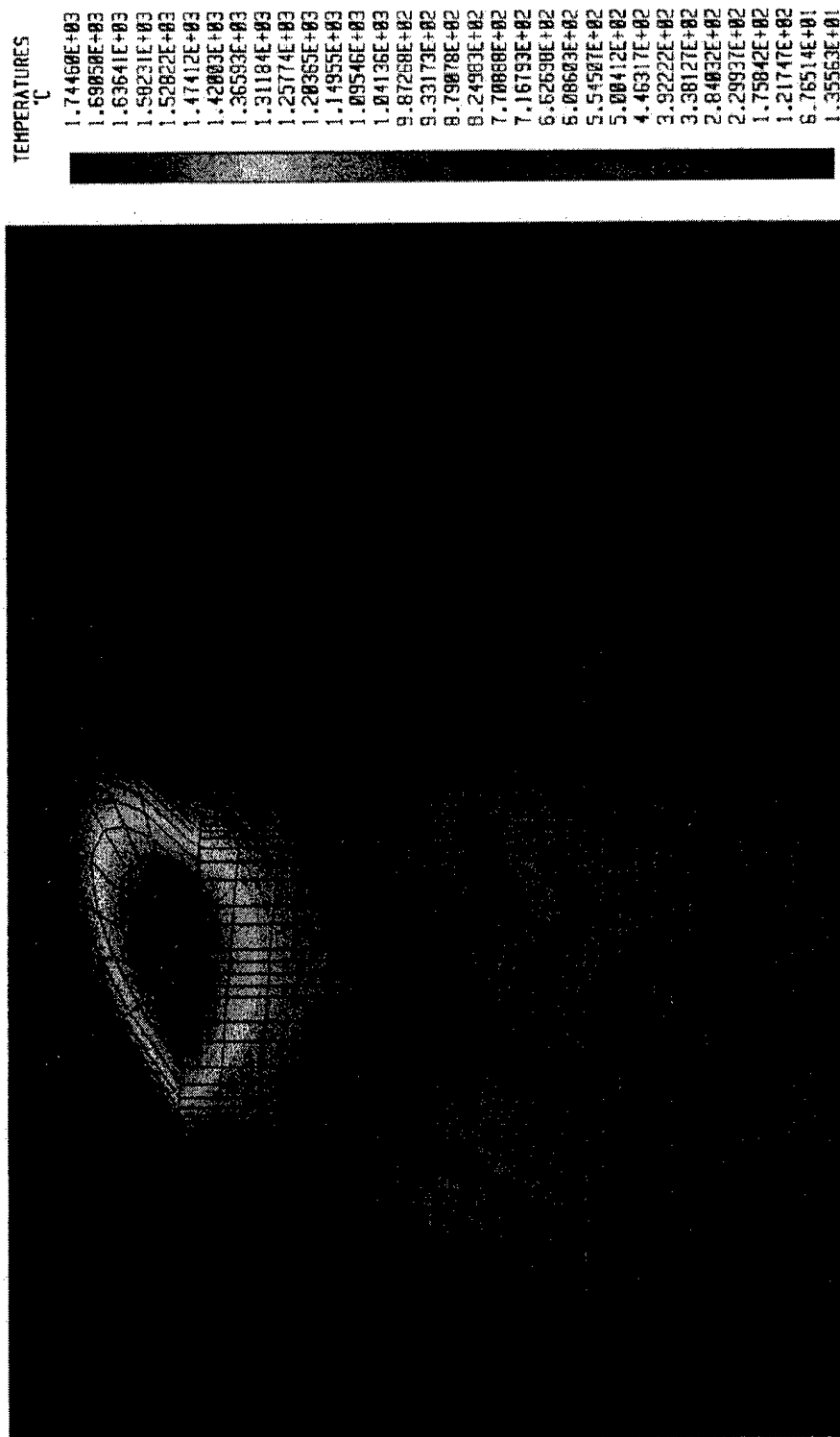


Figure 4-24b. Temperature distribution on a sectional plane along minor axis of contact ellipse resulting from an ellipsoidal heat flux on the surface.

VON-MISES
STRESS
N/(mm²)

1.80454E+09
1.74835E+09
1.69216E+09
1.63596E+09
1.57977E+09
1.52358E+09
1.46739E+09
1.41120E+09
1.35501E+09
1.29882E+09
1.24262E+09
1.18643E+09
1.13024E+09
1.07405E+09
1.01786E+09
9.61667E+08
9.05476E+08
8.49284E+08
7.93093E+08
7.36901E+08
6.80710E+08
6.24518E+08
5.68327E+08
5.12135E+08
4.55944E+08
3.99752E+08
3.43561E+08
2.87369E+08
2.31176E+08
1.74986E+08
1.18795E+08
6.26035E+07
6.41198E+06

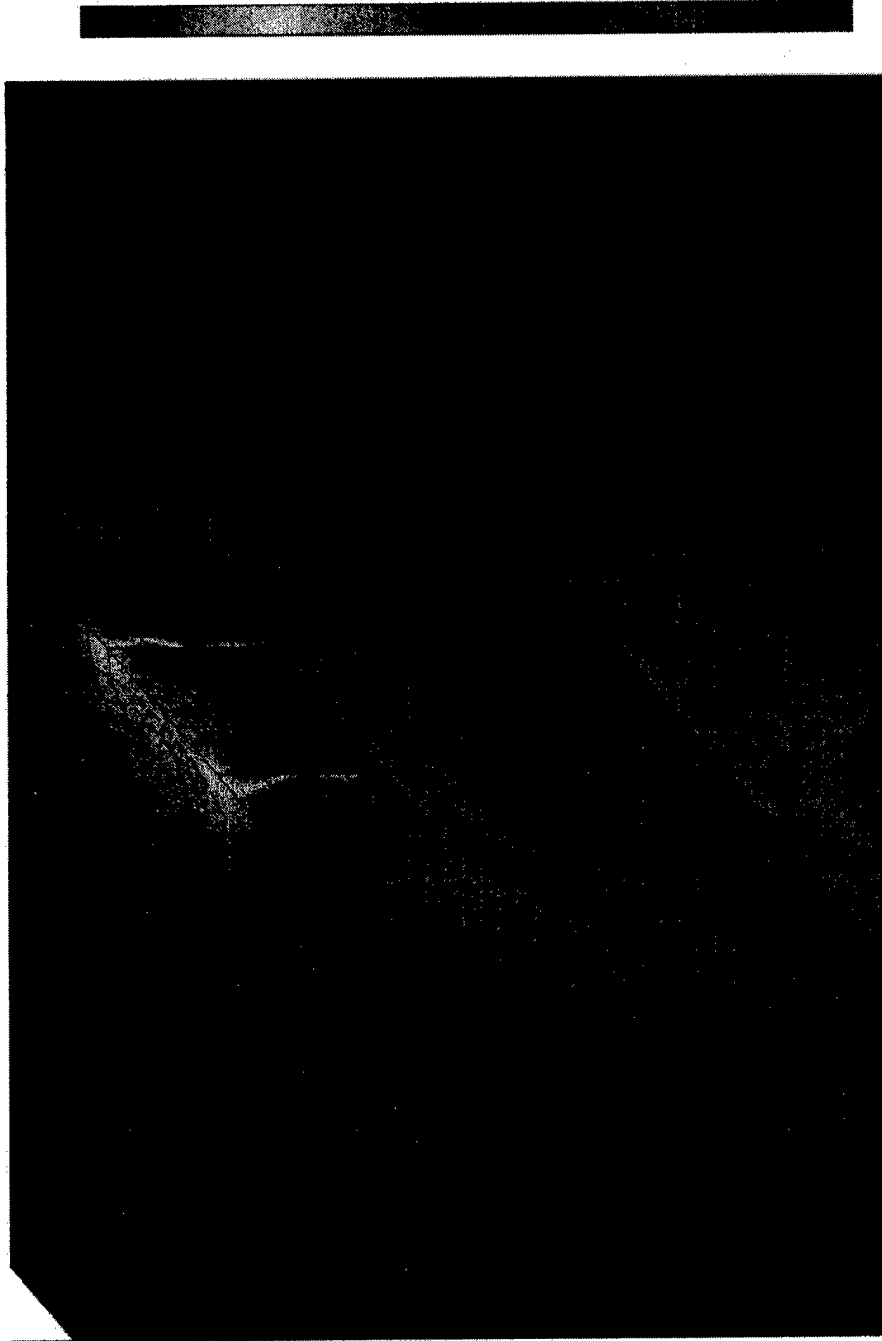


Figure 4-25a. von-Mises stresses on a sectional plane along major axis of contact ellipse resulting from an ellipsoidal heat flux on the surface.

VON_MISES
STRESS
N/(m²)

1.80454E+09
1.74835E+09
1.69216E+09
1.63596E+09
1.57977E+09
1.52358E+09
1.46739E+09
1.41120E+09
1.35501E+09
1.29882E+09
1.24262E+09
1.18643E+09
1.13024E+09
1.07405E+09
1.01786E+09
9.61657E+08
9.05476E+08
8.49284E+08
7.93093E+08
7.36901E+08
6.80710E+08
6.24510E+08
5.68327E+08
5.12135E+08
4.55944E+08
3.99752E+08
3.43561E+08
2.87359E+08
2.31178E+08
1.74986E+08
1.18795E+08
6.26835E+07
5.41190E+06

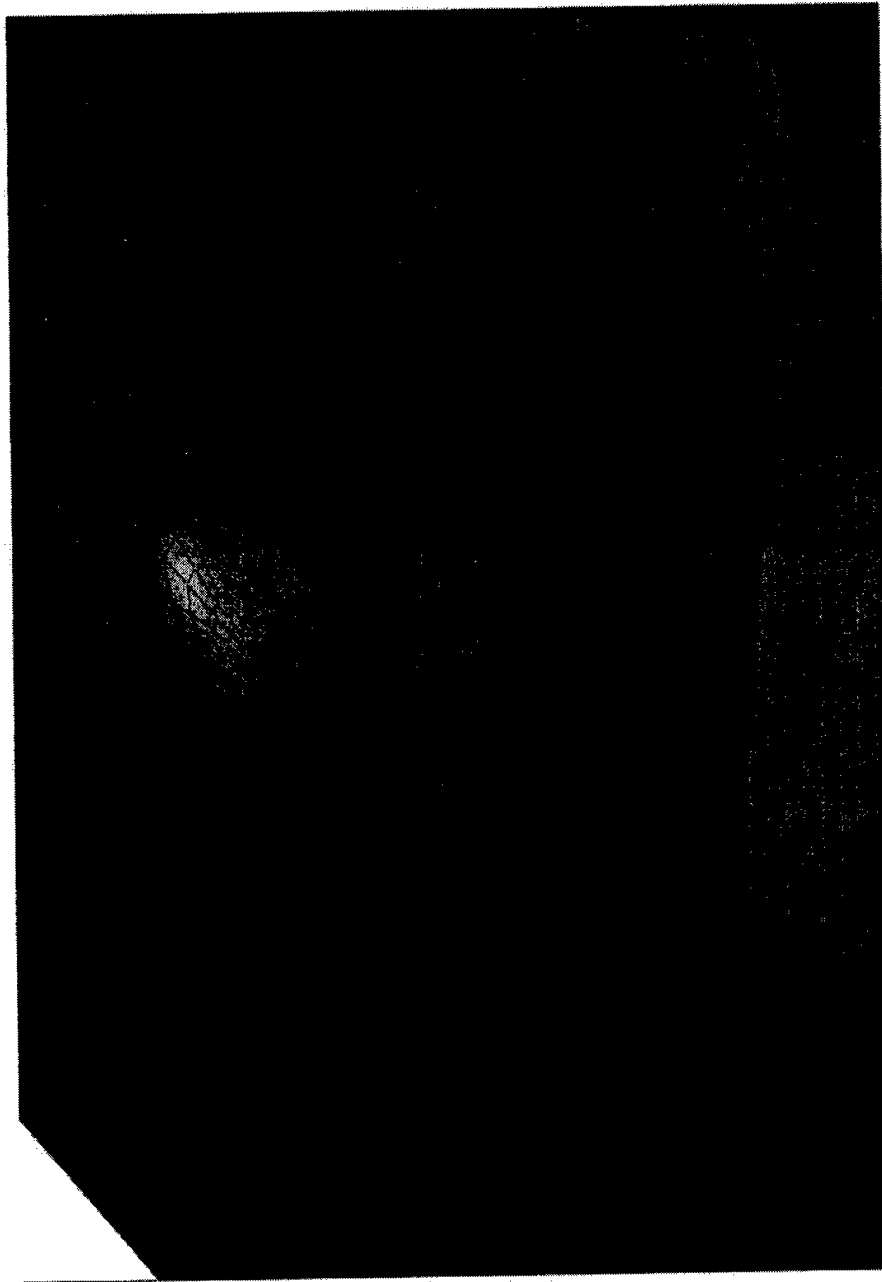


Figure 4-25b. von-Mises stresses on a sectional plane along minor axis of contact ellipse resulting from an ellipsoidal heat flux on the surface.

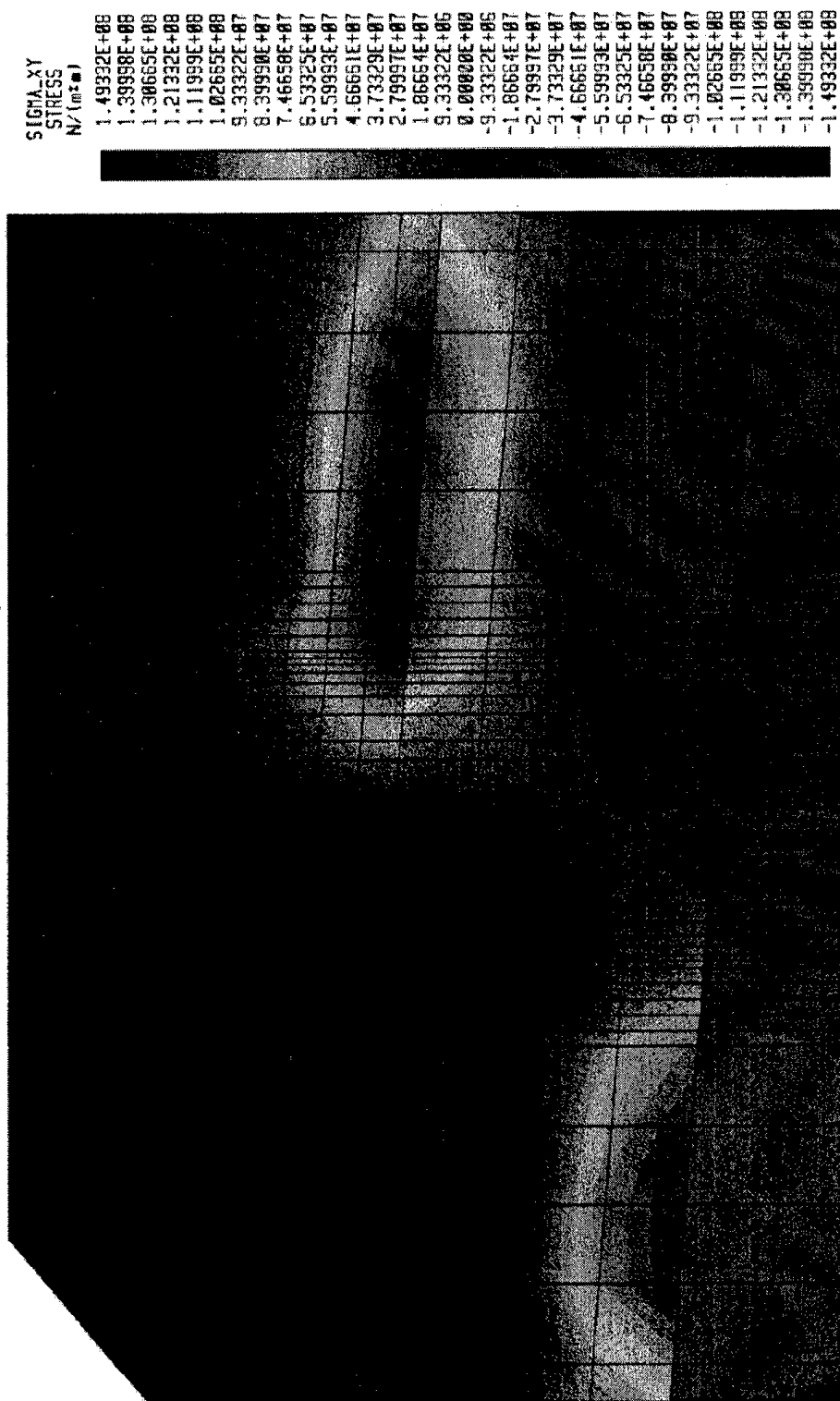


Figure 4-25c. Orthogonal shear stress resulting from an ellipsoidal heat flux on the surface.

VON_MISES
STRESS
N/(mm²)

2.03587E+09
1.97372E+09
1.91158E+09
1.84944E+09
1.78729E+09
1.72515E+09
1.66301E+09
1.60086E+09
1.53872E+09
1.47658E+09
1.41444E+09
1.35229E+09
1.29015E+09
1.22801E+09
1.16586E+09
1.10372E+09
1.04158E+09
9.79432E+08
9.17289E+08
8.55145E+08
7.93002E+08
7.30859E+08
6.68716E+08
6.06572E+08
5.44429E+08
4.82285E+08
4.20143E+08
3.57999E+08
2.95856E+08
2.33713E+08
1.71570E+08
1.09425E+08
4.72839E+07

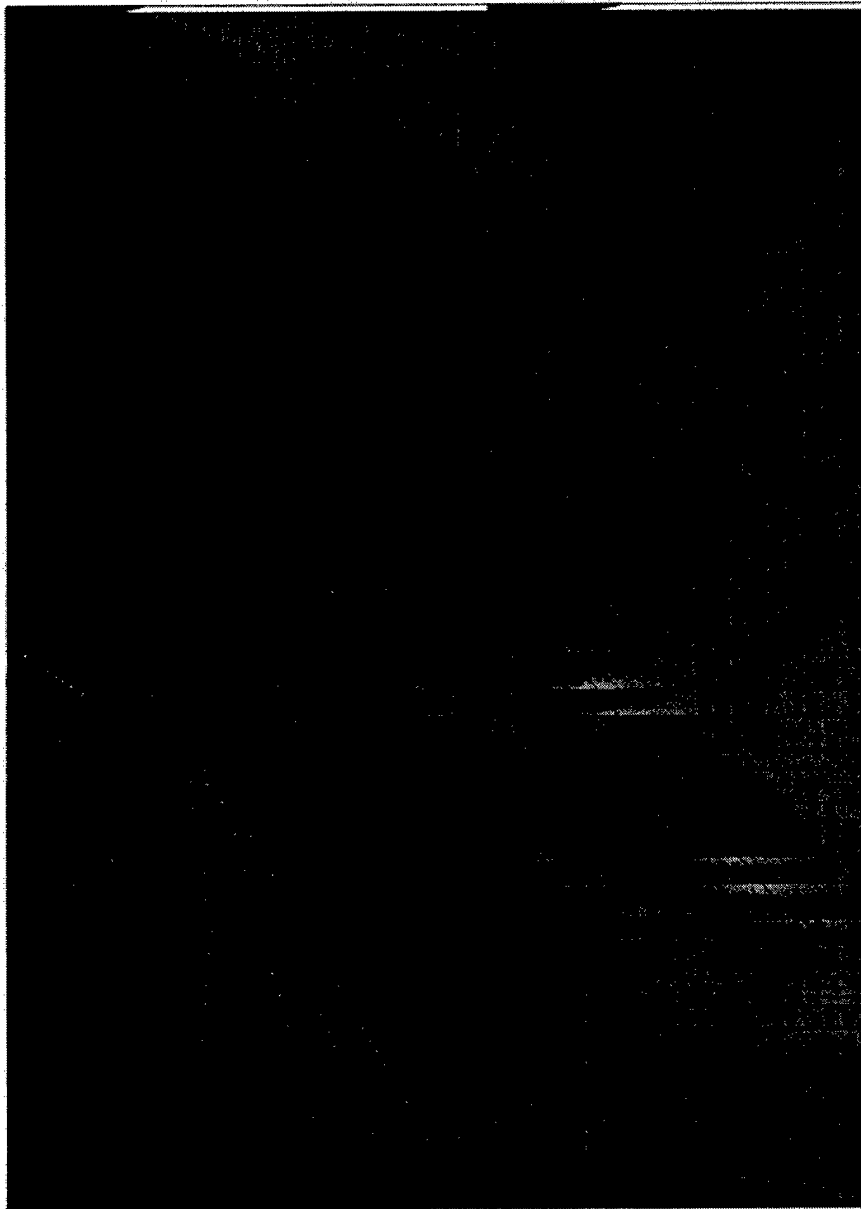


Figure 4-26a. von-Mises stresses on a sectional plane along major axis of contact ellipse resulting from a uniform cooling of the solid from 500 to 20°C.

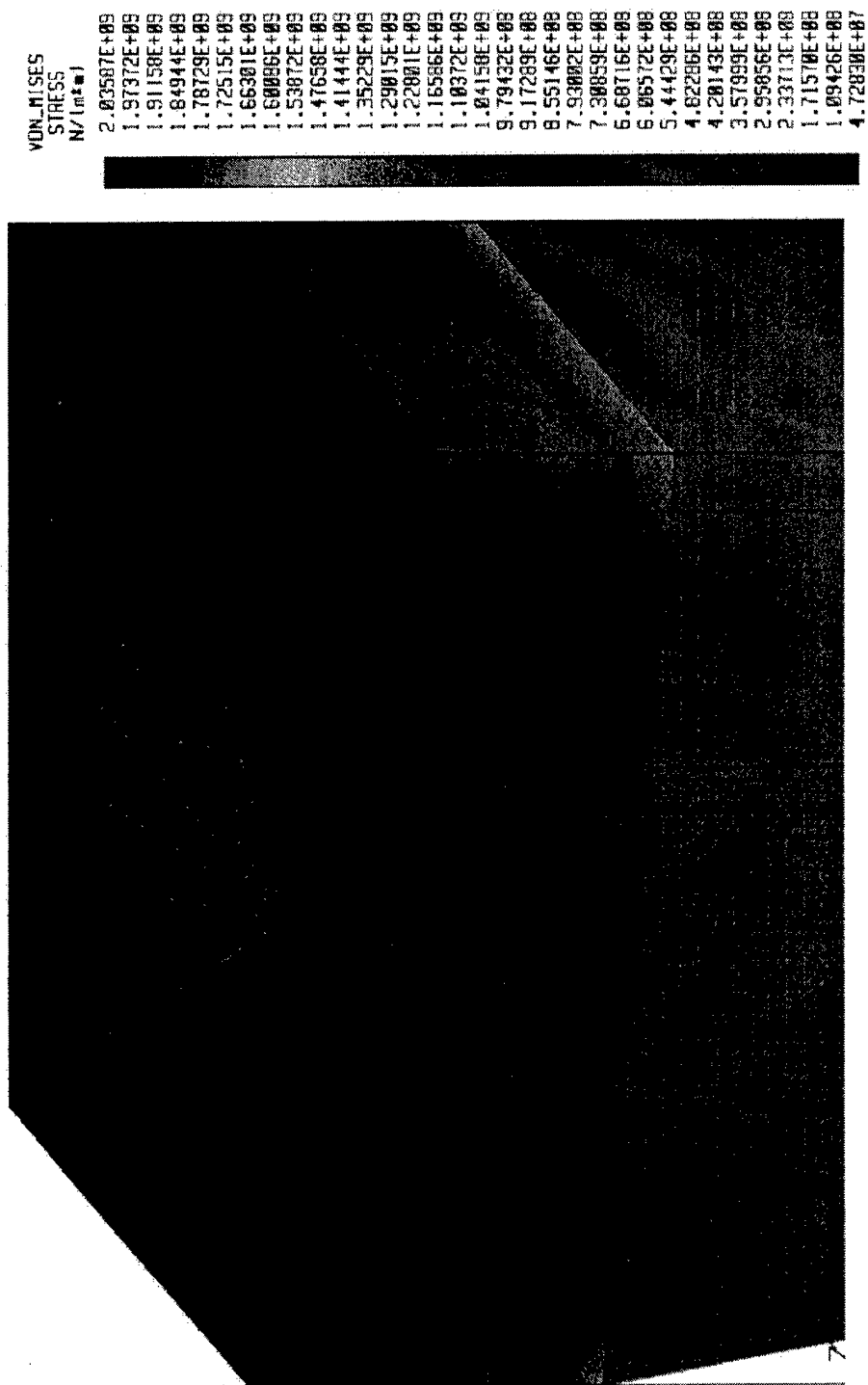


Figure 4-26b. von-Mises stresses on a sectional plane along minor axis of contact ellipse resulting from a uniform cooling of the solid from 500 to 20°C.

5. MODELING OF FRICTIONAL INTERACTIONS

Friction between two mating surfaces is perhaps the most significant interaction which controls the behavior of a wide range of mechanical components. In concentrated contacts where the relative sliding velocity is superposed on nominal rolling velocity, the resulting friction is often referred to traction. In terms of the overall frictional forces the two terms, e.g., friction and traction, are basically equivalent. Aside from the frictional forces resulting from applied slip or sliding velocities, the frictional interactions may produce significant heat in the contact, which in turn affects properties of both the lubricant and the interacting solids. In contacts with liquid lubricants, the contact heat generations affect lubricant temperature, which alters the viscosity, which in turn modifies the shear rates and traction through the lubricant film. Thus modeling the traction problem for such contacts becomes an iterative process consisting of both thermal and mechanical interactions. For solid films the fundamental understanding of the mechanics of friction is still in infancy. It is the complexity associated with closely coupled chemical, mechanical and thermal interactions, which make the problem extremely difficult to formulate. This has led to semi-empirical approaches to modeling the frictional behavior. Friction between two mating specimens is experimentally measured as a function of operating conditions, and then curve fitted to various models. Such an approach, although lacking in physical understanding of the frictional mechanics, provides significant guidance for practical design of mechanical components and materials development. A wide range of experimental investigations have, therefore, been the first step in frictional modeling. The current effort is also based on available experimental data.

Since friction is often greatly affected by thermal and chemical interactions, experimental measurement in a controlled environment has been a difficult task and rather large scatter is commonly associated with most experimental investigations. While an estimate of nominal friction coefficient as a function of the operating environment is adequate for sliding contacts, a closely coupled traction/slip relation is required for rolling sliding contacts, where the acceleration of rolling elements has to be computed at prescribed slip velocities. In fact, the coupling between traction and slip, has been established as one of the most important parameters which control the dynamic behavior of rolling bearings. With such a practical significance, experimental investigations for the measurement of frictional behavior may be classified into two categories:

1. Measurement of nominal friction coefficient for a sliding contact.
2. Measurement of traction as a function of slip in a rolling sliding contact.

Practical applications in the first categories simply require a tabulation of friction coefficient as a function of material properties and operating conditions, such as load and temperature. For the definition of traction as a function of slip, a more extensive modeling effort is required. Thus most of the current effort is dedicated to development of such a model. The modeling approach is semi-empirical where available experimental data is fitted to a model to derive a certain number of constitutive coefficients which are useful in predicting traction in a practical application.

Traction or friction behavior as a function of relative sliding, or slip velocity, for most lubricants, either solid or liquid, has been typically found to be similar to that shown in figure 5-1. The traction coefficient first increases with increasing slip, reaches a maximum and then levels off to an asymptotic value, which is often less than the maximum value. The qualitative similarity

between the traction/slip relation for solid and liquid lubricants suggests a similar mechanism. For liquid lubricants there have been two common models. The first model is based on the viscosity variation as a function of pressure and temperature [15] and the observed traction behavior is explained in terms of viscous heating of the lubricant. In another school of thought, it is postulated that at the high pressures in a rolling/sliding contact, the lubricant viscosity is so high that it behaves almost like a solid, leading to a more complex visco-elastic behavior [16]. In solid films, it will of course be the shear through the film which will contribute to friction. Thus some similarity between liquids and solids is obvious.

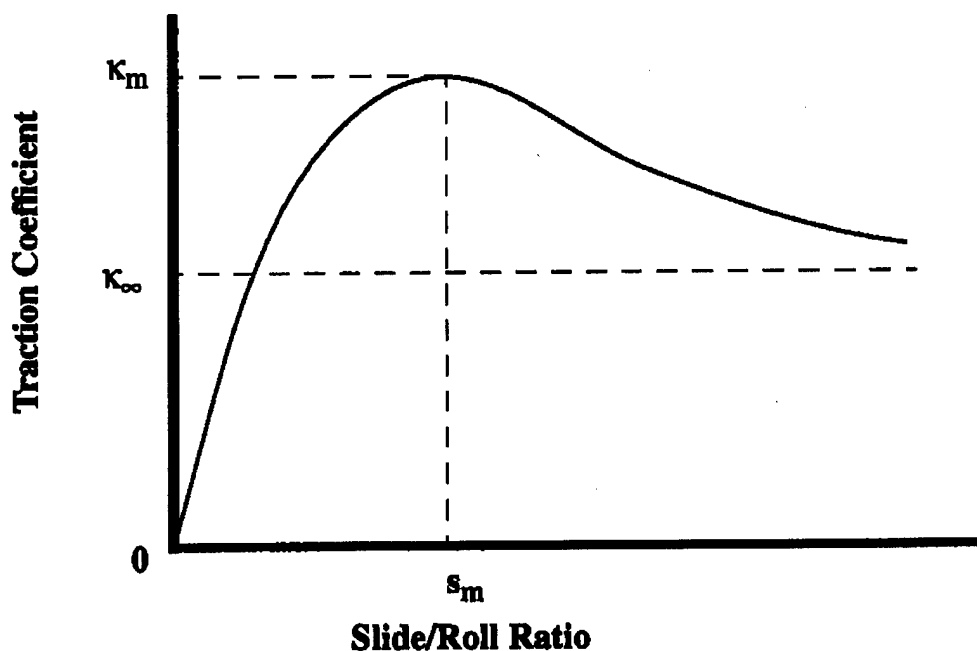


Figure 5-1. Commonly observed traction slip behavior.

5.1 Friction or Traction Models

Various models to simulate the above behavior have been developed. A model based on the viscosity behavior consists of the following fundamental equations:

Energy equation:

$$K_f \frac{\partial^2 T}{\partial z^2} = -\tau s \quad \text{Eqn (5-1)}$$

Geometric compatibility:

$$\frac{\partial u}{\partial z} = s(\tau, p, T) \quad \text{Eqn (5-2)}$$

Constitutive equation:

$$s(\tau, p, T) = \frac{\tau}{\mu(p, T)} \quad \text{Eqn (5-3)}$$

where K_f is the thermal conductivity of the lubricant, T is the absolute temperature, τ is the shear stress, s is the shear strain rate, u is the sliding velocity, p is the pressure, μ is the viscosity, and z is a coordinate across the lubricant film.

Given the temperatures of the two interacting surfaces, the thickness of lubricant film and the rolling velocity, appropriate boundary conditions may be applied to integrate the above equations to obtain a shear stress distribution over the contact, which in turn may be integrated to obtain the total traction force. The main input is the viscosity-pressure-temperature relation, which is commonly assumed to be of the form:

$$\mu = \mu_o \exp[\alpha p + \beta(T_o - T)] \quad \text{Eqn (5-4)}$$

Here the three constitutive constants are μ_o , the viscosity at a reference temperature, T_o , α , the pressure-viscosity coefficient, and β , the temperature viscosity coefficient. These three constitutive coefficients are computed by performing a regression fit of the model to experimental traction data.

For the visco-elastic model the governing equation is:

$$s = \frac{1}{G} \frac{\partial \tau}{\partial t} + \frac{\tau_o}{\mu} f\left(\frac{\tau}{\tau_o}\right) \quad \text{Eqn (5-5)}$$

Here also, there are three constitutive constants: the shear modulus G , viscosity μ , and a critical shear stress τ_o , at which the viscous effect becomes significant. All the three constants may, in general, be functions of pressure and temperature. Knowing the rolling velocity, the convective derivative term can be expressed in terms of derivative with respect to a coordinate along the rolling direction, and then the resulting differential equation may be integrated over the contact to obtain a shear stress distribution.

For both of the above models Gupta, et al. [17], and Gupta [18,19,20] has analyzed a number of lubricating fluids to obtain the constitutive coefficients. The coefficients may be readily used to simulate the traction behavior of the various lubricants.

The primary emphasis in the present investigation is on solid films or lubricants. Although Walowit [21] has attempted to apply the visco-elastic model to solid film, the application is quite complex even after several simplifying assumptions about operating environment and the film

properties. The complexity of the model also has restrictions on use of the model for practical application, once the appropriate coefficients have been derived from experimental data. Particularly for dynamic performance simulation of rolling bearings the model has to be fairly simple because several million traction computations may be required in order to obtain a steady-state dynamic behavior of the bearing [22].

In view of the above complexities of solid film behavior and the required simplicity in the model, technical approach in the present investigation is based on an empirical equation suggested by Kragelskii [23]. The traction or friction coefficient, may be expressed as a function of slide-to-roll ratio, as:

$$\kappa = (A + Bs)e^{-Cs} + D \quad \text{Eqn (5-6)}$$

where κ is the traction, or friction, coefficient, s is the slide-to-roll ratio and A, B, C, D are coefficients, which are generally dependent on material properties and operating conditions. The model yields a traction/slip relation of the form displayed in figure 5-1.

For rolling/sliding contacts, traction is always zero at zero slip. Substituting this condition in equation (5-6) results in $D = -A$, and thus equation (5-6) may be reduced to

$$\kappa = (A + Bs)e^{-Cs} - A \quad \text{Eqn (5-7)}$$

Thus the model once again results in three coefficients, A, B, C . For a given set of experimental data, these coefficients may be estimated from the following three conditions:

1. Maximum traction coefficient = κ_m
2. Traction at infinite slip = κ_∞
3. Slide/roll at maximum traction = s_m

Condition (2) above, will give $A = -\kappa_\infty$, which when substituted in equation (5-7) gives traction variation only in terms of the coefficients B and C

$$\kappa = (-\kappa_\infty + Bs)e^{-Cs} + \kappa_\infty \quad \text{Eqn (5-8)}$$

Setting the derivative of traction with respect to the slide-to-roll ratio equal to zero at $s = s_m$, per condition (3), and denoting the ratio $\frac{B}{C} = \beta$, will result in the following:

$$s_m = \frac{\beta + \kappa_\infty}{B} \quad \text{Eqn (5-9)}$$

which when substituted in equation (4) and combined with condition (1), will result in the follow-

ing equation for computation of β :

$$\kappa_m = \beta e^{\frac{\beta + \kappa_\infty}{\beta}} + \kappa_\infty \quad \text{Eqn (5-10)}$$

With given maximum traction, and traction at infinite slip, the above equation may be solved for β by conventional bisection, and then using equation (5) the coefficients B and C may be computed.

5.2 Regression Analysis for Model Coefficients

Although the above formulation provides an estimate of model coefficients based on certain limiting conditions, it is often desirable to estimate the model coefficients from regression analysis of experimental traction data. To formulate such an analysis, two intermediate variables, η and ζ are defined as

$$\eta = (e^{-Cs} - 1) \quad \text{Eqn (5-11)}$$

$$\zeta = se^{-Cs} \quad \text{Eqn (5-12)}$$

Now in terms of the above variables, equation (5-7) may be written as:

$$\kappa = A\eta + B\zeta \quad \text{Eqn (5-13)}$$

The squared deviation, L , for a set of n experimental data points is defined as

$$L = \sum_{i=1}^n w_i (\kappa_i - \kappa_i')^2 \quad \text{Eqn (5-14)}$$

where κ_i and κ_i' are respectively the computed and measured value of traction at a given point and w_i are arbitrary weights assigned to the data points to control fit over the data range.

For computation of model coefficients, the squared deviation is minimized by using the following conditions:

$$\frac{\partial L}{\partial A} = \frac{\partial L}{\partial B} = \frac{\partial L}{\partial C} = 0 \quad \text{Eqn (5-15)}$$

Since the variables η and ζ contain the coefficient C , the coefficients A and B are computed by the following linear algebraic equations, derived by setting the first two derivatives in equation (5-15) equal to zero, for a given value of C :

$$\begin{bmatrix} \sum_{i=1}^n w_i \eta_i^2 & \sum_{i=1}^n w_i \zeta_i \eta_i \\ \sum_{i=1}^n w_i \zeta_i \eta_i & \sum_{i=1}^n w_i \zeta_i^2 \end{bmatrix} \begin{bmatrix} A \\ B \end{bmatrix} = \begin{bmatrix} \sum_{i=1}^n w_i \eta_i \kappa_i' \\ \sum_{i=1}^n w_i \zeta_i \kappa_i' \end{bmatrix} \quad \text{Eqn (5-16)}$$

For computation of C , equations (5-7) and (5-14) are combined to obtain the following expanded form

$$L = \sum_{i=1}^n w_i \left\{ (A + Bs_i) e^{-Cs_i} - A - \kappa_i' \right\}^2 \quad \text{Eqn (5-17)}$$

The nonlinear equation in C is now written by combining the above with the third derivative expression in equation (5-15)

$$g = \frac{\partial L}{\partial C} = \sum_{i=1}^n w_i s_i \left\{ (A + Bs_i) e^{-Cs_i} - A - \kappa_i' \right\} (A + Bs_i) e^{-Cs_i} = 0 \quad \text{Eqn (5-18)}$$

Equation (5-18) is solved for the coefficient C by conventional Newton-Raphson iterative method. Differentiation of equation (5-18) with respect to C , for computation of correction term, is quite straightforward. Computation of the initial guess may be accomplished by preliminary examination of the experimental data and by using the three limiting conditions discussed above.

5.3 Contact Temperatures

Since the model coefficients and also the material properties are temperature dependent, it is necessary to compute the contact temperature. This may, indeed, depend on the thermal constraints and environment of the practical application. For the present investigation, however, a simple conduction analysis based on the theory of moving heat sources, as documented by Jaeger[24] and applied to rolling bearings by Gupta [25]. Although the analytical formulation has been well documented in reference [25], it is duplicated here, since this reference has not been widely published.

Assume an elliptical contact, as shown in figure 5-2. The direction of rolling is along the minor axis of the contact ellipse. Once, the friction coefficient and load distribution in the contact is known, the distribution of heat generation in the contact may be readily computed.

If the contact zone is divided in incremental strips as shown in figure 5-2, then the temperature distribution, $T(y)$, along the rolling direction (y) is given by the equation

$$T(y) = T_0 + \frac{1}{\sqrt{\pi \rho c k U}} \int_{-b}^y \frac{q(\xi)}{\sqrt{y-\xi}} d\xi \quad \text{Eqn (5-19)}$$

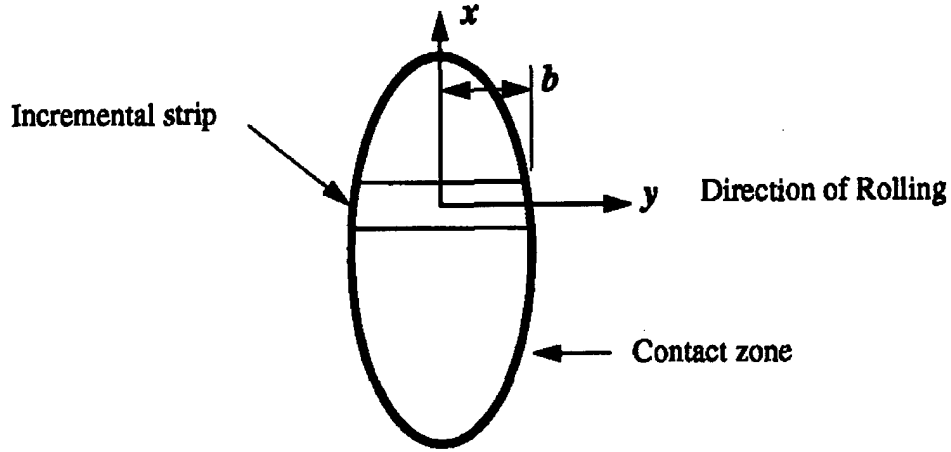


Figure 5-2. Contact zone schematic.

where T_0 is a reference temperature and ρ , c , k , U are, respectively, the density, heat capacity, thermal conductivity, and rolling velocity. The heat flux $q(y)$ for a given pressure distribution $p(y)$, traction coefficient κ , and sliding velocity u_s , is simply written as

$$q(y) = \kappa u_s p(y) \quad \text{Eqn (5-20)}$$

If the two surfaces are separated by a lubricant film of thickness, h , and that the heat generated in the contacts is partitioned into the two surfaces by fractions α and $(1 - \alpha)$, then the heat fluxes going into surfaces 1 and 2, as shown schematically in figure 5-3 are given by

$$q_1(y) = \frac{k_f}{h} (T_2 - T_1) + \alpha q(y) \quad \text{Eqn (5-21)}$$

$$q_2(y) = \frac{k_f}{h} (T_1 - T_2) + (1 - \alpha) q(y) \quad \text{Eqn (5-22)}$$

where k_f is the thermal conductivity of the fluid, or lubricant. The corresponding temperature distributions on the two surfaces, denoted by subscripts 1 and 2, may be written as

$$T_1(y) = T_0 + \frac{1}{\sqrt{\pi\rho_1 c_1 k_1 U_1}} \int_{-b}^y \frac{q_1(y)}{\sqrt{y-\xi}} d\xi \quad \text{Eqn (5-23)}$$

$$T_2(y) = T_0 + \frac{1}{\sqrt{\pi\rho_2 c_2 k_2 U_2}} \int_{-b}^y \frac{q_2(y)}{\sqrt{y-\xi}} d\xi \quad \text{Eqn (5-24)}$$

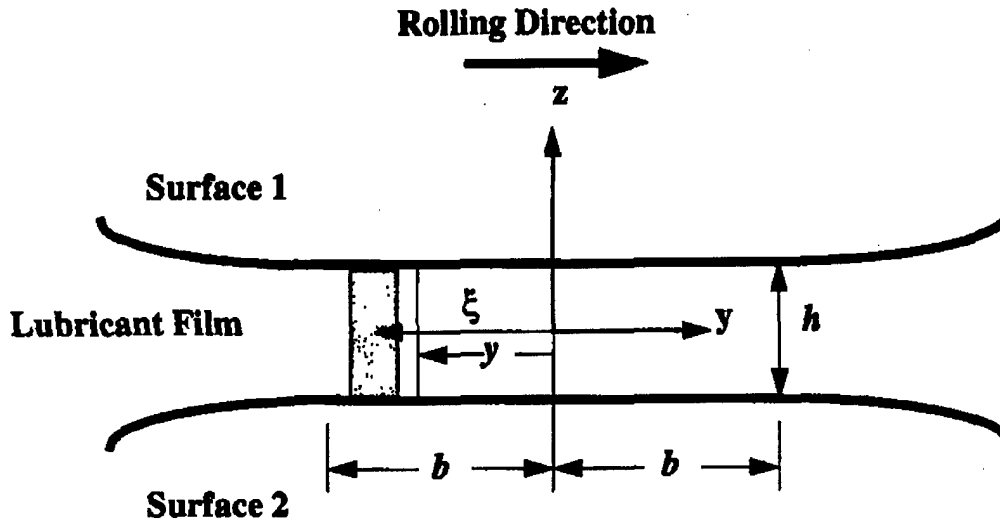


Figure 5-3. Basic coordinates in the contact zone.

For the present investigation, temperatures of the two surfaces shall be assumed to be equal and therefore the conduction term in equations (5-21 and 5-22) will vanish, and the heat partition fraction reduces to

$$\alpha = \frac{1}{\sqrt{\pi\rho_1 c_1 k_1 U_1} + \sqrt{\pi\rho_2 c_2 k_2 U_2}} \quad \text{Eqn (5-25)}$$

The expression for temperature rise, $\Delta T(y) = T(y) - T_0$, in the contact along the rolling direction thereby reduces to

$$\Delta T(y) = \frac{1}{\sqrt{\pi\rho_1 c_1 k_1 U_1} + \sqrt{\pi\rho_2 c_2 k_2 U_2}} \int_{-b}^y \frac{q(y)}{\sqrt{y-\xi}} d\xi \quad \text{Eqn (5-26)}$$

The above equation gives the local temperature rise over an incremental strip in the contact along the rolling direction. For computation of average temperature, this equation may be integrated over the contact area

$$T_{ave} - T_o = \frac{1}{\pi ab} \int_{-a}^a \int_{-b}^b \Delta T(y) dy dx \quad \text{Eqn (5-27)}$$

where a is the contact half width in the direction normal to rolling.

A computer code SLTRAC is written to implement the above analysis to a concentrated contact. Model correlations with the available experimental data are discussed below.

5.4 Model Correlations

Some of the early experimental data on traction-slip behavior of solid lubricants was generated by Winer under contract with Hughes Aircraft Company [26-27]. The overall effort was sponsored by DARPA and the U.S. Air Force, and managed by Gardos of Hughes Aircraft Company. Typical data obtained with 52100 steel specimens with a Ga-In-W-Se₂ film at the interface is shown below in figure 5-4.

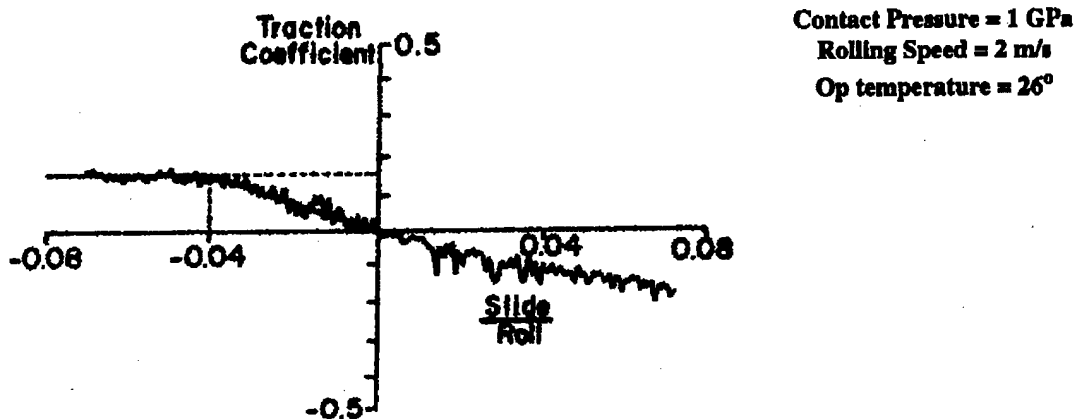


Figure 5-4. Traction behavior of 0.40 μm coating of Ga-In-W-Se₂ 52100 steel specimens.

The data was fitted to a simple slope and threshold value, as shown in figure 5-4, by Gupta [28] and used in simulation of dynamic performance of a solid lubricated ball bearing. The traction slope was shown to be a critical parameter for bearing performance. A more detailed evaluation of bearing performance as a function of traction behavior was carried out later by Gupta [29]. This work also highlights significance of the model discussed above for rolling bearing application.

The data shown in figure 5-4 may be used in regression analysis outlined above to compute the model coefficients, A, B and C. The results are shown in figure 5-5. Although, over the

range of slide to roll ratios, shown in figure 5-4, the normal peak in traction is not seen, the fit between this set of data and the traction model presented above is fairly good.

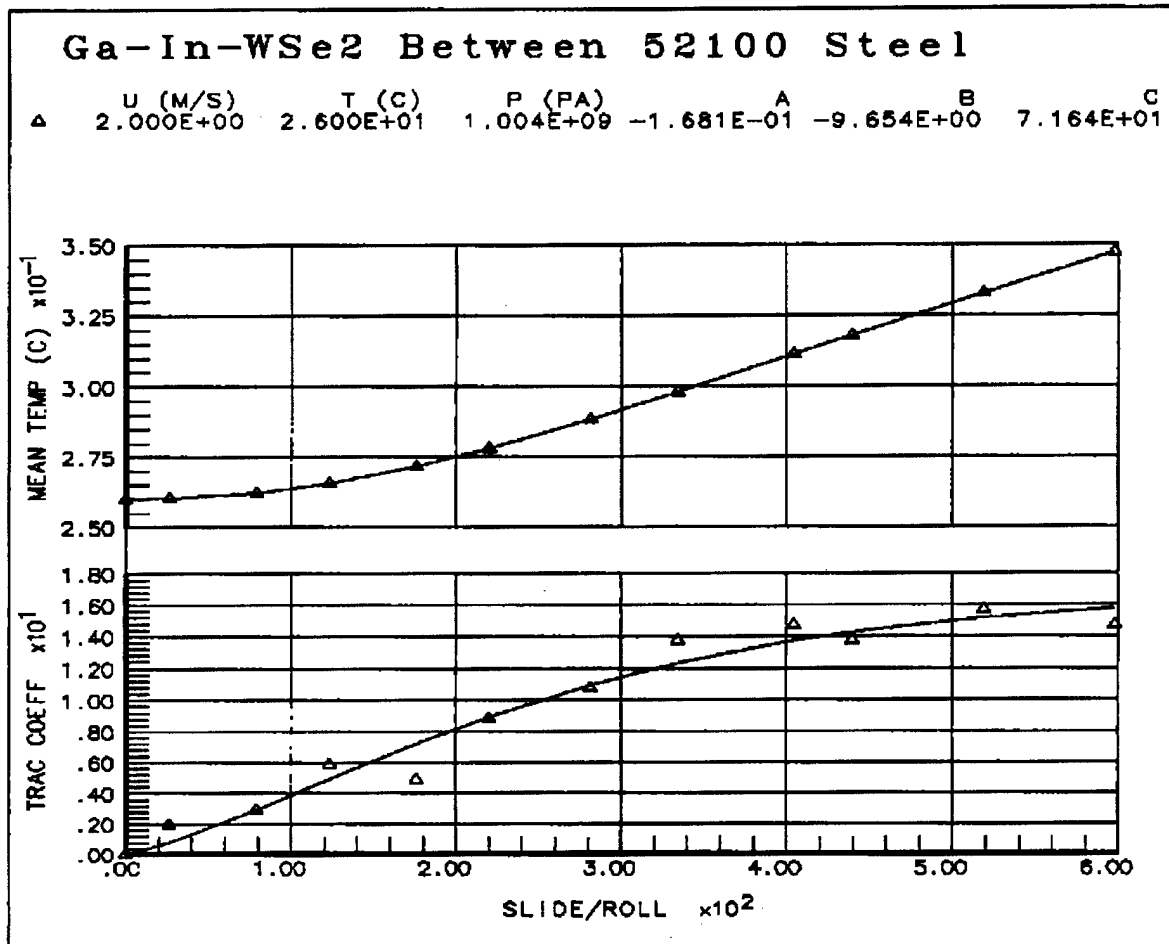


Figure 5-5. Model correlation with experimental traction data obtained with Ga-In-W-Se₂.

A more recent set of traction data with solid lubricants has been generated by Heshmet [30-32]. Most of this data is with a variety of solid lubricants, applied in powder form between two ceramic disk specimens, subjected to rolling sliding interaction.

Figures 5-6 and 5-7 show correlations of the traction model with experimental traction data obtained by Heshmet [30], with silicon carbide and silicon nitride disks in rolling-sliding contact with no lubricant.

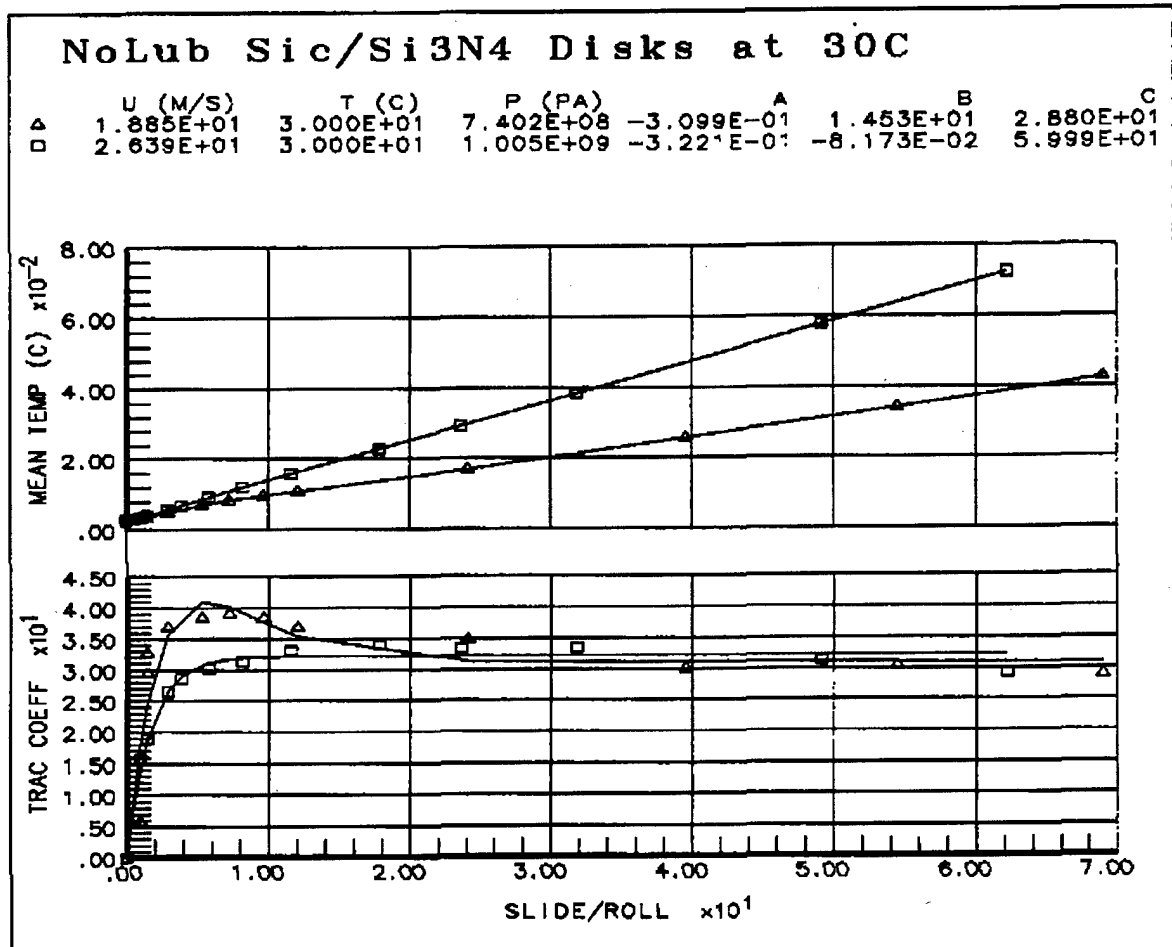


Figure 5-6. Model correlation with experimental traction data obtained with ceramic disk specimens with no lubricant at room temperature.

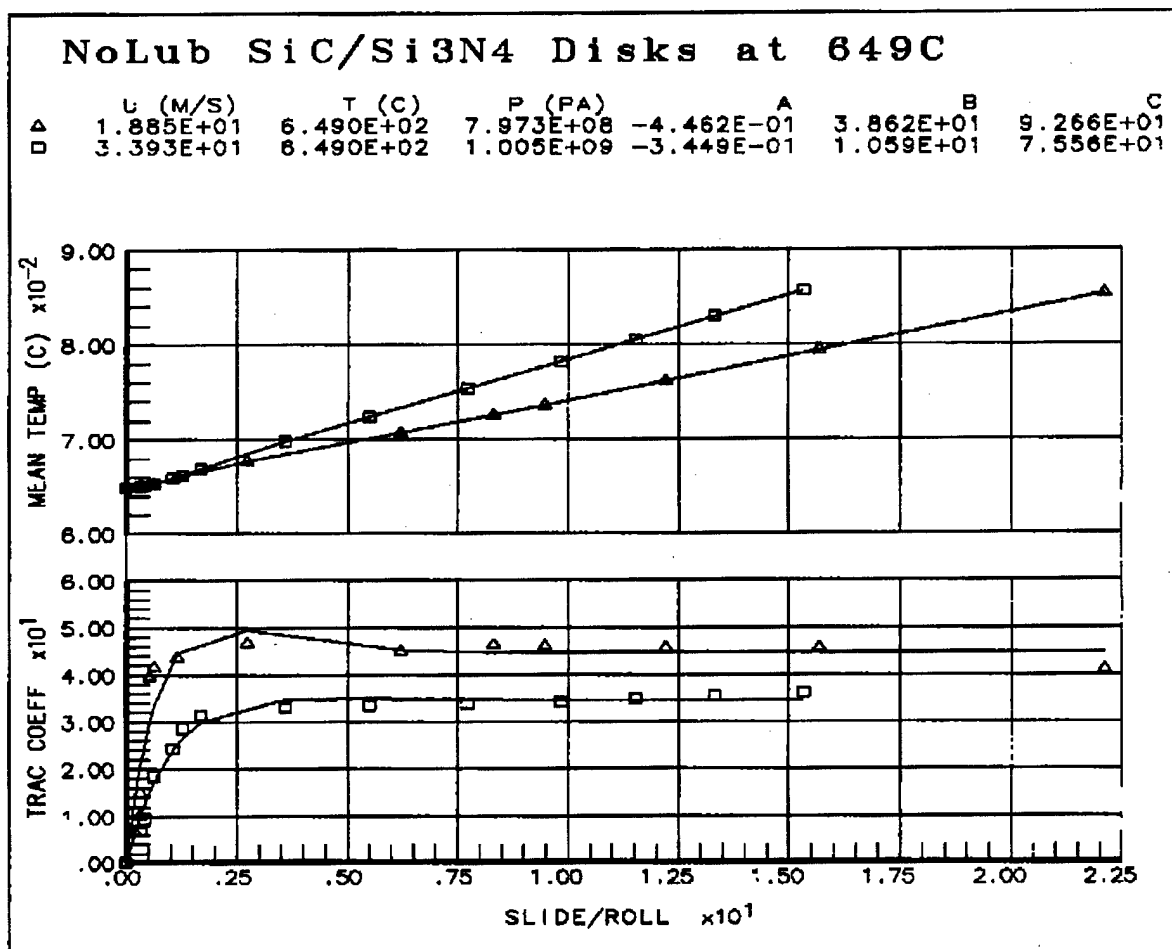


Figure 5-7. Model correlation with experimental traction data obtained with ceramic disk specimens with no lubricant at 649°C.

In the next set of experiments, TiO₂ powder was introduced between the ceramic disks. Model correlations with this set of data obtained at 30 and 649°C are shown, respectively, in figures 5-8 and 5-9. During some of these tests at high temperature, some material from the Inconel 718 thermo-couple was inadvertently transferred to the disks in the midst of the powder lubricant. This contamination did not seem to affect overall traction. Model correlations with this set of data are shown in figure 5-10.

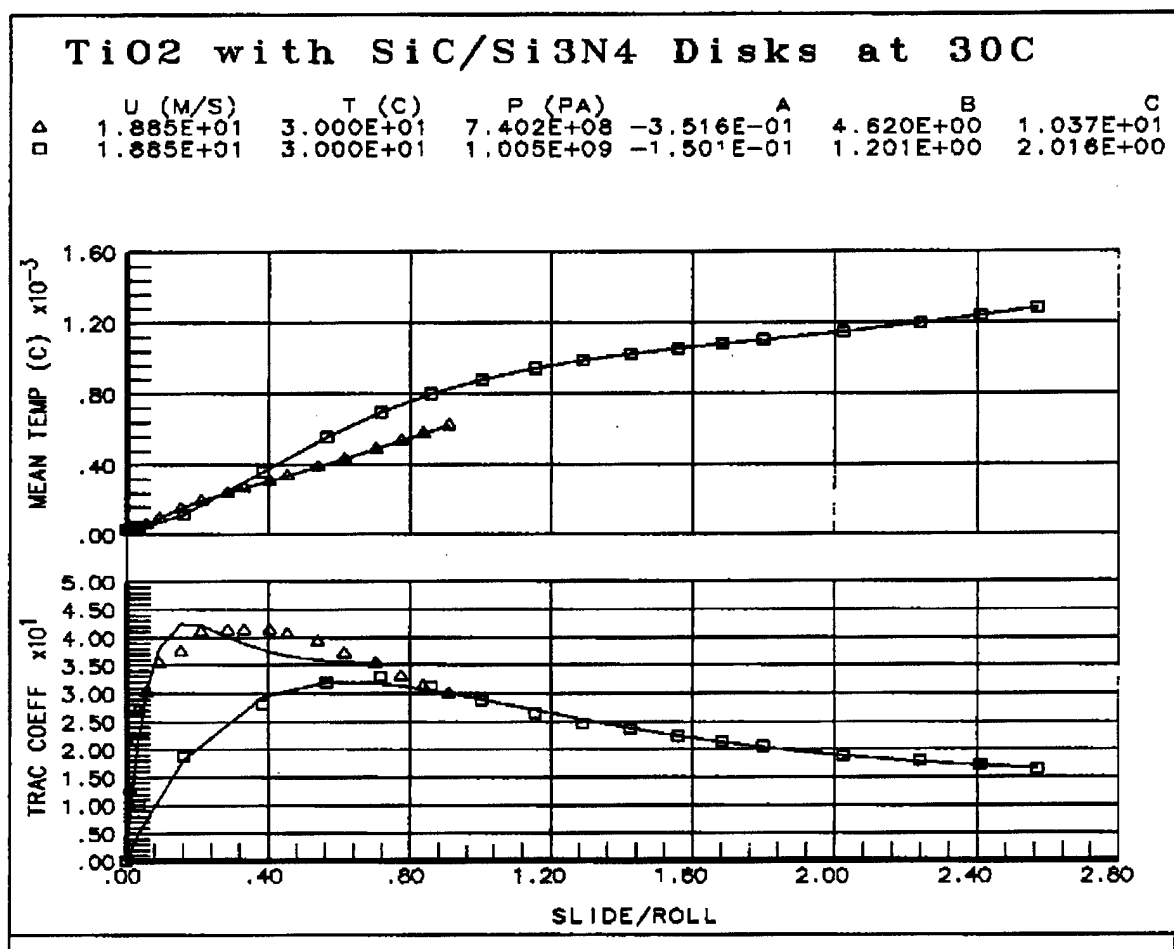


Figure 5-8. Model correlation with experimental traction data obtained with ceramic disk specimens with TiO₂ powder lubricant at room temperature.

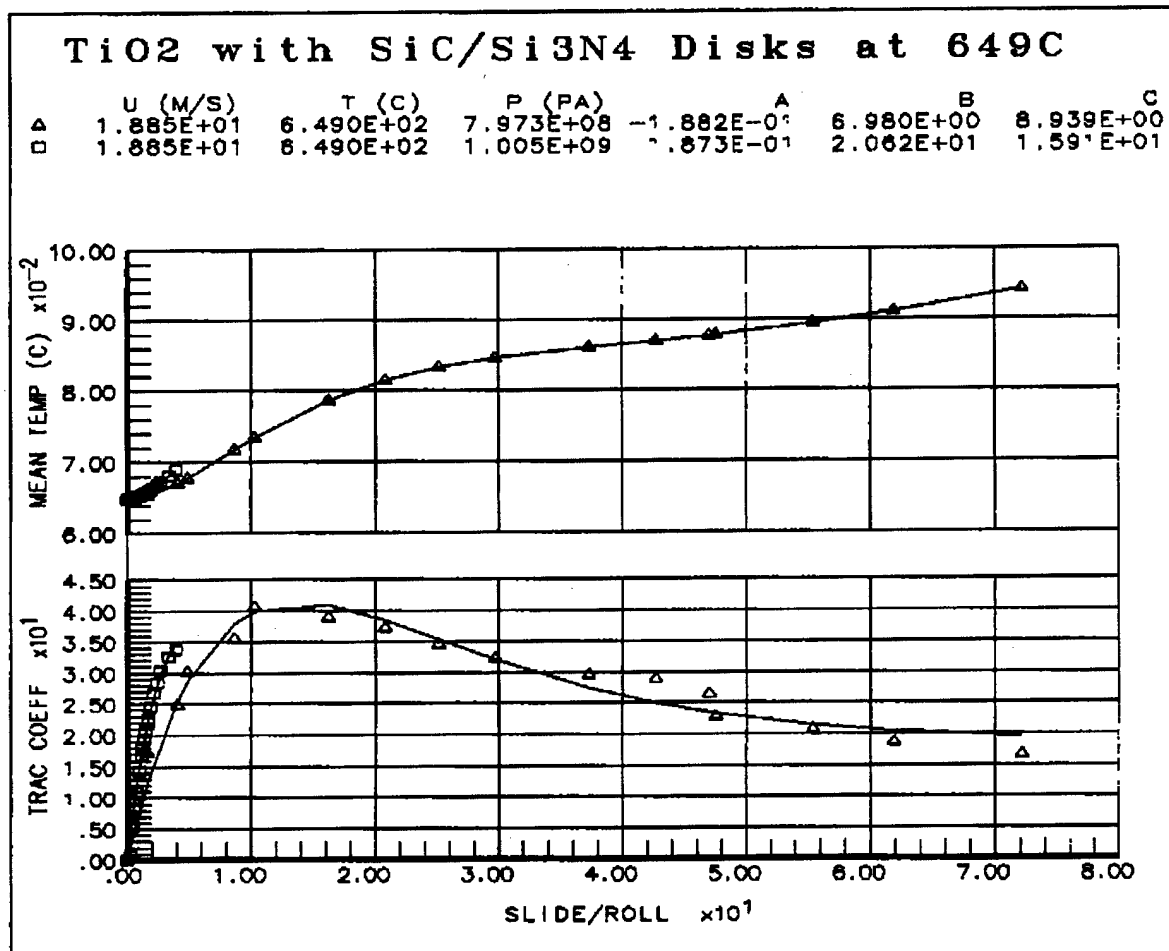


Figure 5-9. Model correlation with experimental traction data obtained with ceramic disk specimens with TiO₂ powder lubricant at 649°C.

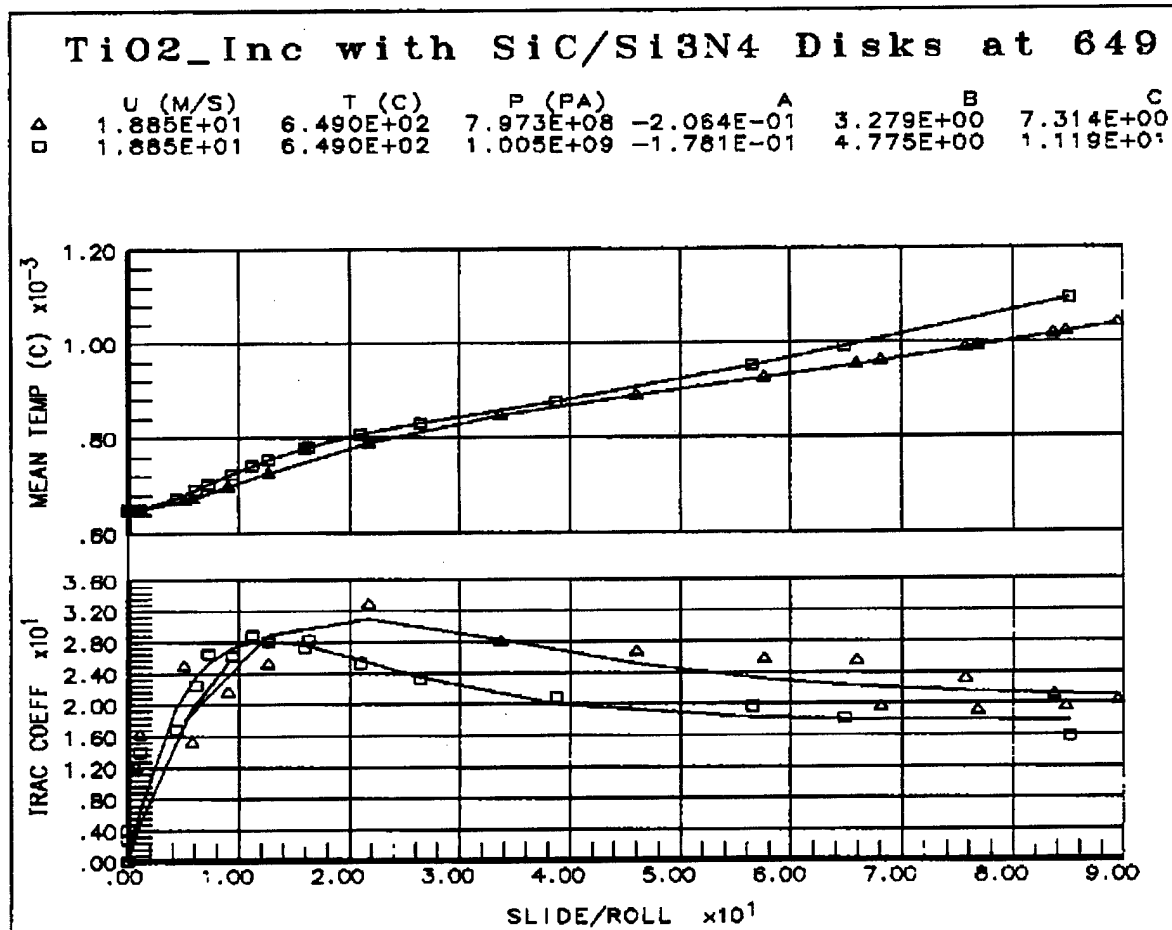


Figure 5-10. Model correlation with experimental traction data obtained with ceramic disk specimens, contaminated with Inconel 718, with TiO₂ powder lubricant at 649°C.

The results obtained with boron nitride powder [30] are shown in figures 5-11 and 5-12. A fair amount of data was also generated with the popular molybdenum disulphide [30], these results are shown in figures 5-13, 5-14 and 5-15.

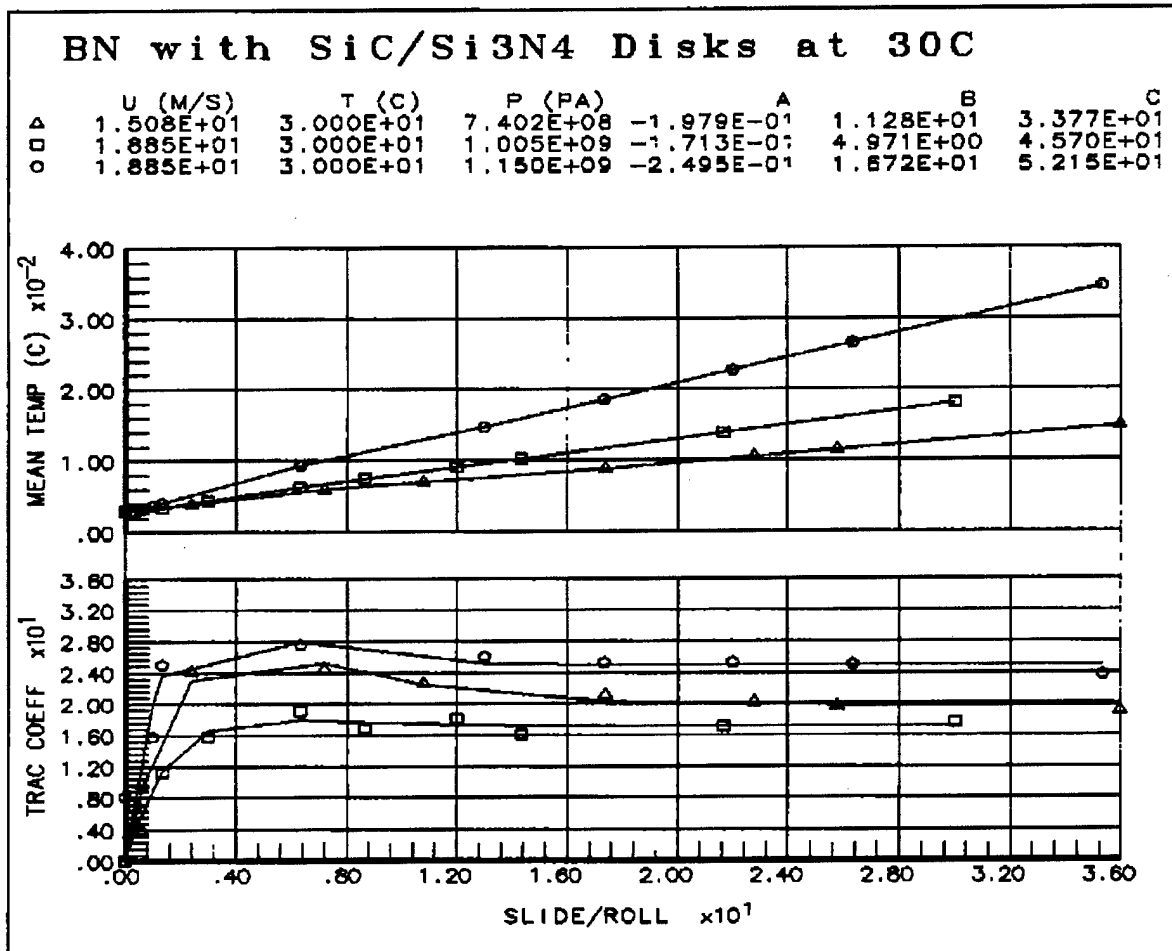


Figure 5-11. Model correlation with experimental traction data obtained with ceramic disk specimens with boron nitride powder lubricant at 30°C.

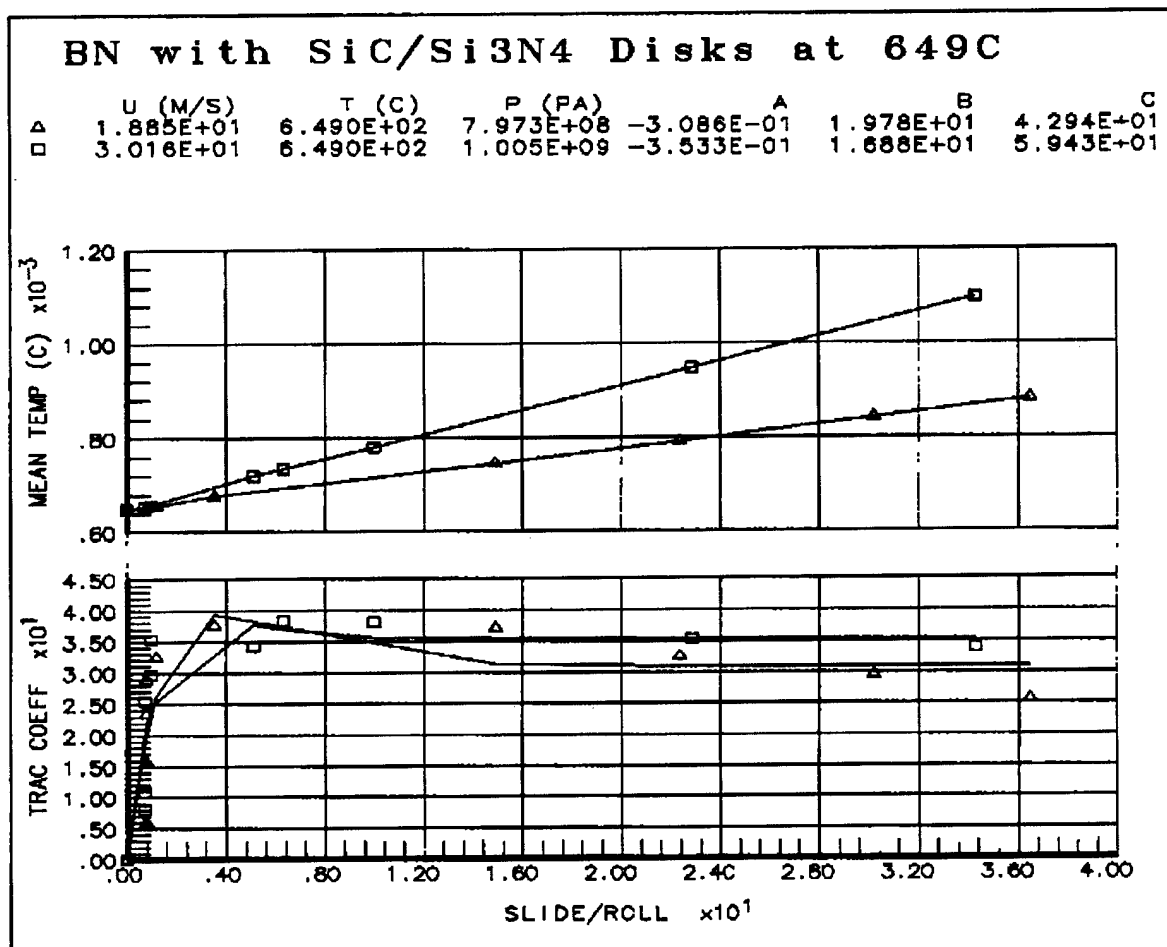


Figure 5-12. Model correlation with experimental traction data obtained with ceramic disk specimens with boron nitride powder lubricant at 649°C.

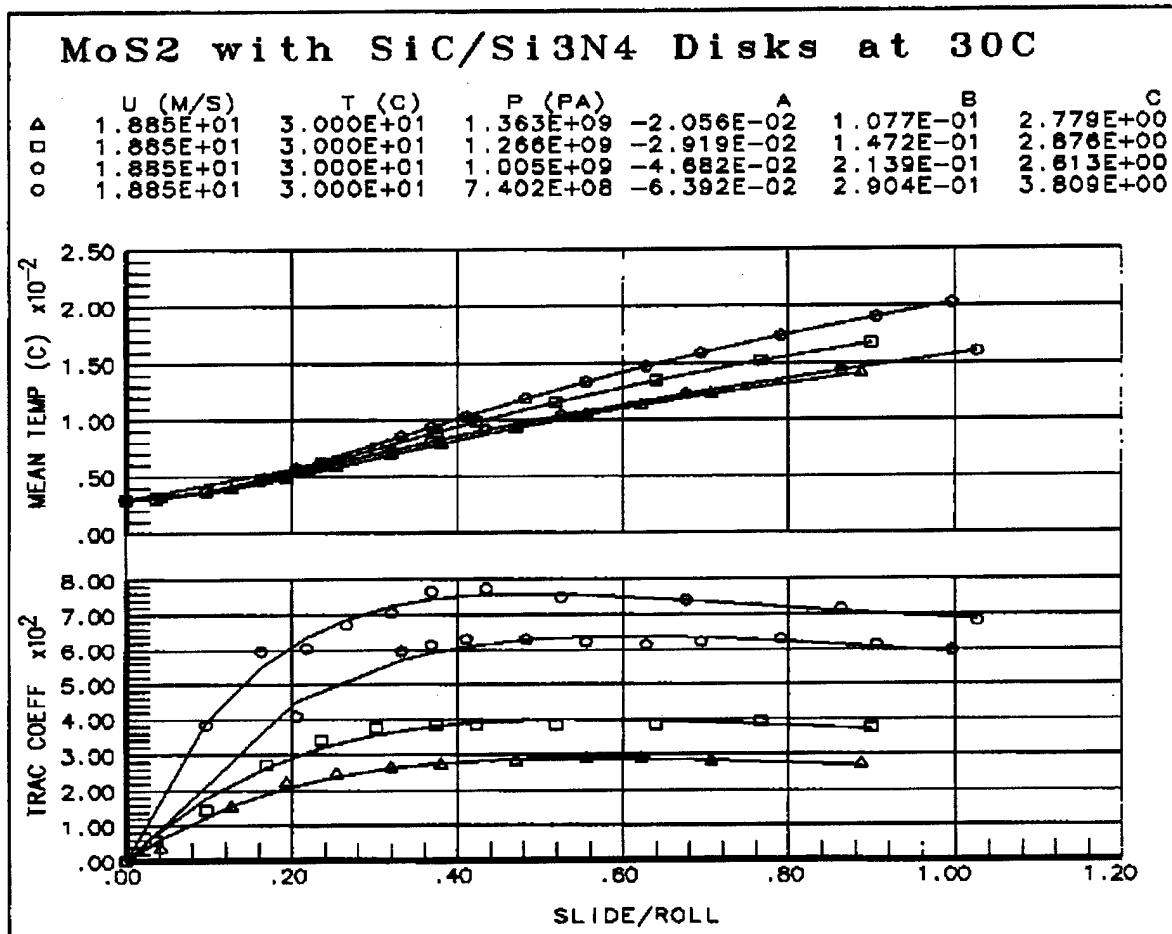


Figure 5-13. Model correlation with experimental traction data obtained with ceramic disk specimens with MoS₂ powder lubricant at 30°C.

MoS₂ with SiC/Si₃N₄ Disks at 427°C

	U (M/S)	T (C)	P (PA)	A	B	C
Δ	1.886E+01	4.270E+02	7.973E+08	-5.274E-02	1.140E-01	4.924E+00
□	1.885E+01	4.270E+02	1.150E+09	-3.161E-02	1.170E-01	2.816E+00
○	3.393E+01	4.270E+02	1.268E+09	-2.470E-02	1.142E-01	7.083E+00

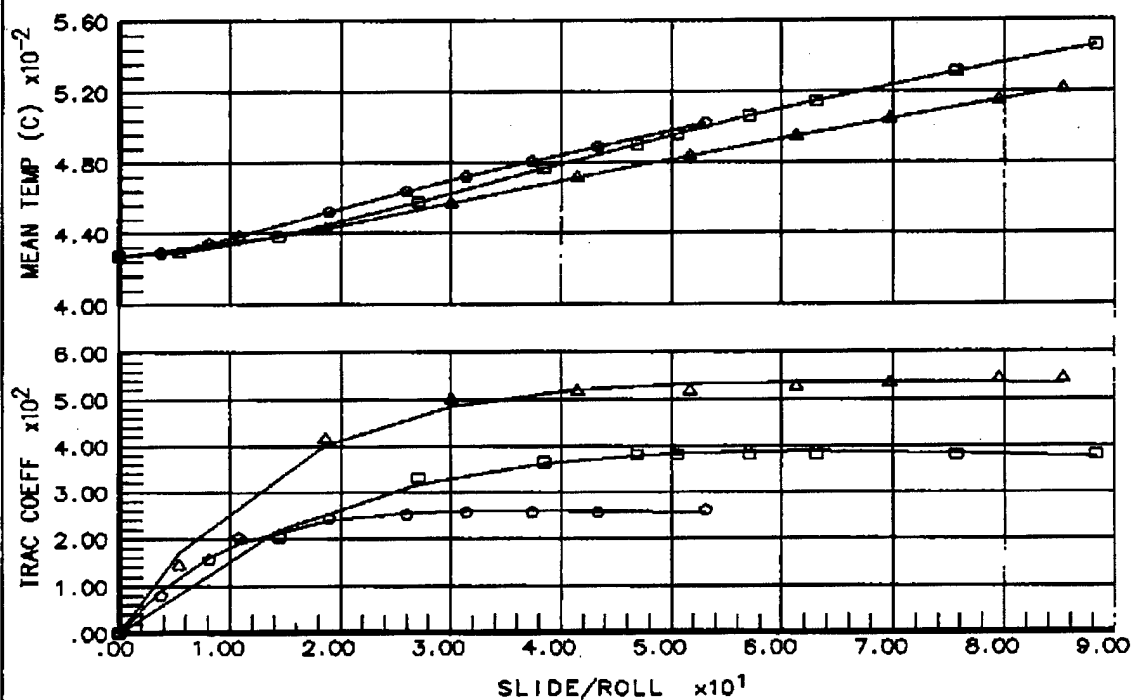


Figure 5-14. Model correlation with experimental traction data obtained with ceramic disk specimens with MoS₂ powder lubricant at 427°C.

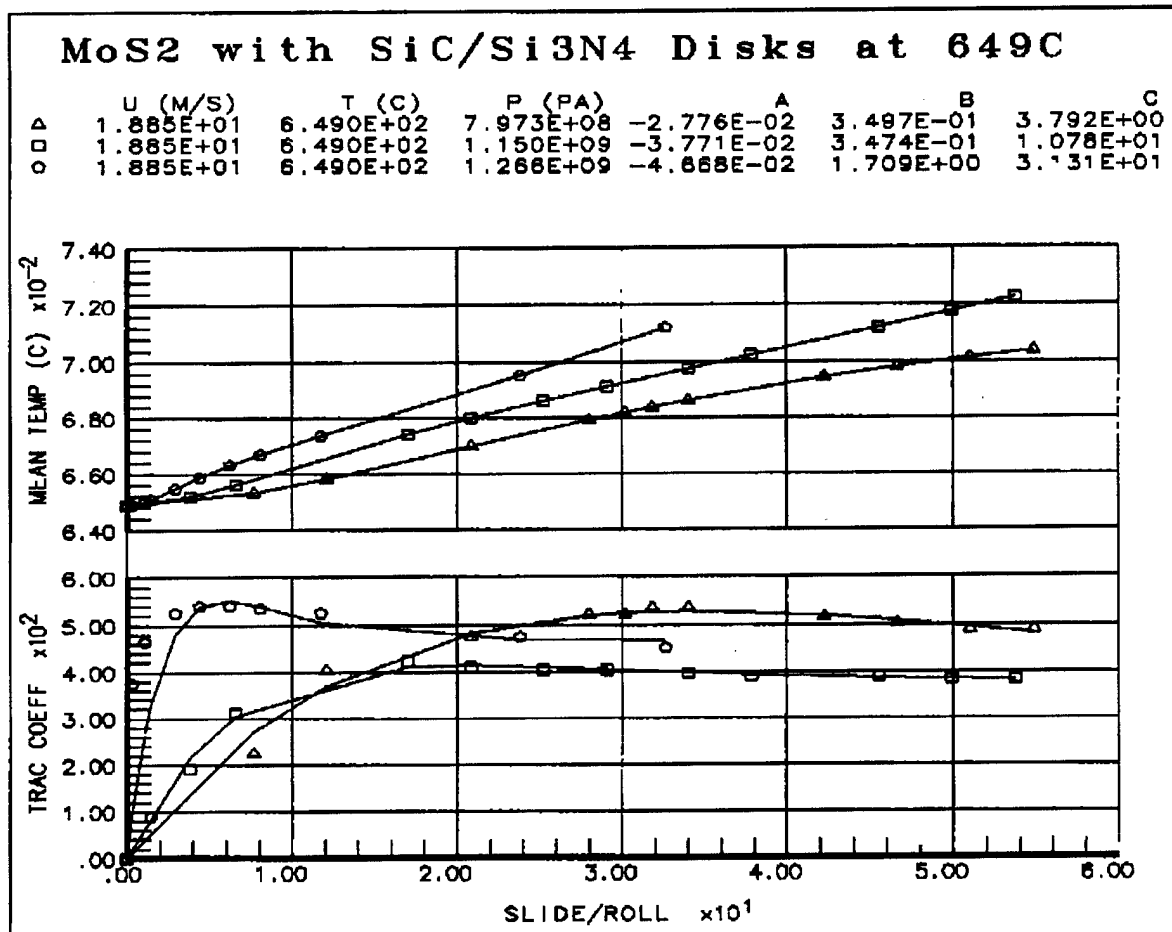


Figure 5-15. Model correlation with experimental traction data obtained with ceramic disk specimens with MoS₂ powder lubricant at 649°C.

A final set of data with powder lubricants was obtained with zinc oxythiomolybdate (ZnMoO₂S₂) between a pair of silicon nitride disks. These results are shown in figure 5-16.

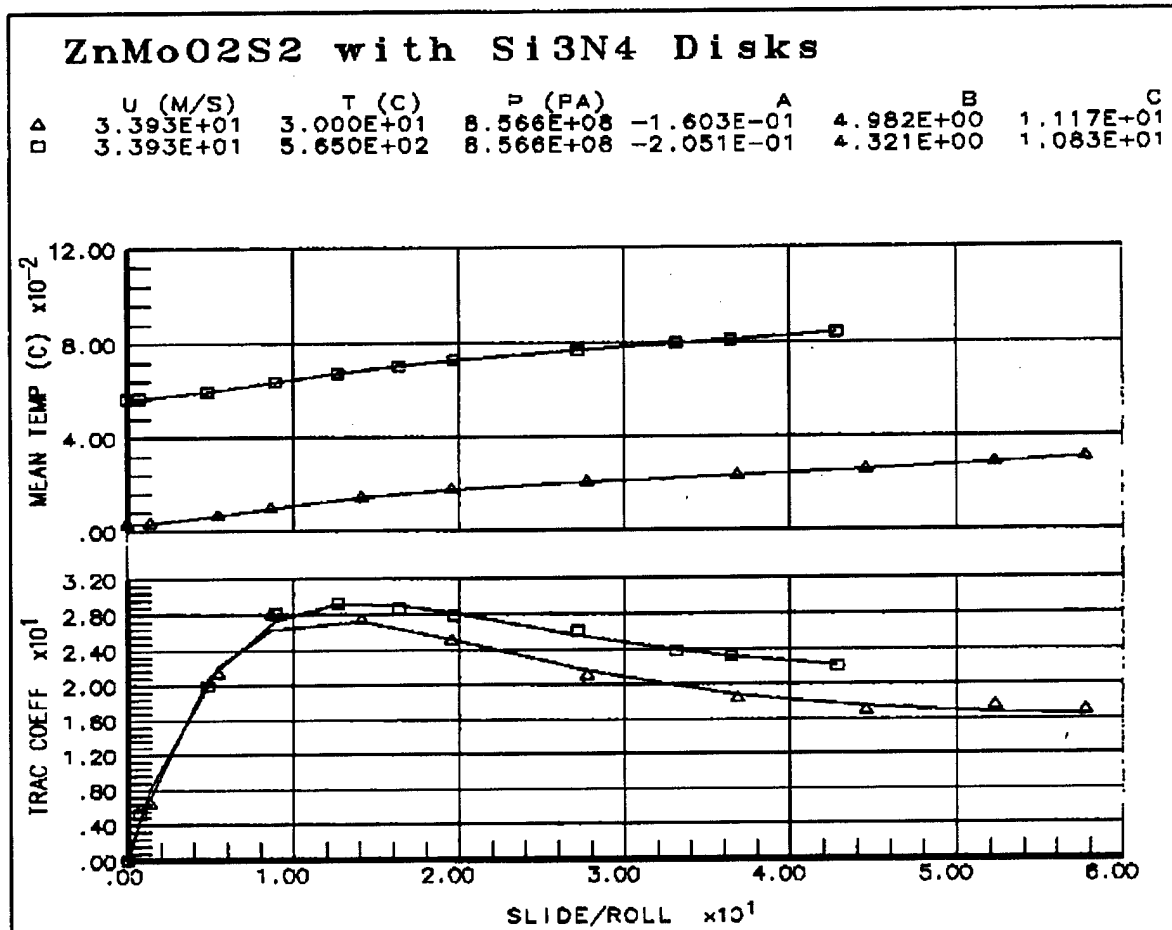


Figure 5-16. Model correlation with experimental traction data obtained with ceramic disk specimens with ZnMoO₂S₂ powder lubricant at 30 and 585°C.

In a very recent investigation, Kukureka, et al. [33], have investigated rolling-sliding contact between polymeric disks. The material is commonly known as POM, polyoxymethylene (acetal) or polyamide (nylon) and it is commonly used for gears. The experimental data reported in this investigation is correlated to the model in figure 5-17. Note, that the temperature calculations are subject to error due to uncertainty in material properties, although the traction correlations are unaffected by any materials constant.

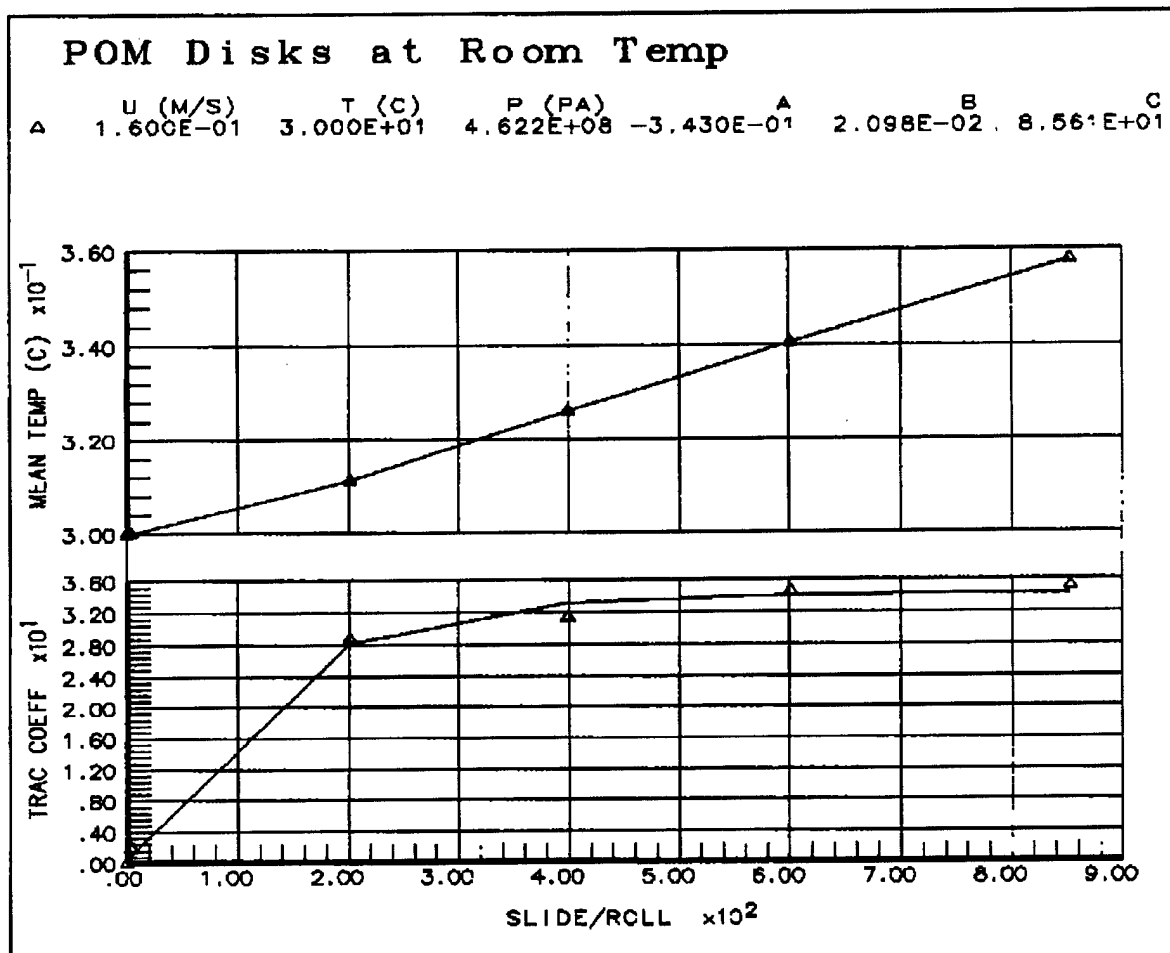


Figure 5-17. Model correlation with experimental traction data obtained with POM disk specimens.

During a course of development of a high-temperature solid lubricated ball bearing, Galbato [53] has carried out traction tests using a K162B (TiC) balls on a silicon nitride flat disk with a number of different lubricants. All these tests were done in a rolling/sliding type of environment. A typical data set with unlubricated contact is correlated in figure 5-18. Here the role of the oxidized surface of the ball at high operating temperature is examined. The model, indeed fits the data well. There may be some uncertainty in the operating conditions and materials property data; however, this will affect only the computed temperatures in the contact.

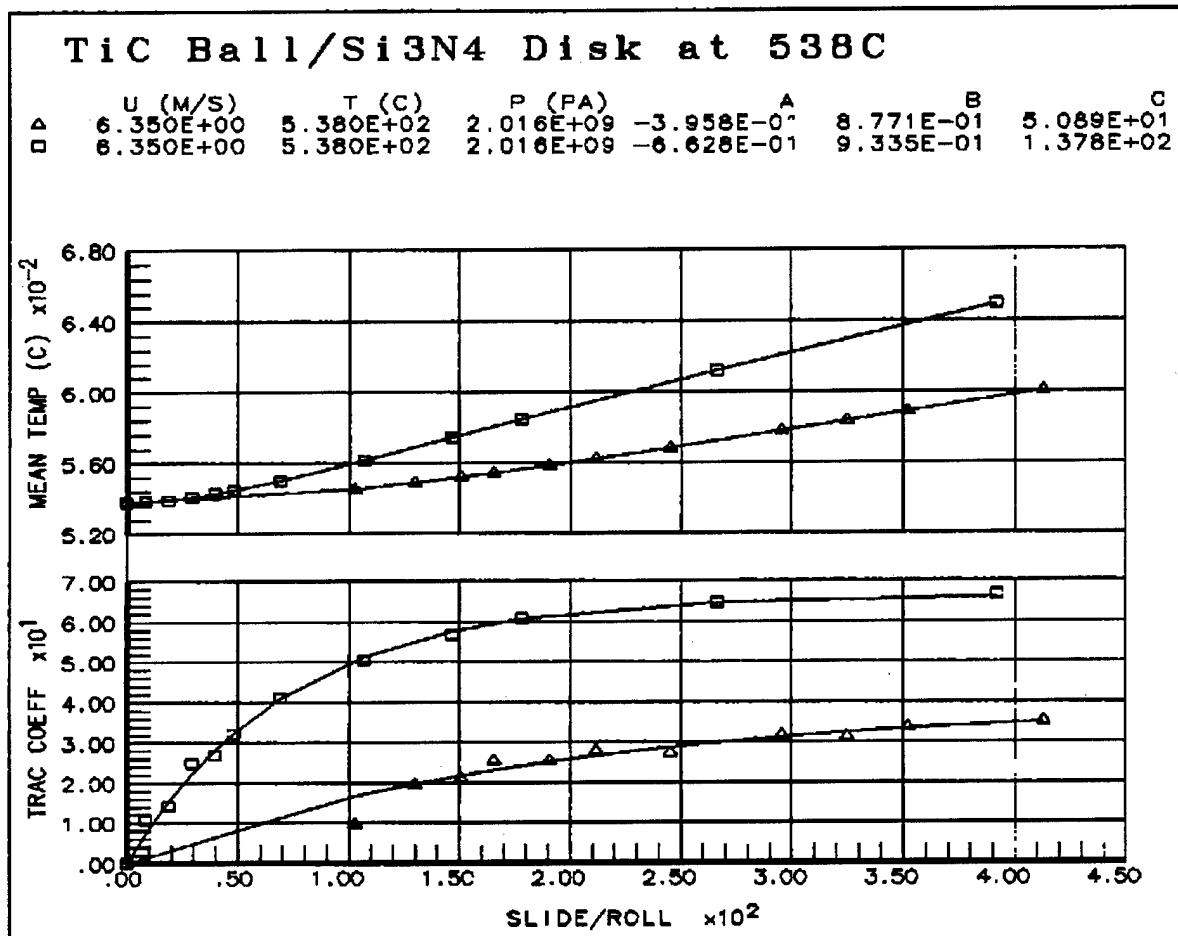


Figure 5-18. Model correlation with experimental traction data obtained with K162B (TiC) ball and silicon carbide disk specimens at high operating temperature.

All of the above correlations demonstrate the practical significance of the model in predicting traction in a given application. The model coefficients, A, B, and C are derived from the regression and correlation of experimental data, as discussed above, and then equation (5-7) may be applied at prescribed operating conditions to predict the traction coefficient.

Clearly, there is a need for more experimental data, particularly with coated solids. Although a number of experimental investigations have been carried out with coated specimens, the friction measurements have been restricted to just measurement of an overall friction coeffi-

cient after sliding the specimens against each other for a set time or duty cycle. This data may be useful in applications where the concentrated contacts are subjected to rather large sliding velocities. For rolling/sliding contacts, however, experimental variation of traction with slip velocities is required.

5.5 Nominal Friction Values for Some Materials

The pin and disk type of friction testers, and other variations, have been employed for friction measurement over several past decades. A detailed review of these investigations is indeed beyond the scope of this investigation. However, some of the very recent data is documented in table 5-1. The nominal friction coefficients compiled in this list will provide some practical guidance for the design of mechanical components with concentrated contacts subject to sliding interaction.

Table 5-1: Nominal Friction Values for Some Materials

Materials	Operating Conditions	Range of Friction Coefficients	Reference
Corundum against TiN, (Ti,Nb)N and (Ti,Al)N coatings	5N load, and 0.1 m/s sliding speed	1.0-1.20	Vancoille, et al. [34]
Corundum against Ti(C,N) coating	5N load and 0.10 m/s sliding speed	0.10-0.20	Vancoille, et al. [34]
Si ₃ N ₄ /SiC disk against SiC and Si ₃ N ₄ pins	Room temp, Pin dia =9.35 mm, Loads = 1-10N, Sliding speed = 0.10 m/s	0.40-0.60	Yust & DeVore [35]
Si ₃ N ₄ /SiC disk against SiC and Si ₃ N ₄ pins with 5W30	Loads = 1-10N, Reciporating sliding, 0.10 m/s	0.080-0.10	Yust & DeVore [35]
Si ₃ N ₄ /SiC disk against SiC and Si ₃ N ₄ pins with 5W30	Loads = 80-300N, Unidirectional sliding 0.10-0.30 m/s	0.015-0.020	Yust & DeVore [35]
Cr ₂ O ₃ Coatings with paraffin oil and additives	Block and ring specimens Load = 539N, Sliding Speed =0.51 m/s	0.080 0.12	Wei, et al. [36]
Steel ball with Ti and TiN coatings against aluminum disk	Coating thickness = 20-74 μm, Load = 98N	~0.40	Kaneta, et al. [37]

Table 5-1: Nominal Friction Values for Some Materials

Materials	Operating Conditions	Range of Friction Coefficients	Reference
Amorphous Hydrogenated Carbon Films on Silicon	Low humidity, contact stress 0.83-1.66 GPa, Sliding speed 0.03-1.0 m/s	0.05-0.16	Gangopadhyay, et al. [38]
Carbon Nitride films on Zirconium	Load = 3.36N, sliding Speed = 32 mm/mn	0.16-0.20	Chen et al [39]
Carbon Graphite Materials against M-50Steel and NBD 100 Silicon Nitride	Oscillating pin/disc, Load = 25N, sliding speed 0.10 m/s	0.10-0.25	Blau and Martin [40]
ZrO ₂ on ZrO ₂ with Ag and Au films with Nb films	Op temp 23-250 °C Cont Stress 208 Mpa Sliding 0.050 m/s	0.14 0.050 0.14	Ajayi, et al. [41]
440C ball against Metal Matrix Composite Polished Disk Etched Disk	Ball Dia 3.125 mm Load 0.2 N, Sliding 0.2 m/s	0.4-0.5 0.15-0.18	Prasad and Mecklenburg [42]
MoS ₂ in Air in Partial Vacuum in Vacuum		0.16-0.18 0.05-0.10 0.003-0.01	Roberts [43]
TiN Films	Thrust Washer Tester Load 222N, sliding 0.7-1.40 m/s	0.35-0.52	Guu, et al. [44]
Steel Pins of Silicon Nitride Disks	200°C 200°C	0.75 0.40	Childs & Mimaroglu [45]
Bonded MoS ₂ Films in rolling/sliding contact	Slid/Roll 0-1.0 Cont Stress 520 MPa	0.10-0.15	Endo, et al. [46]
C ₇₀ Films on Si substrate against 440 SS ball	3.175mm ball, Load 2.5 gm, Sliding 1.40 cm/s	0.50-0.90	Zhao, et al. [47]
Gold & Silver Coatings on silicon again 52100 Steel balls	3.2 mm dia balls 1-100 gm Load	0.10-0.20	Jang and Kim [48]

Table 5-1: Nominal Friction Values for Some Materials

Materials	Operating Conditions	Range of Friction Coefficients	Reference
Coated TiN Couples	Dry Air Dry Nitrogen Humid Air	0.10-0.80 0.20-0.30 0.080-0.10	Santner, et al. [49]
Boron Nitride Films on Silicon against Diamond pins	Reciprocating Tribometer Pin radius 0.25-1.0 mm Load 0.10-0.90 N, Sliding 1.67 mm/s	0.045-0.065 Lower friction at higher load	Watanabe, et al. [50]
Steel ball on (TiAl)N Coat Steel ball on TiN Coat Steel ball on CrN Coat	Load 5-20N, sliding 0.05 to 0.25 m/s	0.60-0.75 0.50-0.60 0.35-0.55	Huang, et al. [51]
M-50 vs NC-132	Ball and Disk, Sliding 0-13 cm/s, Stress 0.70 to 1.7 GPa, Temp 316 °C	0.60-0.80	Bandow, et al. [52]

In addition to the above data, friction behavior as a function of slip rate has been investigated for varying loads and operating temperatures for a number of solid lubricants in a number of programs aimed at development of solid lubricants for rolling element bearings [53-55]. Galbato [53] has documented maximum traction coefficients with silicon carbide and silicon nitride specimens with no lubricant and also with a number of solid lubricants including, Graphite, Cs_2MoOS_3 , ZnMoO_2S_2 , and $\text{BaF}_2/\text{CaF}_2\text{Ag}$. The behavior of ZnMoO_2S_2 powder between ceramic specimens has been more recently examined by Trivedi and Gerardi [54]. Lahrman, et al. [55], have report traction coefficients at 2% slip as a function of temperature with M50 steel balls against M50 disks, M50 balls against Silicon Nitride disks, and Silicon Nitride balls against Silicon Nitride disks, under no lubricants, and with Graphite and MoS_2 mixture, Cesium Oxythiomolybdate and Zinc oxythiomolybdate lubricants. This data was also obtained for design guidance for solid lubricated rolling bearings.

5.6 Other Models for Frictional Interactions

While the traction models and nominal friction coefficients presented above provide design guidance for practical components, a few of the recent investigations have been dedicated to the enhancement of physical understanding of frictional interactions. Komvopoulos [56,57] has postulated that frictional resistance between two interacting surfaces could be divided into the elastic and plastic components of deformation of interacting asperities. Thus, if α represents the fraction of real to apparent area of contact, then the overall friction coefficient, κ , may be defined

as:

$$\kappa = \alpha\kappa_e + (1 - \alpha)\kappa_p \quad \text{Eqn (5-28)}$$

The friction component, κ_e depends on the lubricant shear behavior and elastic properties of the interacting surface, while the plastic component, κ_p depends on the plastic properties of the surface, such as shear strength, strain hardening effects, and interfacial shear stress resulting from adhesion and lubricant effects. The determination of fractional real area of contact, α , is a difficult task, particularly due to the complexities associated with the sliding process. Aside from the sliding mechanism, topographic description and characterization of the surfaces becomes a major input. In some earlier works the terms, "Plasticity Index" introduced by Greenwood and Williamson [58], and "Topographic Index" introduced by Gupta and Cook [59], provide some guidance for elastic and plastic contacts between rough surfaces. Elastic and plastic contacts of interacting asperities have also been modeled by Gupta and Cook [60]. In a more recent investigation Zhang and Kato [61] have further implemented the statistical aspects of rough surfaces into the basic model for frictional interaction proposed by Komvopoulos [56,57]. Friction and wear models based on statistically distributed contact spots, formed by interacting asperities, have also been presented by Zhao and Liu [62]. This work also considers some chemical aspects by dividing the stochastically distributed contact spots into three categories: oxide-oxide, metal-metal and metal-oxide. The friction force is computed by the interfacial shear stress for these three types of contacts and their respective areas of contact. While investigating the behavior of Teflon transfer films in rolling bearings, Dareing [63] has presented a model for computing traction coefficients from elastic deformation in the transfer film, the surface coating and the substrate.

6. WEAR MODELING

Over the past several decades, a rather vast amount of tribological literature has been devoted to the fundamental mechanics of wear and development of models for the prediction of wear rates in mechanical components. A fair review of this literature is clearly beyond the scope of the present discussion. Only a few of the investigations, which have direct relevance to the technical approach presented in the next section, are discussed below. Perhaps, some of the well established texts, such as [23,64], may be referred to for a more complete listing of the early works.

Wear in mechanical components subject to sliding interaction has been known to be a very complex phenomena. Aside from the mechanical deformation of surfaces, the friction at the interface generates heat, which often alters the tribological characteristics of the surfaces and thereby affect the wear rates. Similarly the operating environment may promote chemical processes which alter the surface properties and therefore affect the friction and wear behavior. Due to such complexities in the mechanics of surface interaction, the development of a universal wear model has been a very difficult task. In fact, even well controlled experimental investigations have often failed to produce repeatable results, primarily due to difficulties in controlling all the significant variables. This results in a rather large scatter in experimental wear data which makes even the task of curve fitting a model a difficult one. The more fundamental investigations aimed at understanding the mechanics of wear do result in technically sound hypothesis, but again due to uncertainties in the operational and materials variables, they remain quite weak for prediction of wear in actual practical application. Wear experiments under simulated conditions, have therefore been an integral part of every materials development project.

The objective of this investigation is to formulate a semi-empirical model which integrates the mechanical, thermal and chemical interactions. Rather than modeling the fundamental mechanics of the wear process, the emphasis here is to develop an empirical wear equation which could be used for wear prediction with reasonable caution. The approach is no more than curve fitting of experimental data, as done for friction modeling in the preceding chapter. Similar to the friction model, the wear equation has certain constants which may be computed by regression analysis of experimental data. Unlike the friction or traction problem, however, the difficulty in wear modeling is that the term, "wear coefficient," is not as well established as the friction or traction coefficient. Furthermore, most of the experimental data available is of qualitative form, such as, size and shapes or wear scars, SEM and Auger studies of wear surfaces, the change in surface characteristics due to wear, etc. Whatever quantitative data consisting of wear volume or mass as a function of operating variables is available, it has a rather large scatter, which may permit a fit with many hypothetical models with equal confidence. Thus, the present investigation is restricted to a qualitative comparison of the proposed wear model with available experimental observations, and a rigorous computation of model coefficients is deferred until more experimental data becomes available. Although, due to uncertainty in the coefficients, the model will not have immediate design significance, it will certainly provide some guidance for formulating experimental investigations required for materials development for a given application. Hopefully, with the continued growth of the experimental investigations, a reliable database for model coefficients for prediction of wear may be established, as it is presently done for prediction of friction.

6.1 Proposed Wear Model

The starting point for most of the wear models is generally the simple wear equation, where the wear volume, w , is directly proportional to the applied load, Q , and sliding distance, L , and inversely proportional to the hardness, H . Symbolically,

$$w = K \frac{QL}{H} \quad \text{Eqn (6-1)}$$

where K is a proportionality constant.

In the above fundamental equation, sometimes the sliding velocity, $V = L/t$ may be used in place of the sliding distance to obtain volumetric wear per unit time, $W = w/t$, and the wear equation may be written as

$$W = K \frac{QV}{H} \quad \text{Eqn (6-2)}$$

By analyzing interactions between micro asperities, Archard [65] has shown that if k is the probability of a wear fragment being formed, when two spherical asperities interact with each other, then the proportionality constant K in the above equations is found to be equal to $k/3$. With such a physical significance, the coefficient K is commonly referred to as Archard-type wear coefficient.

With equations (6-1) or (6-2) as a starting point, there has been a rather large number of investigations dedicated to the more extensive physical significance of the wear coefficient. Also, varying amount of regression analysis has been used to improve the fit between experimental wear data and a wear rate relation, similar to equation (6-2). The works by Mecklenburg [66], and Meeks and Bohner [67], present some examples of power law variations, rather than direct proportionality. In a very general form such a relation is written as

$$W = K \frac{Q^a V^b}{H^c} \quad \text{Eqn (6-3)}$$

where, a , b and c are exponents to be determined from regression analysis of experimental wear data. Also, the values of these exponents may be constrained to keep the wear coefficient dimensionless. Clearly, when all exponents are equal to one, the wear rate equation reduces to the basic Archard-type relation.

In all of the above type of wear equations there is no direct input for temperature, and wear is basically postulated as a mechanical phenomena. With modern development of composite materials and solid lubricants for use in high-temperature environments, however, thermal interaction and its effect on friction and wear has become a subject of significant interest. Some friction and wear experiments have been conducted as a function of temperature, although the available data is too little for development of a model. Aside from the overall operating temperature, the

interfacial temperature rise, resulting from friction, has been known to alter the tribological behavior of interacting surfaces. The interfacial temperature affects both surface friction and stress distribution in the solid. In addition, the properties of some of the modern materials are temperature dependent. Based on such an understanding, dependence of wear rate on temperature is a very logical question.

Wear of cutting tools, where a concentrated sliding contact is formed between the tool surface and the chip of material being cut, has been shown to strongly depend on the contact temperature. Again, there is a large amount of literature available on this subject, the early works by Cook and Nayak [68], and Gupta [69], are just two examples. Here the wear process is considered as a thermally activated phenomena, where the wear rate, W , is written as

$$W = W_0 e^{-\Phi/(RT)} \quad \text{Eqn (6-4)}$$

Here R is the universal gas constant, T is the absolute temperature, and Φ is the activation energy.

In more recent investigation, Gautier and Kato [70] have related the wear phenomena to the frictional dissipation represented by κQV , where κ is the effective friction coefficient. Vancoille, et al. [71], have applied the thermal activation principal, similar to equation 6-4, to sliding wear of TiN coatings. The wear process has also been related to oxidation of the surfaces, which is a thermal phenomena. Kukureka, et al. [33], while studying wear of polyoxymethylene (POM) surfaces have shown that the wear phenomena changes mild to severe as the temperature at the surfaces rises above a certain level. Pathak, et al. [72], have parametrically measured wear of bearing alloys, as a function of composition, applied load and sliding velocities; they have shown that the contact temperature depends on the test conditions and amount of cadmium in the alloy. Thoma [73] and Suzuki, et al. [74] have shown that the wear rates for the materials tested reduce to a minimum value, before they increase with increasing temperature.

Based on the above investigations, it is clear that the thermal impact on wear is more complicated than the mechanical counter part, where the wear is proportionally related to loads and sliding velocities. If wear is related to chemical reaction of surfaces as a function of temperature, and the property distribution in the sliding contact, then it is quite reasonable to assume that more than one phenomena will contribute to wear. Such a speculation is similar to what has been done in modeling friction of rough surfaces [56-62]. Also, Ramesh, et al. [75], while investigating wear of composite coatings have considered the wear process in terms of four different mechanisms, which are grouped into two categories: wear due to pure sliding and wear resulting from all other mechanisms. We can postulate that the total wear rate in the basic wear equation [6-2] may be partitioned into several parts, with each part representing a given mechanism. Symbolically, the wear equation may then be written as

$$W = \sum_{i=0}^n W_i \quad \text{Eqn (6-5)}$$

In the above equation, the first partition may represent Archard-type wear, while the other partitions may be thermally activated according to the relation of the type shown in equation (6-

4). Furthermore, in the thermal activation equation, it may be more convenient to express the temperature as a temperature difference, rather than absolute temperature; also this difference in temperature may be scaled relative to a reference temperature. Thus, if T_o is a reference temperature and T is the absolute temperature, then we may define a dimensionless temperature,

$$T^* = \frac{T - T_o}{T_o} \quad \text{Eqn (6-6)}$$

and the thermal activation process may be written in the form:

$$W^* = W_o^* e^{\Phi^* T^*} \quad \text{Eqn (6-7)}$$

Now in equation (6-5) if we assume the first term, $i = 0$, to be the Archard term, the remaining terms, $i = 1, n$, to be thermally activated per equation (6-7), then combination of equations (6-5) and (6-7) will yield:

$$W = \frac{KQV}{H} \left[a_o + \sum_{i=1}^n a_i e^{\Phi_i T} \right] \quad \text{Eqn (6-8)}$$

Here we have dropped the asterisks on Φ and T for brevity. Also, the reference temperature T_o in equation (6-6) may be defined such that at this temperature the total wear reduces to the Archard-type equation. Thus, at $T = 0$, equation (6-8) should reduce to equation (6-2). Hence

$$a_o + \sum_{i=1}^n a_i = 1 \quad \text{Eqn (6-9)}$$

Now combining equations (6-8) and (6-9) to eliminate a_o , and scaling the wear rate relative to the Archard-type wear at temperature $T = 0$, yields

$$W^* = \frac{W}{\frac{KQV}{H}} = \left(1 - \sum_{i=1}^n a_i \right) + \sum_{i=1}^n a_i e^{\Phi_i T} \quad \text{Eqn (6-10)}$$

Finally, by dropping the asterisk, once again, the final form of the wear model may be expressed as a dimensionless wear equation:

$$W = \left(1 - \sum_{i=1}^n a_i \right) + \sum_{i=1}^n a_i e^{\Phi_i T} \quad \text{Eqn (6-11)}$$

For practical application of equation (6-11) note that the dimensionless wear rate is a ratio of actual wear rate to the Archard-type wear rate at the selected reference temperature, at which all exponential temperature terms are unity. In most wear experiments the data is presented in terms of wear volume per unit load per unit sliding distance and the Archard-type wear rate in equations (6-1) and (6-2) is written as

$$\tilde{w} = \frac{w}{QL} = \frac{W}{QV} = \frac{K}{H} \quad \text{Eqn (6-12)}$$

Thus, the normalizing Archard-type wear rate can be either in the common units of wear volume per unit load per unit sliding distance, or in terms of wear volume per unit time. When correlating the model to the experimental data, the measured wear rates in either units are converted to ratios, using the base as Archard-type wear rate at the reference temperature.

Clearly, extensive experimental investigations are required to physically substantiate the above wear model. At present, the model is no more than an algebraic equation which could be used to correlate any available experimental data. Such correlations, although lacking physical justification, they may offer significant potential for practical design and materials development.

6.2 Model Correlations

For the present investigation, the small amount of data obtained by Thoma [73] and Suzuki, et al. [74] is used to just validate the model significance by showing a somewhat qualitative comparison between the model and experimental observations. Both sets of these data show that the wear rate reduces to a minimum at about 200°C, and then increases with increasing temperature. The general form of the wear-temperature curve resembles a hyperbolic cosine function. Such an observation immediately suggests using two terms in equation (6-11). Symbolically,

$$W = 1 + a_1(e^{\Phi_1 T} - 1) + a_2(e^{\Phi_2 T} - 1) \quad \text{Eqn (6-13)}$$

For the data obtained by Thoma [73] for titanium alloys, model correlations are shown in figure 6-1. Note that since the number of data points available are not adequate to perform a detailed regression analysis, Φ_1 and Φ_2 are set equal to +1 and -1, respectively. This will give a hyperbolic cosine variation if the coefficients a_1 and a_2 are equal. However, these coefficients are calculated by fitting the model at the first and last point in the experimental data set. The reference point was selected at 200 °C where the wear was minimum. The computed values of the coefficients are documented in the legend in figure 6-1. Also documented in the figure are the wear quantities at reference temperature, in units of wear volume per unit load per unit sliding distance, and the value of reference temperature.

Correlations of the model with the data obtained by Suzuki, et al. [74] with a composite material are shown in figure 6-2. The data was obtained with a composite pin against an M50 steel disk. The base composite material consists of 80% MoS₂ + 10% MoO₂ + 10% Nb. In the second set, 5% 304 steel was added while MoS₂ was reduced to 75%. Again, due to a limited number of

data points in the curves, the procedure discussed above is used to compute the coefficients. The reference point was again selected at 200 °C at which the wear rates were minimum and maximum, respectively, for the two data sets shown in the figure.

Indeed, the correlations of the model to both the above experimental data sets are quite encouraging. When applying the computed coefficients to a practical application, it must be remembered that the wear rate in equation (6-12) is in dimensionless form. It must be multiplied by the wear rate at reference temperature to get the actual wear rate. These reference wear rates are documented in the data correlation plots in figure 6-1 and 6-2. Also, care must be used when extrapolating the model beyond the range of experimental data. This is particularly significant when the wear rate is maximum at the reference temperature and it reduces with both lower and higher temperatures, as shown in the second data set in figure 5-2. The extrapolation may yield a negative value which has no practical significance.

Similar to the approach used in friction model, equation (6-11) may be fitted to a set of experimental data to derive the various coefficients by regression. Although the amount of data presently available is not adequate to perform a rigorous correlation of the model, it is anticipated that with increasing interest in high-temperature data the required wear data as a function of temperature may soon become available.

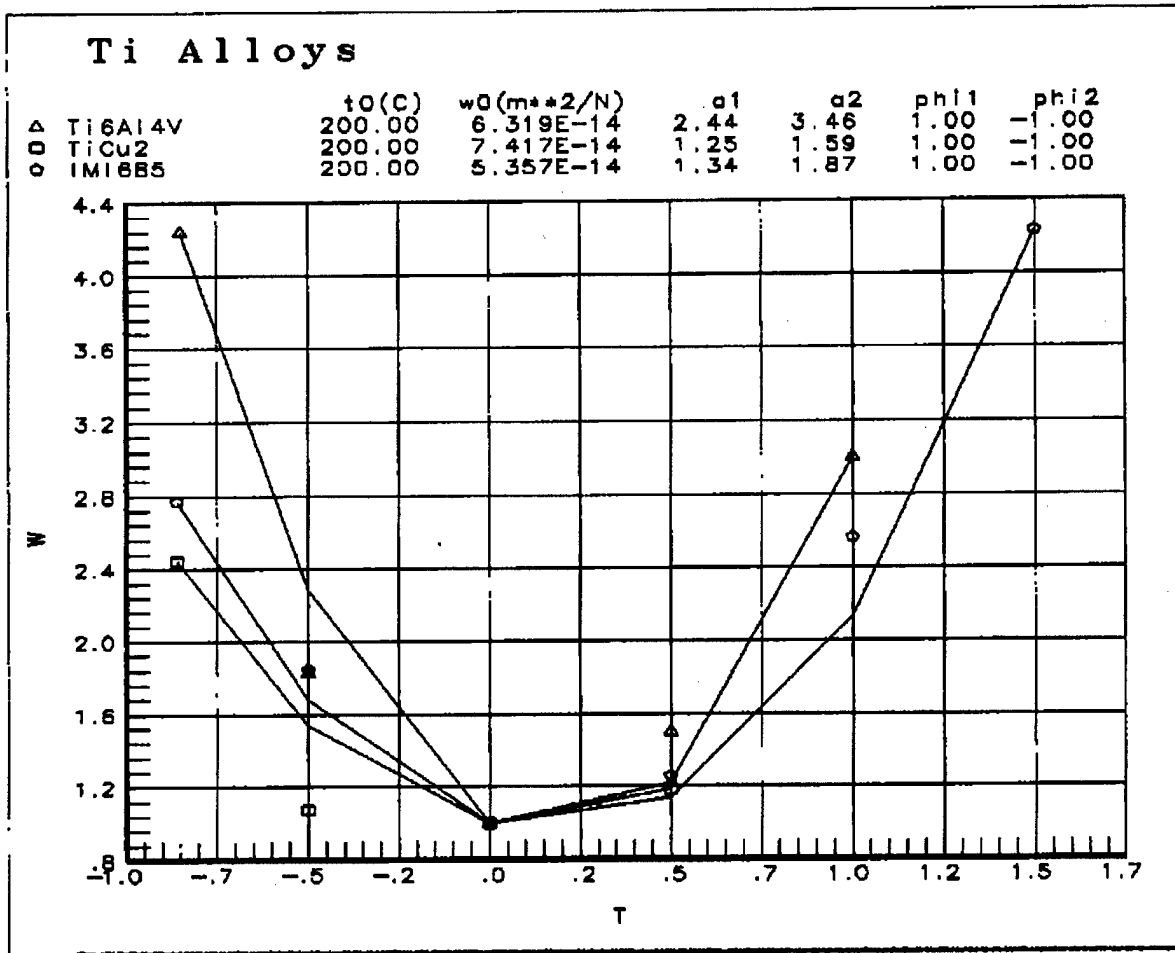


Figure 6-1. Model correlation to experimental wear data obtained with titanium alloys [73].

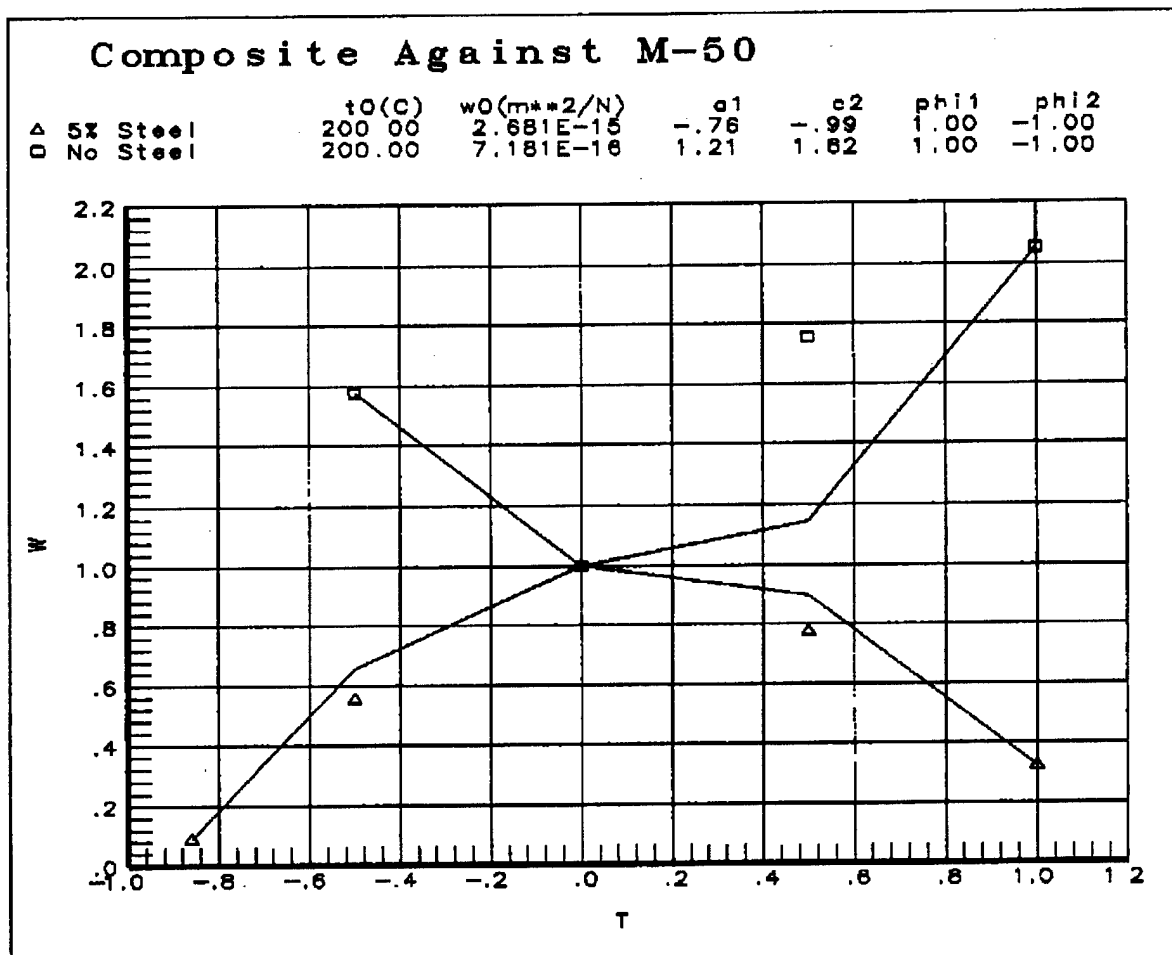


Figure 6-2. Model correlations to experimental wear data obtained with a pin of composite material against an M50 steel disk [74].

7. MODEL INTEGRATION AND DESIGN GUIDANCE

Once the basic models for stresses, friction and wear have been developed, they may be applied, in an integrated fashion, to obtain practical design of mechanical components. Although the models presented in preceding chapters require additional experimental validation and correlation, for the purpose of discussion in this chapter let us assume that the models have been fully validated and are available for design purposes. Then the design of a tribological design of a component shall consist of the following steps:

1. Determine the operating environment
2. Component analysis
3. From tribological behavior of the materials select potential materials
4. Perform stress analysis to determine coatings thicknesses
5. Predict friction and interfacial temperatures
6. Go back to the stress model and recompute thermal stresses
7. Compute wear rates and life over prescribed duty cycles

7.1 Operating Environment

Normally a systems analysis, which is not a part of the present model development, is required to determine the operating environment the particular component shall be exposed to. For example, for the design of a rolling bearing, the operating loads, speeds, temperatures, stiffness and life requirements have to be determined by carrying out an analysis of the entire system. Depending on the application, such an analysis may be quite cumbersome. If the anticipated operating conditions cannot be easily determined, it may suffice to determine an envelope of conditions which include the anticipated conditions.

7.2 Component Analysis

After establishing the range of operating conditions, a component model may be employed to parametrically evaluate component performance as a function of tribological behavior. For rolling bearings, this will constitute overall bearing behavior as a function of traction at rolling element to contact contacts, and friction at the cage contacts. Such a parametric evaluation shall provide a range of desirable tribological behavior for acceptable component performance.

7.3 Potential Materials

Databases for available materials may then be searched to select potential materials. This will include selection of base materials, any potential coating materials and lubricants. In the event the existing materials do not meet the desired needs, the parametric studies in step 2 shall provide guidance to the materials scientist for the development of new materials. In this case, it will also be necessary to carry out the basic friction and wear testing to estimate appropriate coefficients of the friction and wear models outlined in the preceding chapters.

7.4 Stress Analysis of Coatings

After establishing the potential materials, the stress model may be used to compute mechanical stresses in the coatings and at the interfaces between coatings and coating and substrate. The computer code LAYER, presented earlier, shall be very effective in carrying out this task. Of course, LAYER is a plane-strain model; it will, therefore, model only two-dimensional contacts. In the event the contact geometry is such that a full three-dimensional treatment is necessary, then using the finite element models will be more appropriate. These techniques for a single concentrated contact have been discussed earlier in chapter 4.

7.5 Surface Friction and Thermal Dissipations

The friction models may now be used to estimate surface shear stresses and energy dissipation in the rolling sliding contacts. Since the component performance is often sensitive to the frictional behavior, it may be necessary to perform the component analysis again to determine the slip patterns and overall thermal dissipations in the contacts.

7.6 Combined Mechanical and Thermal Stress Analysis

Coating stresses are now updated for the frictional and thermal contributions. For surface friction the boundary loading may be prescribed as surface shear in both the two-dimensional analysis in LAYER and in the more generalized finite element model. The stresses computed in the coatings will eventually have to be superposed on the stresses computed earlier under normal loading. Before, such a superposition, however, the finite element model may be used to model the thermal problem. This will be a two step process: first the temperature distribution in the solid is estimated by prescribing a surface heat flux, then the thermal stresses resulting from the temperature field are computed. Here variation in thermal coefficient of expansion of the different coating materials shall also be taken into consideration. In addition to these stresses, there may also be residual stresses in the coatings resulting from the fabrication process if the material deposition is carried out at a high temperature and the solid is subsequently cooled. This can also be easily accomplished by the finite element model as illustrated in chapter 4. Total stresses in the coated solid, therefore, consist of the following four components:

- a. Stresses due to normal loading on the surface
- b. Stresses resulting from surface shear stresses due to friction
- c. Thermal stresses resulting from frictional dissipation on the surface
- d. Residual stresses arising from the coating deposition process

All of these components of stresses may be linearly superposed to determine the total stress field and thereby evaluate possible failures of coatings. The output post-processors in the finite element package provide the tools for convenient superposition of various solutions.

7.7 Analysis of Wear and Component Life

The final step in the design process will be model wear based on the wear models presented in the preceding chapter. These models for a given contact will have to be incorporated in

the component model to compute overall wear as a function of applied conditions. As the materials at the various contacts wear, the coating thickness will reduce and in the event of active chemical processes during wear, the mechanical properties of the coating may change as well. This will require recomputation of stresses. If the stresses resulting of these modified coating thicknesses and properties indicate potentials for failure, then the amount of time it takes for the wear process to produce these critical conditions will define the wear life of the component. For applications, such as rolling bearings, the changing clearances, resulting from the wear process, may trigger certain instabilities which may lead to potential bearing failure [76]. In such an event the time required for the wear process to produce the critical change in clearances shall define wear life of the bearing.

Based on the above discussion, figure 7-1 schematically outlines the integrated modeling approach. It is clear that in addition to the three basic tribological models formulated in this investigation, models for system analysis and overall components performance are integral parts of the development process.

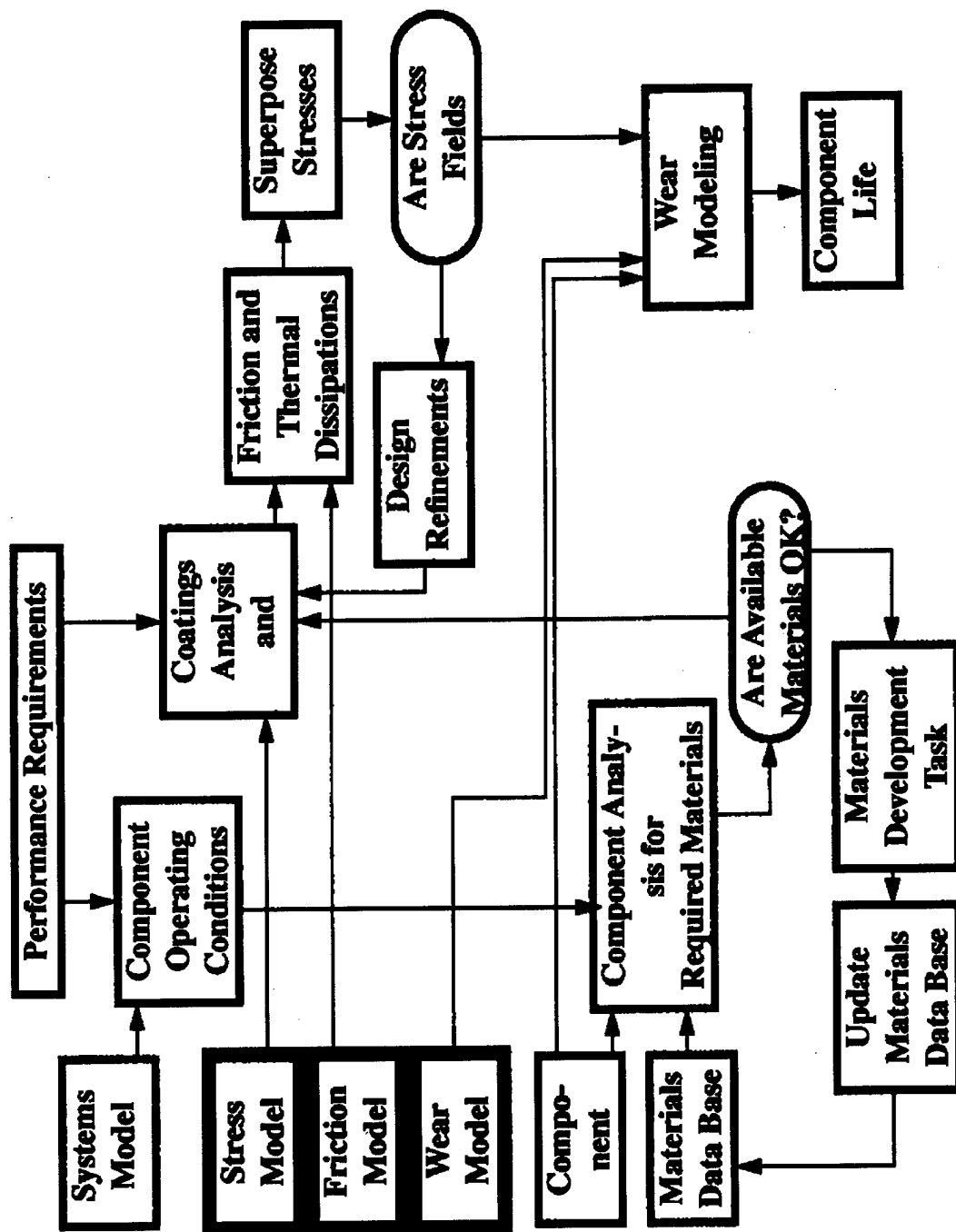


Figure 7-1. Model application for practical design.

8. RECOMMENDATIONS FOR FUTURE DEVELOPMENT

Models for prediction of stresses, surface friction, and wear of solids subjected to sliding or rolling/sliding interaction have been developed in the present investigation. The stress models are based on well established theories of applied mechanics and techniques for finite element modeling. They are therefore quite strong in predictive capability. The only limitation is that the materials have been assumed to be homogeneous. When applying these models to practical problem, the only uncertainties will be in terms of materials properties and input operating conditions. The friction model consists of an empirical equation which can be curve fitted to experimental data to derive the significant model coefficients. Model correlations have been performed with some experimental data, however, there is a need for further validation. In order to model wear, a multi-process model is postulated where one of the wear processes consists of conventional Archard-type wear while other processes are thermally activated. The model shows strong potential for correlating experimental wear-temperature data which cannot be treated with conventional models. Although correlations with two sets of available experimental data show reasonable fit to the model, more extensive experimental work is required before the model can have acceptable design significance. On the whole, it is anticipated that the following development will enhance the models developed under the present investigation:

1. Traction experiments using a rolling/sliding type of contact are required for the newly developed high temperature materials and lubricants. The experimental data should include traction as a function of slip rate with prescribed rolling speed, contact load and nominal temperature. Such data when correlated with the model developed herein, will result in a coefficients database which can be readily applied to the design and performance simulation of mechanical components, such as, rolling bearings and gears.

2. Pin and disk types of friction tests should be run at sliding speeds higher than the values reported in the literature (generally less than 1 m/s). This will permit realistic modeling of sliding contacts, as encountered in ball/cage interactions in a ball bearing.

3. Carefully controlled pin and disk type of experiments can also provide wear data as a function of operating loads, speed and temperature. Such data when correlated with the multi-process model developed in the present investigation will result in a wear equation with good predictive capability.

4. A thorough microscopic examination and chemical analysis of the worn surfaces may provide valuable insight into the most dominant processes of wear, and thereby provide physical justification to the correlated coefficients of the model.

9. REFERENCES

1. Aleksandrov, V. M., "Asymptotic Methods in Contact Problems in Elasticity Theory," *Prikladnaya Matematika y Mekhanika*, vol 32, in English translation, pp 691, 1968.
2. Aleksandrov, V. M., "Asymptotic Solution of the Contact Problem for a Thin Elastic Layer," *Prikladnaya Matematika y Mekhanika*, vol 33, in English translation, pp 49, 1969.
3. Meijers, P., "The Contact Problem of a Rigid Cylinder on an Elastic Layer," *Applied Scientific Research*, vol 18, pp 353, 1968.
4. Wu, T. and Chiu, Y. P., "On the Contact Problem of Layered Elastic Solids," *Quarterly of Applied Mathematics*, XXV, pp 233, 1967.
5. Pao, Y. C., Wu, T. and Chiu, Y. P., "Bounds on Maximum Contact Stress of an Indented Elastic Layer," *Journal of Applied Mechanics*, vol 38, No. 3, Trans ASME, vol 93E, pp 638, 1971.
6. Gupta, P. K. and Walowit, J. A., "Contact Stresses Between an Elastic Cylinder and a Layered Elastic Solid," *Journal of Lubrication Technology*, ASME Trans, vol 96F, No. 2, pp 250, 1974.
7. Lemcoe, M. M., "Stresses in Layered Elastic Solids," *Proc ASCE*, EM4, pp 1, August 1960.
8. Barovich, D., Kingsley, S. C. and Ku, T. C., "Stresses on a Thin Strip or Slab with Different Elastic Properties From That of the Substrate Due to Elliptically Distributed Load," *International Journal of Engineering Sciences*, vol 2, pp 253, 1964.
9. Ku, T. C., Kingsley, S. C. and Ramsey, H., "Stresses in a Thin Slab With Different Elastic Properties From That of the Substrate Due to Distributed Normal and Shearing Forces on the Surface of the Slab," *International Journal of Engineering Sciences*, vol 3, pp 93, 1965.
10. Gupta, P. K., Walowit, J. A. and Finkin, E. F., "Stress Distributions in Plane Strain Layered Elastic Solids Subjected to Arbitrary Boundary Loading," *Journal of Lubrication Technology*, ASME Trans, vol 95F, pp 427, 1973.
11. Gupta, P. K., *LAYER - A Computer Code for Analysis of Plane- Strain Layered Elastic Solids*, PKG Inc, 1984.
12. Dio, F.F., Kato, K. and Hayashi, K., "The Maximum Tensile Stress on a Hard Coating Under Sliding Friction," *Tribology International*, vol 27, #4, pp 267-272, 1994.
13. Lovell, M.R., Khonsari, M.M., and Marangoni, R.D., "A finite Element Analysis of the Frictional Forces Between a Cylindrical Bearing Element and MoS₂ Coated and Uncoated Surfaces," *Wear*, vol 194, pp 60-70, 1996.
14. MSC/NASTRAN Computer codes with ARIES pre- and post-processors, MacNeal and Schwinder Corporation.
15. Kanel, J.W. and Walowit, J.A., "Simplified Analysis for Traction Between Rolling Sliding

- Elastohydrodynamic Contacts," J. Lub Tech., ASME Trns, vol 93, pp 39-46, 1971.
16. Johnson, K.L. and Tevaarwerk, J.L., "Shear Behavior of EHD Oil Film," Proc Royal Soc, London, A356, pp 215, 1977.
 17. Gupta, P.K., Flamand, L., Berthe, D. and Godet, M., "On the Traction Behavior of Seeral Lubricants," J. Lub Tech, ASME Trans, vol 103, pp 55-64, 1981.
 18. Gupta, P.K., "Traction Behavior of Military Lubricants," Air Force Technical Report WRDC-TR-89-2064, PKG Inc., August 1989.
 19. Gupta, P.K., "Traction Data Analysis, Part I: Perfluoropolyalkylether Fluids," Air Force Technical Report WL-TR-95-4117, PKG Inc, April 1995.
 20. Gupta, P.K., "Traction Data Analysis, Part II: Behavior of Some Aerospace Fluids and Lubricants," Air Force Technical Report WL-TR-97-4036, PKG Inc., January 1997.
 21. Walowit, J.A., "A Continuum Approach Towards Modeling the Mechanics of Solid Lubricating Films," Jed A. Walowit Inc, Technical Report prepared for Office of Naval Research, Arlington, VA, under contract number N00014-90-C-0087, September 1990.
 22. Gupta, P.K., ADVANCED DYNAMICS OF ROLLING ELEMENTS, Springer-Verlag, 1984.
 23. Kragelskii, I.V., FRICTION AND WEAR, Butterworths, 1965.
 24. Carlson, H. S. and Jaeger, J. C., CONDUCTION OF HEAT IN SOLIDS, Second Edition, Oxford Press, 1959.
 25. Gupta, P.K., "Thermal Interactions in Rolling Bearing Dynamics," PKG Inc, SBIR Phase I Report, Prepared for US Air Force under contract number F33615-95-C-2528, October 1995.
 26. Gardos, M.N., "Solid Lubricated RollingElement Bearings," Semiannual Status Report No. 4 & 5 - Part I: Executive Summary, DARPA Order NO. 3576, AFWAL Contract Nuo. F33615-78-C-5196, Hughes Aircraft Company Report NO. FR 81-76-661, March 1981.
 27. Gardos, M.N., "Solid Lubricated Rolling Element Bearings," Air Force Technical Report AFWAL-TR-83-4129, February 1984.
 28. Gupta, P.K., "Some Dynamic Effects in High-Speed Solid-Lubricated Ball Bearing," ASLE Transactions, vol 26, #3, pp 393-400, 1983.
 29. Gupta, P.K., "Frictional Instabilities in Ball Bearings," ASLE Tribology Transactions, vol 31, #2, pp 258-268, 1988.
 30. Heshmat, H., Albrecht, P. and Dill, J., "Friction and Wear Testing of Ceramic Materials," Mechanical Technology Inc Technical Report MTI 90TR1, prepared for Hughes Aircraft Company under contract S-9-316055 SAC, January 1990.

31. Heshmet, H., "Solid-Lubricated Roller Bearing Development: Static and Dynamic Characterization of High-Temperature, Power-Lubricated Materials," Air Force Technical Report, WL-TR-92-2050, Aero Propulsion and Power Directorate, Wright-Patterson Air Force Base, Ohio, June 1992.
32. Heshmet, H., "Traction Characteristics of High-Temperature Power-Lubricated Ceramics ($\text{Si}_3\text{N}_4/\alpha\text{SiC}$)," STLE Tribology Transactions, vol 35, #2, pp 360-366, 1992.
33. Kukureka, S.N., Chen, .K., Hooke, C.J., and Liao, P., "The Wear Mechanisms of Acetal in Unlubricated Rolling-sliding Contact," Wear, vol 185, pp 1-8, 1995.
34. Vancoille, E., Celis, J.P. and Roos, J.R., "Dry sliding Wear of TiN based ternary PVD Coatings," Wear, vol 165, pp 41-49, 1993.
35. Yust, C.S., and DeVore, C.E., "The Friction and Wear of Lubricated $\text{Si}_3\text{N}_4/\text{SiC}(w)$ Composites," STLE Tribology Transactions, vol 34, #4, pp 497-504, 1991.
36. Wei, J., Xue, Q. and Wang H., "Effects of Anti-Wear Additives on Friction and Wear Properties of Cr_2O_3 Coating," Tribology International, vol 26, #3, pp 241-244, 1993.
37. Kaneta, M., Matsuda, K., Matsuda, J. and Utsumi, A., "Friction and Wear Properties of Titanium Film formed on Aluminium by Laser Thermal Spraying," wear, vol 156, pp 161-173, 1992.
38. Gangopadhyay, A.K., Vassell, W.C., Tamor, M.A., Willermet, P.A., "Tribological Behavior of Amorphous Hydrogenated Carbon Films on Silicon," Journal of Lubrication Technology, ASME Trans, vol 116, pp 454-462, 1994.
39. Chen, M.Y., Lin, X., Dravid, V.P., Chung, Y.W., Wong, M.S. and Sproul, W.D., "Synthesis and Tribological Properties of Carbon Nitride as a Novel Superhard Coating and Solid Lubricant," STLE Tribology Transactions, vol 36, #3, pp 491-495, 1993.
40. Blau, P.J., and Martin, R.L., "Friction and Wear of Carbon-Graphite Materials against Metal and Ceramic Counterfaces," Tribology International, vo 27, #5, pp 413-422, 1994.
41. Ajayi, O.O., Erdemir, A., Fenske, G.R., and Erck, R.A., "Effect of Metallic-Coating Properties on the Tribology at Coated and Oil-Lubricated Ceramics," STLE Tribology Transactions, vol 37, #3, pp 656-660, 1994.
42. Prasad, S.V., and Mecklenburg, K.R., "Friction Behavior of Ceramic Fiber-Reinforced Aluminum Metal-Matrix Composites against a 440C Steel Counterface," Wear, vol 162-164, pp 47-56, 1993.
43. Roberts, E.W., "toward an Optimized MoS_2 Film," Proc 20th Aerospace Mech Symp, NASA CP-2423, pp 103-119, 1986.
44. Guu, Y.Y., Lin, J.F., and Ai, C., "The Tribological Characteristics of Titanium Nitride Coat-

ings, Part I Coating Thickness Effects," *Wear*, vol 194, pp 12-21, 1996.

45. Childs, T.H.C. and Mimaroglu, A., "Sliding Friction and Wear up to 600 °C of High-Speed Steels and Silicon Nitrides for Gas Turbine Bearings," *Wear*, vol 162-164, pp 890-896, 1993.
46. Endo, T., Iijima, T., Kaneko, Y., Miyakawa, Y., and Nishimura M., "Tribological Characteristics of Bonded MoS₂ Films Evaluated in Rolling-Sliding Contact in a Vacuum," *Wear*, vol 190, pp 219-225, 1995.
47. Zhao, W., Jinke, T., Yuxin, L. and Chen, L., "High Friction Coefficient of Fullerene C₇₀ Film," *Wear*, vol 198, pp 165-168, 1996.
48. Jang, D., and Kim, D.E., "Tribological Behavior of Ultra-Thin Soft Metallic Deposits on Hard Substrates," *Wear*, vol 196, pp 171-179, 1996.
49. Santner, E., Klaffke, D., and Kocker, G.M., "Comprehensive Tribological Characterization of Thin TiN-based Coatings," *Wear*, vol 190, pp 204-211, 1995.
50. Watanabe, S., Miyake, S., and Murakawa, M., "Tribological Behavior of cubic Boron Nitride Film sliding Against Diamond," *ASME Journal of Tribology*, vol 117, pp 629-633, 1995.
51. Huang, Z.P., Sun, Y. and Bell, T., "Friction Behavior of TiN, CrN and (TiAl)N Coatings," *Wear*, vol 173, pp 13-20, 1994.
52. Bandow, H.E., Gray, S.E., and Gupta, P.K., "Performance Simulation of a Solid-Lubricated Ball Bearing," ASLE Paper No. 85-AM-4E-3, Presented at the 40th Annual Meeting in Las Vegas, Nevada, May 6-9, 1985.
53. Galbato, A.T., "High-Temperature Solid Lubricant Bearing Development," Air Force Technical Report WRDC-TR-90-2085, Aero Propulsion and Power Directorate, Wright-Patterson Air Force Base, Ohio, November 1990.
54. Trivedi, H.K., and Gerardi, D.T., "High Temperature Bearing Material and Lubricant Evaluation," Air Force Technical Report WL-TR-96-2120, Aero Propulsion and Power Directorate, Wright-Patterson Air Force Base, Ohio, August 1996.
55. Lahrman, K., Bristol, B., and Anstead, D., "Dry Lubricated Bearing Development," Air Force Technical Report WL-TR-92-2074, Aero Propulsion and Power Directorate, Wright-Patterson Air Force Base, Ohio, May 1992.
56. Komvopoulos, K., "Sliding Friction Mechanisms of Boundary-Lubricated Layered Surfaces: Part I-Basic Mechanical Aspects and Experimental Results," *STLE Tribology Transactions*, vol 34, #2, pp 266-280, 1991.
57. Komvopoulos, K., "Sliding Friction Mechanisms of Boundary-Lubricated Layered Surfaces: Part II-Theoretical Results," *STLE Tribology Transactions*, vol 34, #2, pp 281-291, 1991.

58. Greenwood, J.A., and williamson, J.B.P., "Contact of Nominally Flat Surfaces," Proc Royal Soc, A, vol 295, pp 300-319, 1966.
59. Gupta, P.K., and Cook, N.H., "Statistical Analysis of Mechanical Interaction of Rough Surfaces," ASME Journal of Lubrication Technology, vol 94F, #1, pp 19-26, 1971.
60. Gupta, P.K., and Cook, N.H., "Junction Deformation Models for Asperities in Sliding Interaction," Wear, vol 20, pp 73-87, 1972.
61. Zhang, X., and Kato, K., "Friction Model of Thin Solid Film Lubrication," ASM Journal of Tribology, vol 118, pp 693-697, 1996.
62. Zhao, Y. and Liu J., "The Friction and Wear Model of Steels and Their Probable Stitistic Claculations", STLE Tribology Transactions, vol 35, pp 673-678, 1992.
63. Dareing, D.W., "Traction Coefficients for Coated Bearing Races Lubricated with Teflon Transfer Films," ASME Journal of Tribology, vol 113, pp 343-348, 1991.
64. Rabinowicz, E., FRICTION AND WEAR OF MATERIALS, John Wiley, 1965.
65. Archard, J.F., "Contact and Rubbing of Flat Surfaces," J. Appl Phys, vol 24, pp 981-988, 1953.
66. Mecklenburg, K.R., "Lubricant Compact Wear Rate Techniques," Air Force Technical Report AFWAL-TR-81-4014, Air Force Materials Laboratory, Wright-Patterson Air Force Base, Ohio, March 1981.
67. Meeks, C.R., and Bohner, J., "Predicting Life of a Solid-Lubricated Ball Bearing," ASLE Transactions, vol 29, #2, pp 203-213, 1986.
68. Cook, N.H., and Nayak, P.N., "The Thermal Mechanics of Tool Wear," ASME Paper #65-Prod-9, 1965.
69. Gupta, P.K., "An Investigation of Crater Wear of Cemented Carbide Tools," S.M. Thesis, Massachusetts Institute of Technology, Dept of Mech Engg, December 1967.
70. Gautier, P. and Kato, K., "Wear Mechanisms of Silicon Nitride, Partially Stabilized Zirconia and Alumina in Unlubricated Sliding Against Steel," Wear, vol 162-164, pp 305-311.1993.
71. Vancoille, E., Celis, J.P., and Roos, J.R., "Dry Wear of TiN based ternary PVD Coatings," Wear, vo 165, pp 41-49, 1993.
72. Pathak, J.P., Karimi, D., and Tiwari, S.N., "Room Temperature Wear Characteristics Al-Si-Cd Bearing Alloys," Wear, vol 170, pp 109-117, 1993.
73. Thoma, M., "Wear Behavior Titanium-Coating Combinations at Elevated Temperatures," Wear, vol 162-164, pp 1045-1047, 1993.

74. Suzuki, M., Moriyama, M., Nishimura, M. and Hasegawa, M., "Friction and Wear of Self-Lubrication Composites at Temperatures to 450 °C in Vacuum," *Wear*, vol 162-164, pp 471-479, 1993.
75. Ramesh, C.S., Seshadri, S.K., and Iyer, K.J.L., "A model for Wear Rates of Composite Coatings," *Wear*, vol 156, pp 205-209, 1992.
76. Gupta, P.K., "Modeling of Instabilities Induced by Cage Clearances in Ball Bearings," *STLE Tribology Transactions*, vol 34, pp 93-99, 1991.

Appendix A

Macros for Building the Coated Solid

A.1 Macro "startup"

```
/* This macros setup the starting variables */
setup
coordsystem
axis
unit
length
m
force
n
mass
kg
temperature
c
energy
joule
////////
axis
align
to_global
////////
quit
```

A.2 Macro "solid2d"

```
/* This macro creates the 2d solid for plane strain problem */
/* ---- name of solid ----*/
prompt "Enter name of solid"
input_string $b
/* ---- contact half width ---- */
prompt "Enter contact half width "
input $a
/* ---- size of solid ---- */
$x = 10.*$a
$y = $x
$z = $a
/* ----- frac of half width for fine mesh ----- */
prompt "Enter fraction of half width for fine mesh "
input $f
/* ----- */
axis
move
```

```

to_point
digitize
-$x/2. $y/2. 0 v 1
;;;
quit
/* --- base solid ---- */
edit
edit_target
$b
;
quit
add
solid
box
at_axis
ax
  $x
ay
  -$y
az
  -$z
;;;
/* ----- construct contact region ---- */
axis
move
to_point
digitize
  ($x/2.-$a*(1.+$f)) 0.001 -$z-0.001 v 1
;;;
quit
add
solid
box
at_axis
ax
  2.*$a*(1.+$f)
ay
  -$y-0.002
az
  $z+0.002
;;;
quit
construct
region
solid_cut
;;;

```

```

/* ----- construct sub regions near edge of contact ---- */
for ($i=1; ($i<3); $i=$i+1)
    axis
    move
    to_point
    digitize
    $f*$a 0 0 v 1
    ;;
    quit
    add
    solid
    box
    at_axis
    ax
    2.*$a*(1.+$f-$f*$i)
    ;;
    quit
    construct
    region
    solid_cut
    ;;
end_for
;;
/* ----- move axis to bottom of solid ---- */
axis
move
to_point
digitize
-$x*0.50+$a-$f*$a-0.001 -$y-0.002 0 v 1
;;
quit
/* --- regioning for layers ----- */
prompt "Enter first coating thickness to half width ratio"
input $h
$hs=$h
while ($h > 0.)
    add
    solid
    box
    at_axis
    ax
    $x+0.002
    ay
    $y-$hs*$a+0.001
    az
    $z+0.002

```

```

    !!!!
    quit
    construct
    region
    solid_cut
    !!!
    quit
    prompt "Enter next coating thickness to half width ratio (0. to
terminate) "
    input $h
    $hs=$hs+$h
end_while
!!!!
/* ---- set axis to center of contact zone ----*/
axis
align
to_global
;
move
to_point
digitize
0 0.50*$y 0 v 1
!!!!
view
show
dimetric
!!!!
view
show
front
!!!!
quit
quit
quit
quit

```

A.3 Macro "ell_pres"

```

/* Macro to prescribe elliptical pressure variation */
prompt " Enter maximum pressure "
input $p
prompt " Enter contact halfwidth "
input $a
interpolation
piecewise_linear
number_of_values
25

```

1 x -1.00*\$a;
 2 x -0.95*\$a;
 3 x -0.90*\$a;
 4 x -0.85*\$a;
 5 x -0.80*\$a;
 6 x -0.70*\$a;
 7 x -0.60*\$a;
 8 x -0.50*\$a;
 9 x -0.40*\$a;
 10 x -0.30*\$a;
 11 x -0.20*\$a;
 12 x -0.10*\$a;
 13 x 0.;
 14 x 0.10*\$a;
 15 x 0.20*\$a;
 16 x 0.30*\$a;
 17 x 0.40*\$a;
 18 x 0.50*\$a;
 19 x 0.60*\$a;
 20 x 0.70*\$a;
 21 x 0.80*\$a;
 22 x 0.85*\$a;
 23 x 0.90*\$a;
 24 x 0.95*\$a;
 25 x 1.00*\$a;
 1 VALUE 0.;
 2 VALUE -0.3122*\$p;
 3 VALUE -0.4359*\$p;
 4 VALUE -0.5268*\$p;
 5 VALUE -0.6000*\$p;
 6 VALUE -0.7141*\$p;
 7 VALUE -0.8000*\$p;
 8 VALUE -0.8660*\$p;
 9 VALUE -0.9165*\$p;
 10 VALUE -0.9539*\$p;
 11 VALUE -0.9798*\$p;
 12 VALUE -0.9950*\$p;
 13 VALUE -1.0000*\$p;
 14 VALUE -0.9950*\$p;
 15 VALUE -0.9798*\$p;
 16 VALUE -0.9539*\$p;
 17 VALUE -0.9165*\$p;
 18 VALUE -0.8660*\$p;
 19 VALUE -0.8000*\$p;
 20 VALUE -0.7141*\$p;
 21 VALUE -0.6000*\$p;

```

22  VALUE  -0.5268*$p;
23  VALUE  -0.4359*$p;
24  VALUE  -0.3122*$p;
25  VALUE  0.;

```

A.4 Macro "solid3d"

```

/* Macro for creating a 3d solid */
/* ---- name of solid ----*/
prompt "Enter name of solid"
input_string $n
/*----- contact type -----*/
prompt "Enter contact type (0=rectangular, 1=elliptical) "
input $icon
/* ---- contact half widths ---- */
prompt "Enter major to minor contact half width ratio"
input $ab
$b = 0.060
$a = $ab*$b
/* ---- size of solid (half lengths) ---- */
$x = 4.*$b
$y = 2.*$x
$z = 4.*$a
/* ---- frac of half width for central rect region */
$f = 0.1561
$fmin = $f
$fmaj = $f
/*----- number of points on elliptical contour -----*/
$m = 40
/* ---- set origin and fix axis ----- */
$dy = 0.0050
$x0 = 0.
$y0 = 0.
$z0 = 0.
axis
move
to_point
digitize
  $x0 $y0 $z0  v 1
;;;
axis
fix
;;
quit
/* --- base solid ---- */
edit
edit_target

```



```

$n
;
quit
axis
move
to_point
digitize
-$x 0 -$z
;;;
quit
add
solid
box
at_axis
ax
2.*$x
ay
2.*$y
az
2.*$z
;;;
quit
/*----- rectangular zone inside the contact -----*/
axis
move
to_point
digitize
($x - $b*$fmin) -$dy ($z - $a*$fmaj) v 1
;;;
quit
$xi = 2.*$b*$fmin
$yd = 2.*$y + 2.*$dy
$zi = 2.*$a*$fmaj
add
solid
box
at_axis
ax
$xi
ay
$yd
az
$zi
;;;
quit
construct

```

```

region
solid_cut
;;;
quit
/*----- move axis to center of contact -----*/
$xi = 0.50*$xi
$zi = 0.50*$zi
axis
move
to_point
digitize
$xi 0 $zi v 1
;;;
quit
/*----- main regions -----*/
for ($i=1; $i<3; $i=$i+1)
  if ($i == 1) then
    $sig = -1. ;;
  else
    $sig = 1. ;;
  end_if
/*---- subregion 1 & 2 ----*/
add
curve
exact
digitize
-$xi 0 $sig*$zi
lineseg
digitize
exact
$xi 0 $sig*$zi
digitize
exact
$x 0 $sig*$z
digitize
exact
-$x 0 $sig*$z
;
close
;;;
add
solid
extrusion
ext_x_direction
0
ext_y_direction

```

```

1
ext_z_direction
0
pick curve -$x 0 $sig*$z
depth
$yd
////
quit
construct
region
solid_cut
////
delete
pick curve -$x 0 $sig*$z
////
quit
/*----- subregion 1a & 2a -----*/
add
curve
exact
digitize
-$x 0 $sig*0.50*$z
lineseg
digitize
exact
-$xi 0 $sig*0.50*$zi
digitize
exact
$xi 0 $sig*0.50*$zi
digitize
exact
$x 0 $sig*0.50*$z
digitize
exact
$x 0 $sig*$z
digitize
exact
-$x 0 $sig*$z
;
close
///
add
solid
extrusion
ext_x_direction
0

```

```

ext_y_direction
1
ext_z_direction
0
pick curve -$x 0 $sig*$z
depth
$yd
;;;
quit
construct
region
solid_cut
;;;
delete
pick curve -$x 0 $sig*$z
;;;
quit
/*----- subregion 1b & 2b -----*/
add
curve
exact
digitize
0.50*$sig*$x 0 -$z
lineseg
digitize
exact
0.50*$sig*$xi 0 -$zi
digitize
exact
0.50*$sig*$xi 0 $zi
digitize
exact
0.50*$sig*$x 0 $z
digitize
exact
$sig*$x 0 $z
digitize
exact
$sig*$x 0 -$z
;
close
;;;
add
solid
extrusion
ext_x_direction

```

```

0
ext_y_direction
1
ext_z_direction
0
pick curve $sig*$x 0 -$z
depth
$yd
;;;
quit
construct
region
solid_cut
;;;
delete
pick curve $sig*$x 0 -$z
;;;
quit
end_for
/*----- contact zone -----*/
$dth = 2.*3.14159265/$m
$ff = 1.
for ($j=1; ($j < 10); $j=$j+1)
  if ($j == 2) then
    $ff = 0.9539
  end_if
  if ($j == 3) then
    $ff = 0.9165
  end_if
  if ($j == 4) then
    $ff = 0.8660
  end_if
  if ($j == 5) then
    $ff = 0.8000
  end_if
  if ($j == 6) then
    $ff = 0.7141
  end_if
  if ($j == 7) then
    $ff = 0.6000
  end_if
  if ($j == 8) then
    $ff = 0.4359
  end_if
  if ($j == 9) then
    $ff = 0.3122

```

```

end_if
$bj = $b*$ff
$aaj = $a*$ff
/*----- rectangular contact zone -----*/
if ($icon == 0) then
  axis
  move
  to_point
  digitize
  -$bj 0 -$aaj v 1
  ;;;
  quit
  add
  solid
  box
  at_axis
  ax
  2.*$bj
  ay
  $yd
  az
  2.*$aaj
  ;;;
  axis
  move
  to_point
  digitize
  $bj 0 $aaj v 1
else
/*----- elliptical contact area -----*/
  $xi = $bj
  $yi = 0.
  $zi = 0.
  $theta = 0.
  $i = 1
  add
  curve
  exact
  digitize
  $xi $yi $zi v 1
  spline
  through
  for ($i = 1; ($i < $m); $i = $i + 1)
    $theta = $theta + $dth
    $xi = $bj * cos($theta)
    $zi = $aaj * sin($theta)

```

```

        digitize
        exact
        $xi $yi $zi v 1
    end_for
    digitize
    exact
    $bj 0 0
    ;;
    close
    ;;
    quit
    add
    solid
    extrusion
    ext_x_direction
    0
    ext_y_direction
    1
    ext_z_direction
    0
    pick curve $bj 0 0
    depth
    $yd
    ;;
    quit
    delete
    pick curve $bj 0 0
    ;;
end_if
quit
construct
region
solid_cut
;;
quit
end_for
/*----- zone around the contact -----*/
$xi = 1.50*$b
$zi = 1.50*$a
axis
move
to_point
digitize
-$xi 0 -$zi v 1
;;
quit

```

```

add
solid
box
at_axis
ax
2.*$xi
ay
$yd
az
2.*$zi
;;;
quit
construct
region
solid_cut
;;;
quit
axis
move
to_point
digitize
$xi 0 $zi v 1
;;;
quit
/*----- region solid along z axis -----*/
$zd = 2.*($z+$dy)
$xd = 2.*($x+$dy)
axis
move
to_point
digitize
0 0 -($z + $dy) v 1
;;;
quit
add
solid
box
at_axis
ax
$x+$dy
ay
$yd
az
$zd
;;;
quit

```



```

construct
region
solid_cut
!!!!
quit
/*----- region solid along x axis -----*/
axis
move
to_point
digitize
~($x+$dy) 0 0 v 1
!!!!
quit
add
solid
box
at_axis
ax
$xd
ay
$yd
az
($z+$dy)
!!!!
quit
construct
region
solid_cut
!!!!
quit
/* --- regioning for layers ----- */
prompt "Enter first coating thickness to half width ratio"
input $h
$hs=$h
while ($h > 0.)
    add
    solid
    box
    at_axis
    ax
    $xd
    ay
    2.*$y-$hs*$b+$dy
    az
    $zd
    !!!!

```

```

quit
construct
region
solid_cut
iii
quit
prompt "Enter next coating thickness to half width ratio (0. to
terminate) "
input $h
$hs=$hs+$h
end_while
iiii
/* ---- set axis to center of contact zone ----*/
axis
move
to_point
digitize
($x+$dy) (2.*$y+$dy) ($z+$dy) v 1
iiii
view
show
dimetric
iiii
quit
quit

```

A.5 Macro "mesh1"

```

/*-----*/
/* Macro to generate mesh around the outer */
/* region in the top layer. This is the first */
/* macro which must be executed to start */
/* meshing the coated solid. */
/*-----*/
/*---- input data -----*/
prompt " Enter half width ratio "
input $ab
prompt " Enter number of circumferential mesh points "
input $n
$x = 0.24
$z = $x*$ab
/*---- mesh zone 2 -----*/
pick
region 0.25*$x 0 $z
;
edge_nodes
num_elem

```

```

$n
pick
edge 0.25*$x 0 $z
;;
mesh
;
/*----- mesh zone 3 -----*/
pick
region -0.25*$x 0 $z
;
edge_nodes
num_elem
$n
pick
edge -0.25*$x 0 $z
;;
mesh
;
/*----- mesh zone 4 -----*/
pick
region -0.75*$x 0 $z
;
edge_nodes
num_elem
$n
pick
edge -0.75*$x 0 $z
;;
mesh
;
/*----- mesh zone 5 -----*/
pick
region -$x 0 0.75*$z
;
edge_nodes
num_elem
$n
pick
edge -$x 0 0.75*$z
;;
mesh
;
/*----- mesh zone 6 -----*/
pick
region -$x 0 0.25*$z
;

```

```

edge_nodes
num_elem
$n
pick
edge -$x 0 0.25*$z
;;
mesh
;
/*----- mesh zone 7 -----*/
pick
region -$x 0 -0.25*$z
;
edge_nodes
num_elem
$n
pick
edge -$x 0 -0.25*$z
;;
mesh
;
/*----- mesh zone 8 -----*/
pick
region -$x 0 -0.75*$z
;
edge_nodes
num_elem
$n
pick
edge -$x 0 -0.75*$z
;;
mesh
;
/*----- mesh zone 9 -----*/
pick
region -0.75*$x 0 -$z
;
edge_nodes
num_elem
$n
pick
edge -0.75*$x 0 -$z
;;
mesh
;
/*----- mesh zone 10 -----*/
pick

```

```

region -0.25*$x 0 -$z
;
edge_nodes
num_elem
$n
pick
edge -0.25*$x 0 -$z
;;
mesh
;
/*----- mesh zone 11 -----*/
pick
region 0.25*$x 0 -$z
;
edge_nodes
num_elem
$n
pick
edge 0.25*$x 0 -$z
;;
mesh
;
/*----- mesh zone 12 -----*/
pick
region 0.75*$x 0 -$z
;
edge_nodes
num_elem
$n
pick
edge 0.75*$x 0 -$z
;;
mesh
;
/*----- mesh zone 13 -----*/
pick
region $x 0 -0.75*$z
;
edge_nodes
num_elem
$n
pick
edge $x 0 -0.75*$z
;;
mesh
;

```

```

/*----- mesh zone 14 -----*/
pick
region $x 0 -0.25*$z
;
edge_nodes
num_elem
$n
pick
edge $x 0 -0.25*$z
;;
mesh
;
/*----- mesh zone 15 -----*/
pick
region $x 0 0.25*$z
;
edge_nodes
num_elem
$n
pick
edge $x 0 0.25*$z
;;
mesh
;
/*----- mesh zone 16 -----*/
pick
region $x 0 0.75*$z
;
edge_nodes
num_elem
$n
pick
edge $x 0 0.75*$z
;;
mesh
;

```

A.6 Macro "mesh2"

```

/*-----*/
/* This macro is used to mesh the sixteen regions */
/* of either the rectangular of elliptical area. */
/* This is second macro, which is executed in the */
/* in the meshing process. */
/*-----*/
/*----- input data -----*/
prompt " Enter half width ratio "

```

```

input $ab
prompt " Enter normalized half width "
input $bb
$b = 0.060*$bb
$a = $ab*$b
prompt " Enter mesh region type (0=rectangular, 1=elliptical) "
input $icon
prompt " Enter starting region number "
input $izone
if ($icon == 0) then
    $x1 = 0.75*$b
    $z1 = $a
    $x2 = 0.25*$b
    $z2 = $a
    $x15 = $b
    $z15 = 0.25*$a
    $x16 = $b
    $z16 = 0.75*$a
else
    /*---- zone 1 coordinates ----*/
    $t = 0.75*$b/$a
    $aa = ($ab*$t)**2
    $x1 = $b * sqrt($aa/(1.+$aa))
    $z1 = $a/sqrt(1.+$aa)
    /*---- zone 2 coordinates ----*/
    $t = 0.25*$b/$a
    $aa = ($ab*$t)**2
    $x2 = $b * sqrt($aa/(1.+$aa))
    $z2 = $a/sqrt(1.+$aa)
    /*---- zone 15 coordinates ----*/
    $t = 0.25*$a/$b
    $aa = ($t/$ab)**2
    $x15 = $b/sqrt(1.+$aa)
    $z15 = $a*sqrt($aa/(1.+$aa))
    /*---- zone 16 coordinates ----*/
    $t = 0.75*$a/$b
    $aa = ($t/$ab)**2
    $x16 = $b/sqrt(1.+$aa)
    $z16 = $a*sqrt($aa/(1.+$aa))
end_if
/*---- mesh zone 1 ----*/
if ($izone == 1) then
    pick
    region $x1 0 $z1
    ;
    mesh

```

```

;
end_if
/*----- mesh zone 2 -----*/
pick
region $x2 0 $z2
;
mesh
;
/*----- mesh zone 3 -----*/
pick
region -$x2 0 $z2
;
mesh
;
/*----- mesh zone 4 -----*/
pick
region -$x1 0 $z1
;
mesh
;
/*----- mesh zone 5 -----*/
pick
region -$x16 0 $z16
;
mesh
;
/*----- mesh zone 6 -----*/
pick
region -$x15 0 $z15
;
mesh
;
/*----- mesh zone 7 -----*/
pick
region -$x15 0 -$z15
;
mesh
;
/*----- mesh zone 8 -----*/
pick
region -$x16 0 -$z16
;
mesh
;
/*----- mesh zone 9 -----*/
pick

```



```

region  -$x1  0  -$z1
;
mesh
;
/*----- mesh zone 10 -----*/
pick
region  -$x2  0  -$z2
;
mesh
;
/*----- mesh zone 11 -----*/
pick
region  $x2  0  -$z2
;
mesh
;
/*----- mesh zone 12 -----*/
pick
region  $x1  0  -$z1
;
mesh
;
/*----- mesh zone 13 -----*/
pick
region  $x16  0  -$z16
;
mesh
;
/*----- mesh zone 14 -----*/
pick
region  $x15  0  -$z15
;
mesh
;
/*----- mesh zone 15 -----*/
pick
region  $x15  0  $z15
;
mesh
;
/*----- mesh zone 16 -----*/
pick
region  $x16  0  $z16
;
mesh
;

```

A.7 Macro "mesh3"

```
/*-----*/
/* Macro to the twelve rectangular regions in */
/* in the interior of contact. This is third */
/* macro to be executed in meshing process */
/*----- input data -----*/
prompt " Enter half width ratio "
input $ab
prompt " Enter normalized half width "
input $bb
$b = 0.060*$bb
$a = $ab*$b
  $x1 = 0.75*$b
  $z1 = $a
  $x2 = 0.25*$b
  $z2 = $a
  $x12 = $b
  $z12 = 0.25*$a
/*----- mesh zone 1 -----*/
  pick
  region $x1 0 $z1
  ;
  mesh
  ;
/*----- mesh zone 2 -----*/
  pick
  region $x2 0 $z2
  ;
  mesh
  ;
/*----- mesh zone 3 -----*/
  pick
  region -$x2 0 $z2
  ;
  mesh
  ;
/*----- mesh zone 4 -----*/
  pick
  region -$x1 0 $z1
  ;
  mesh
  ;
/*----- mesh zone 5 -----*/
  pick
  region -$x12 0 $z12
  ;
```

```

mesh
;
/*----- mesh zone 6 -----*/
pick
region  -$x12  0  -$z12
;
mesh
;
/*----- mesh zone 7 -----*/
pick
region  -$x1  0  -$z1
;
mesh
;
/*----- mesh zone 8 -----*/
pick
region  -$x2  0  -$z2
;
mesh
;
/*----- mesh zone 9 -----*/
pick
region  $x2  0  -$z2
;
mesh
;
/*----- mesh zone 10 -----*/
pick
region  $x1  0  -$z1
;
mesh
;
/*----- mesh zone 11 -----*/
pick
region  $x12  0  -$z12
;
mesh
;
/*----- mesh zone 12 -----*/
pick
region  $x12  0  $z12
;
mesh
;
;

```

A.8 Macro "mesh4"

```
/*-----*/
/* Macro to mesh the four rectangular regions at */
/* center of contact in the top layer. This is the */
/* macro used to complete meshing of the top layer */
/*-----*/
/*---- input data -----*/
prompt " Enter half width ratio "
input $ab
prompt " Enter normalized half width "
input $bb
$b = 0.060*$bb
$a = $ab*$b
    $x1 = 0.50*$b
    $z1 = $a
    $x2 = -0.50*$b
    $z2 = $a
/*---- mesh zone 1 -----*/
    pick
    region $x1 0 $z1
    ;
    mesh
    ;
/*---- mesh zone 2 -----*/
    pick
    region $x2 0 $z2
    ;
    mesh
    ;
/*---- mesh zone 3 -----*/
    pick
    region $x2 0 -$z2
    ;
    mesh
    ;
/*---- mesh zone 4 -----*/
    pick
    region $x1 0 -$z1
    ;
    mesh
    ;
```

Appendix B

Manual Analysis Procedure

Normally in the ARIES preprocessor for MSC/NASTRAN, the analysis mode is set to "automatic." This means that no input data set is directly submitted to NASTRAN for analysis. When output data from one solution is transferred as input to another case, such as transfer of computed temperature field from the thermal problem to the stress problem, manual mode of analysis is desired. This is accomplished as follows:

1. Build the finite element model as usual.
2. In FEM application, pick Analysis mode as "Manual Analysis."
3. Type in name for input deck, for example "heatxfer1."
4. In a separate unix window execute the following command:
 aries f_nastran.sh input_deck_name heatxfer1
- 5 When the unix prompt returns execute the command:
 aries anf2ari NASTRAN.ANF

The last step puts the output data back in ARIES for post-processing and graphic viewing of the results.

This page is left blank